THE WAKSMAN FOUNDATION OF JAPAN INC.

Honorary Patron

H.I.H. Prince Akishino

Board of Directors

Chairman : Ichiro Kitasato, Adviser, The Kitasato Institute.
Former Chairman of The Board, Meiji Seika Kaisha, Ltd.
Satoshi Omura, Honorable Emeritus Professor, Kitasato Univ.
Teruhiko Beppu, Prof. Emeritus, Tokyo Univ.
Takeji Nishikawa, Prof. Emeritus, Keio Univ.
Shoji Kudoh, Chairman, Board of Directors Japan Anti-Tuberdulosis Association.
Masahiro Koya, President, Keio University Press Inc.

Managing Director : Yuko Kitagawa, Prof., Keio Univ. Sch. Med.

Comptroller : Yoshiharu Wakiyama, Senior Adviser, Kaken Pharmaceutical, Co., Ltd.
Shirow Enoki, Former President, Seikagaku Corporation.

Councilors

Ryoichi Mori, Prof. Emeritus, Kyushu Univ.
Keizo Takemi, Member,The House of Councilors.
Koichi Yamanishi,,Director General,The Research Foundation for Microbial Diseases of Osaka Unoversity.
Shigeo Koyasu, Executive Director, RIKEN.
Takashi Shoda, Senior Corporate Adviser, Daiichi Sankyo Co., Ltd.
Tadakatsu Shimamura, Prof. Emeritus, Showa Univ.
Yoshinobu Sumiyama, Chairman of the Board of Directors, Toho University.
Professor Emeritus, Toho University.
Shuzo Kaihori, Chaiman of the Board, Yokogawa Electric Corporation.

Special Adviser

Akira Uehara, Chairman & CEO, Taisho Pharmaceutical Holdings Co., Ltd.
Osamu Nagayama, Chairman & CEO, Chugai Pharmaceutical Co., Ltd.
Haruo Naito, President & CEO, Eisai Pharmaceutical Co., Ltd.
Seiichi Sato, President & CEO, Sato Pharmaceutical Co., Ltd.
Yoshihiro Miwa, President & CEO, Kowa Co., Ltd.

2016

Published by
THE WAKSMAN FOUNDATION OF JAPAN INC.
26-1 Daikyo-cho, Shinjuku-ku,
Tokyo 160-0015, Japan
http://www.waksman.or.jp/
E-mail: toshihisa-sato@waksman.or.jp

Preface to the First Report (1962)

It is indeed a privilege to take this opportunity to write a few words of introduction to the first report of the Waksman Foundation of Japan Inc., covering five years of its activities and comprising the results of the work of the first two years of research carried out by various scholars in Japan in the fields of microbiology and medical science, supported by this Foundation.

In 1952, I accepted the invitation from Keio University and the Kitasato Institute, to deliver the centennial lecture in honor of the great Japanese bacteriologist, Shibasaburo Kitasato. Before departing for Japan, I proposed to the trustees of the Rutgers Research and Educational Foundation which owned the patents on streptomycin, to share the royalties under the patent in Japan, for the support of research in microbiology and allied fields in that country. The trustees heartily approved my recommendation that I make such announcement to that effect.

Soon upon my arrival in Japan (December 17, 1952), I invited a group of eminent microbiologists, biochemists, and clinical investigators to meet with me in order to discuss the plan. Everyone present was very enthusiastic about the proposal. It was decided that a proper committee be selected to work out the plan of a Foundation under which the royalties were to be received and distributed for the support of Japanese investigators working in different universities in Japan and elsewhere, in the fields of microbiology and medical research. The committee recommended that a Board of Directors be selected and the proposed Foundation be named THE WAKSMAN FOUNDATION OF JAPAN INCORPORATION.

The Rutgers Research and Educational Foundation approved at once the above recommendations and issued a statement, signed by Dr. Lewis Webster Jones, President of the Foundation, to the effect that

"The Rutgers Research and Educational Foundation desires to emphasize that its principal concern is the advancement of scientific knowledge in the public interest and that it confidently expects that the Waksman Foundation for Microbiology and Medical Research in Japan will be similarly motivated, thereby serving the peoples of both countries."

This announcement was received with enthusiasm both by the scientific world and the popular press in Japan and in the United States. It took several years before the Waksman Foundation of Japan Inc. was properly organized, and before applications were received and approved. In 1958, I had the privilege of participating in the first official

meetings of the Board of Directors of the Japanese Foundation and to greet personally the first group of scholars to whom grants had been made.

In summarizing these brief remarks in connection with the first cinqueannual report of the Waksman Foundation of Japan Inc., I would like to enphasize that this example of collaboration between universities and scientists of the United States and Japan may serve to encourage collaboration between scientific workers throughout the world towards a better understanding between men and women and towards a happier and healthier human race, so that all the nations on this earth can live in peace and that man may finally "break his swords and build out of them plowshares" for the betterment of mankind as a whole.

Selman A. Waksman
Professor Emeritus
Rutgers-State University N. J., U. S. A.

The "Waksman Foundation of Japan Inc." was established in 1957 with the spirit of humanity by Dr. S.A. Waksman, Professor of Microbiology, Rutgers University, U.S.A. The Foundation's operations are possible only because Dr. S.A. Waksman and the Rutgers Research and Educational Foundation donated patent royalties he received from the production in Japan of the discovery, Streptomycin.

Because of these royalties, each year many Japanese scholars and research workers in the fields of Microbiology and medical science are encouraged and find it possible to continue their work. Especially, in accordance with Dr. Waksman's suggestion, the funds are distributed to scholars in local and economically hampered schools and laboratories and to those developing research workers who are endeavoring to expand in their fields. This thought of Dr. Waksman's is most appreciated, as it matches our Oriental phylosophy, and results in the search for a jewel among ordinary stones, which is the highest work of the science-leader.

Some five years have now passed since the start of this Foundation, and many persons have received aid through this period.

The reports which are presented herein cover the first and second group of research workers who received financial assistance from the Foundation.

Toshio Katow, M. D.
Executive Director

Contents

——Report of Researches in 2013,2014,2015——

Mechanisms of pathogen invasion into the central nervous system via the inflammation amplifier

Masaaki Murakami

Molecular Neuroimmunology, Institute for Genetic Medicine, Hokkaido University

Introduction

The central nervous system (CNS) excludes the migration of blood circulating cells into the sophisticated tissue due to the presence of blood-brain barrier (BBB). BBB is constituted and maintained by endothelial cells, pericytes and astrocytic end-feet (1). The tight junction is responsible for sealing blood vessels by the interactions of tight junction molecules such as claudins and occludins (2). Dysfunction of BBB and migration of immune cells into the CNS are known to be associated with many chronic neurodegenerative disorders and autoimmune diseases (3, 4). Furthermore, BBB can be cross by some bacteria, viruses and parasites to cause meningitis and encephalitis (5, 6).

Listeria monocytogenes is Gram-positive intracellular bacteria responsible for a severe food borne infection in humans, characterized by gastroenteritis, meningitis, encephalitis, and perinatal infections. Internalins are listeria factors that mediate bacterial invasion into target cells by binding to host receptors including c-Met and E-cadherin (5, 7). ActA is another virulent factor of *Listeria* and used for the actin-based motility of the bacteria within the host cells (5). Herpes simplex virus (HSV) is a member of the Herpesviridae that is a large family of double-stranded DNA viruses. HSV causes localized infections in mucosal sites, but it can also cause meningitis and encephalitis (8). *Neisseria meningitidis* (meningococcus) is Gram-negative bacteria responsible for cerebrospinal meningitis in humans. It is reported that β2 adrenergic receptor mediates adhesion of the bacteria to endothelium (9). *Streptococcus pneumoniae* is a Gram-positive bacterium, and a leading cause of life-threatening infections such as pneumonia, meningitis and sepsis, especially in children (10, 11). However, it is not fully clear how and where these pathogens can pass over the BBB to cause CNS infections.

Under a healthy condition, BBB provides a tight barrier between the circulating blood cells and CNS by dense tight junction proteins, which close the space between adjacent endothelial cells. However, immune cells can be found in the case of tumors or infections in the CNS, suggesting that there is an entry site of immune cells into the CNS. It had been unclear until recently how and where these immune cells migrate into the CNS. Using a murine model of multiple sclerosis,

experimental autoimmune encephalomyelitis (EAE), in which the CNS is attacked by adoptively transferred pathogenic CD4 T cells, we found that the dorsal vessels of fifth lumber spinal cord (L5) are the entry site (i.e. gateway) for immune cells to enter the CNS at an early preclinical phase of EAE (12). Imaging analysis using MRI confirmed the alteration of L5 spinal cord during an initial phase of EAE (13). The dorsal vessels of the L5 spinal cord showed excessive expression of chemokines induced by an inflammation-inducing mechanism, termed the inflame- mation amplifier (14). The inflammation amplifier is defined as a molecular mechanism that induces a large amount of proinflammatory mediators such as chemok- ines and IL-6 in non-immune cells including endothelial cells and fibroblasts, and it has been demonstrated that the inflammation amplifier plays a critical role in the pathogenesis of various chronic inflammatory diseases (12, 14-17). Experiments using RNA interference-mediated knock down in a cell line or mouse embryonic fibroblasts from knock out mice revealed that activation of the inflammation amplifier is dependent on two transcription factors NF-κB and STAT3, which are stimulated by IL-17 and IL-6, respectively (15). In fact, knock-in mice that show enhanced activation of the inflammation amplifier due to a lack of negative regulation of IL-6 signaling pathway (called F759 mice) spontaneously develop autoimmune arthritis that highly resembles rheumatoid arthritis in humans (18). On the contrary, mice deficient in the inflammation amplifier activation in non-immune cells were resistant to various inflammatory animal models (12, 14-17). Furthermore, evidence of the amplifier activation is obtained in a human clinical sample (19). To explore detailed molecular mechanisms of the inflammation amplifier, we have identified target genes of the inflammation amplifier by DNA microarray analysis, and also genes that are required for the activation of the amplifier by small-hairpin RNA-mediated functional screening (20). These identified genes showed high enrichment of human disease-associated genes. The disease types include not only autoimmune diseases, but also metabolic syndromes, neurodegenerative diseases, and cancers (14, 20). All these results suggest that the inflammation amplifier is a molecular basis of many chronic inflammatory diseases.

Mechanistic analyses why the pathogenic CD4 T cells utilize the L5 gateway in EAE model revealed that sensory nerve activation in the soleus muscles by gravity force of the Earth stimulates the activation of sympathetic neurons nearby, which lead to secretion of noradrenaline and enhance the inflammation amplifier preferentially at L5 region of the spinal cords (12). This study provided solid evidence that regional neural signals can be translated into immune signals to promote local inflammation. This neuro-immune response is named “gateway reflex” (21-23). These studies demonstrated that L5 dorsal vessels are a specific gateway for immune cells

to enter the CNS via the activation of the inflammation amplifier. Importantly, the selective activation of the inflammation amplifier is also observed under a normal non-diseased condition, suggesting a certain physiological and/or pathological role of the gateway reflex other than autoimmune conditions. In this study, we hypothesized that pathogens that invade the CNS would also utilize the L5 cord gateway to infect hosts depending on the gateway reflex. Based on this hypothesis, we aimed to characterize molecular mechanisms to establish infections in the CNS.

Materials and Methods

Mice

C57BL/6 mice at 6 – 8 weeks old were purchased from Japan SLC, Inc. All mice were maintained under specific pathogen-free conditions according to the protocols of Osaka University Graduate School of Medicine. All animal experiments were performed following the guidelines of the Institutional Animal Care and Use Committees of the Graduate School of Frontier Biosciences and Graduate School of Medicine, Osaka University.

Infection models

Listeria monocytogenes was grown in brain-heart infusion broth (Beckton Dickinson) at 37 °C, and a log-phase duplicating bacteria was stored in 10% glycerol/PBS (Sigma-Aldrich) at -80 °C. Serial dilutions of the bacteria suspension were made and plated on brain-heart infusion plates to determine the titer of the stock. The frozen stocks of the other bacteria were similarly prepared. Herpes-simplex virus 2 (HSV2) was propagated in BHK-21 cells and titrated using a plaque assay in Vero cells. These pathogens were obtained from ATCC. A lethal dose, which causes mortality in C57BL/6 mice around 4 to 6 days post infection, was injected i.p. on day 0. The mice were sacrificed on day 1, and CNS tissues were harvested. In some experiments, HSV2 was inoculated at ankle joints and the L5 spinal cord was isolated 5 days later. A c-Met inhibitor SU11274 (Sigma-Aldrich) was administered i.p. at 10 mg/kg.

DNA microarray

Normal C57BL/6 mice were sacrificed and cardiac perfusion using PBS was performed. The dorsal vessels of spinal cords at L1 or L5 level were isolated under a stereomicroscope. Total RNA extracted from the dorsal vessels of L1 or L5 spinal cords was processed into biotinylated cRNA, which was then hybridized to GeneChip Mouse Genome 430 2.0 Array (Affymetrix). Raw data were processed with the MAS5 algorithm for normalization.

Genomic DNA extraction and quantitative PCR

One day after the infection, the infected mice were sacrificed, and the brain, L1 and L5

spinal cords were harvested after cardiac perfusion using phosphate-buffered saline. Genomic DNA of the infected mice was extracted from the tissues using proteinase K digestion (Sigma-Aldrich) at 55 °C overnight, followed by isopropanol precipitation (Sigma-Aldrich) to purify the DNA. The genomic DNA was suspended in TE buffer and DNA concentrations were adjusted among samples. The presence of genomic DNA of the pathogens in the tissue DNA samples was examined using quantitative PCR specific for bacterial or viral antigens. A 7300 Fast Real-Time PCR system (Applied Biosystems), and SYBR Green or PROBE FAST qPCR Master Mix (KAPA Biosystems) were used for the quantitative PCR. Primer sequences were as follows: Lm_ActA-P, FAM-TCGAATTTCC-ACCGCCTCCAACAGAAGA-TAMRA; Lm_ActA-F, 5'-GCTCCTGCTACATCGGAAC-C-3'; Lm_ ActA-R, 5'-GTGCTGTTTCCCGCA-TAATTTCTA-3'; Lm_Internalin-P, FAM-AC-CGCGCCAGATTTAGCAAGAAGCACT-TAM-RA; Lm_Internalin-F, 5'-GCGGTTAACTCGA-ACGA TATTTCA-3'; Lm_Internalin-R, 5'-GCT-TCGTCGTATAGATCCGTAAC-3; HSV2-F, 5'-CGCATCAAGACCACCTCCTC-3'; HSV2-R, 5'-GCTCGCACCACGCGA-3'; HSV2-P, FAM-GCGGCGATGCGCCCCAG-TAMRA; NmB-1646-F, 5'-TTCAATACTTACAGCCATTTGAG-C-3'; NmB1646-R, 5'-CATCGTTTACAAACCA-GTAAATGC-3';Sp_CS109-F, 5'-AATGGGATT-ACCTATGCCAATATG-3'; Sp_CS109-R, 5'-CA-TCTGAGTTTCCATGAAAGATTG-3'; Insulin-F, 5'-CCACCCAGGCTTTTGTCAA-3'; and Insulin-R,5'-ATGCTGGTGCAGCACTGATC-3'.

Statistical analysis

Student's t-tests (two-tailed) were used for the statistical analysis of differences between two groups. p values less than 0.05 was considered statistically significant.

Results and Discussion

In previous studies, we identified the dorsal vessels of fifth lumber (L5) spinal cord as a gateway for encephalitogenic autoreactive CD4 T cells to enter the CNS (12). This L5 gateway is created even in normal mice by selective upregulations of various molecules including chemokines (12). The L5 gateway formation is dependent on the activation of the inflammation amplifier in endothelial cells of the L5 vessels (12, 14). These results indicated that the L5 vessels have a unique transcriptional profile due to selective activation of the amplifier. We first performed DNA microarray using total RNA from L1 and L5 dorsal vessels, and assessed the expression levels of known host receptors for pathogens that can invade the CNS. As shown in Table 1 , several molecules known as host receptors of CNS-invading pathogens including c-Met, E-cadherin, Nectin-1, Her2, and β2 adrenergic receptor were upregulated in the dorsal vessels of L5 spinal cords, as compared to those of L1 cords. This result raised possibility that bacteria and viruses using these host receptors such as *Listeria monocytogenes, Streptococcus pneumoniae, Neisseria meningitis,* and herpes-simplex

Table 1 Expression of host receptors used by CNS-invading pathogens in L1 and L5 dorsal vessels

Gene names	Gene symbols	Pathogens	Fold difference (L5/L1)
c-Met	Met	L. monocytogenes	5.0
E-cadherin	Cdh1	L. monocytogenes, S. pneumoiae	1.4
Nectin-1	Pvrl1	HSV	6.5
HVEM	Tnfrsf14	HSV	0.4
HER2	Erbb2	HSV	1.4
Adrenergic receptor, beta 2	Adrb2	N. meningitis	5.6

RNA from dorsal vessels in L1 and L5 spinal cords from normal C57BL/6 mice was subjected to DNA microarray analysis. Fold increase (L5/L1) is shown for genes encoding host receptors used by CNS-invading pathogens.

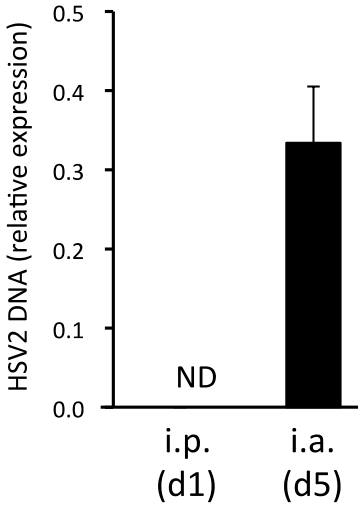

Figure 1 HSV2 DNA levels in L5 cord after intraperitoneal or intraarticular infection.
C57BL/6 mice were infected with HSV2. HSV2 DNA was measured by qPCR on day 1 (intraperitoneal infection, i.p.) or day 5 (intraarticular infection, i.a.). Data represent mean + SD. ND, not detected

virus (HSV) may enter the CNS from the L5 spinal cord. CNS infections are seen in patients at a progressive stage of infection by these pathogens. To replicate this situation, C57BL/6 mice were infected i.p. with a lethal dose of these bacteria and HSV. In order to identify an entry site of the CNS-invading pathogenis, the CNS tissues including L1 or L5 spinal cords, cerebellum, cerebrum, and midbrain were harvested at an early phase of infection (day 1). After genomic DNA extraction from these tissues, the invasion of the bacterial and viral pathogens in the CNS tissues was detected by PCR specific for the

genes of these pathogenic agents. Intraperitoneal infections of C57BL/6 mice with some CNS-invading pathogens including HSV2, *N. meningitis,* and *S. pneumonia* did not show detectable L5 invasion on day 1 (Fig. 1 and data not shown). Since HSV2 DNA was Detected in the L5 cord on day 5 after ankle inoculation via inter-synaptic transmission of HSV, time and/or route of infections may vary for each pathogen to successfully detect entry points of these pathogens in the CNS. On the points of these pathogens in the CNS. On the other hand, Listeria gene internalin was clearly observed in genomic DNA from the L5 spinal cords 1 day post infection with an intraperitoneal inoculation of *Listeria monocytogenes* (Fig. 2A). Quantitative PCR analysis revealed that *Listeria* genes ActA and internalin were detected at significantly higher levels in L5 cords than L1 cords or several brain regions, suggesting that L5 is a possible gateway for the intracellular bacteria, similar to immune cells (Figs. 2B and 2C).

We next examined molecular mechanisms of the *Listeria* invasion from L5 spinal cord. It is known that *Listeria* utilizes c-Met and E-cadherin as host receptors to enter inside host cells (5), and both genes were upregulated in L5 dorsal vessels (Table 1). In a preliminary experiment, blocking c-Met signaling with a pharmacological inhibitor SU11274 altered the distribution of *Listeria* at the L5 cord, suggesting the possibility that c-Met signaling could be involved in the CNS invasion of *Listeria* from L5 spinal cord. These results suggest that CNS-invading pathogen, at least *Listeria monocytogenes,* utilizes the physiological L5 gateway to cause infection in the CNS.

Conclusion

The L5 spinal cord is a specific site because Sensory neurons in the dorsal-root ganglion beside the L5 cord are constantly stimulated by the Earth gravity though the soleus muscles (24). In humans, the dorsal-root ganglion of L5 cord is also the largest among lumber cords (25), suggesting a similar mechanism of anti-gravity response. We previously reported that this anti-gravity neural response creates a gateway for immune cells into the CNS by expressing larger amount of chemokines via the inflammation amplifier (12). The activation of the amplifier is observed even under a normal non-disease condition, albeit a lower degree than that during EAE disease (12). This study showed that one of the CNS-invading pathogens Listeria monocytogenes can invade the L5 spinal cord more significantly than the L1 cord or brain. These results suggest that this pathogen exploit the L5 gateway to cause infection in the CNS, and represent a pathological role for the L5 gateway created by anti-gravity response. Further studies including the contributions of nervous systems and gravity will be performed to analyze this Listeria invading mechanism in detail to publish his study, which will provide an

(4)Bennett, J., J. Basivireddy, A. Kollar, K. E. Biron, P. Reickmann, W. A. Jefferies, and S.

implication that inhibition of the inflammation amplifier can be used to prevent the progression from peripheral infections to life-threatening CNS infections.

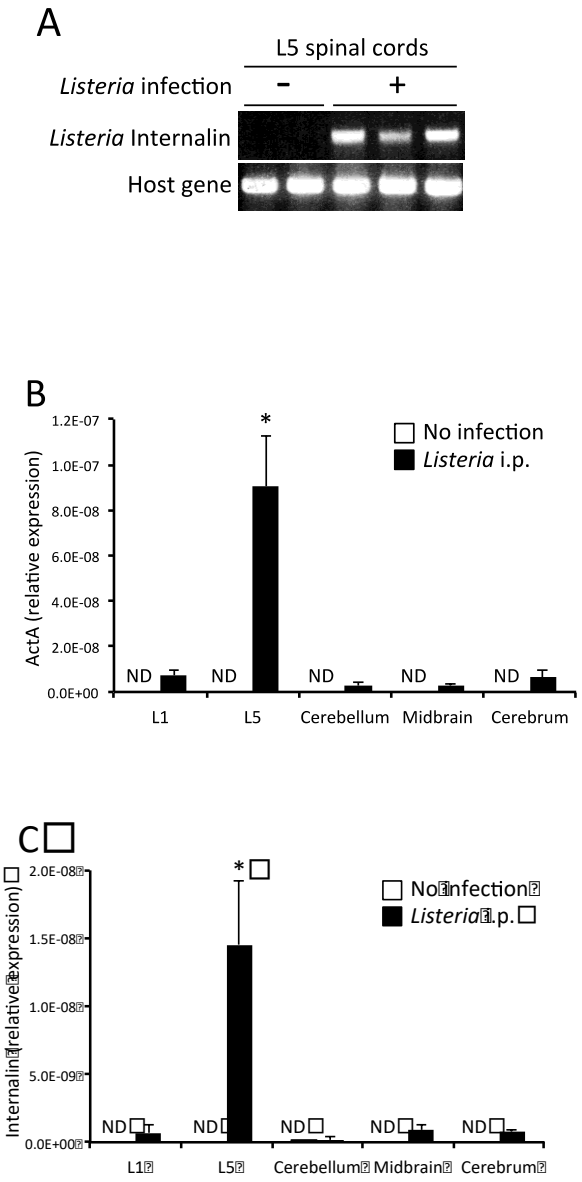

Figure 2 Listeria gene levels in L1, L5 cords and brain regions after intraperitoneal infection. C57BL/6 mice were infected intraperitoneally with L. monocytogenes. (A) Genomic DNA from L5 spinal cords 1 day after infection was amplified for Listeria internalin gene, or host gene (insulin) for a positive control reaction. Listeria gene ActA (B) and internalin (C) levels by qPCR are shown. Data represent mean + SD. * $p < 0.05$ and ND, not detected.

References

1. Abbott, N. J., L. Ronnback, and E. Hansson. 2006. Astrocyte-endothelial interactions at the blood-brain barrier. *Nat Rev Neurosci* 7: 41-53.
2. Steed, E., M. S. Balda, and K. Matter. 2010. Dynamics and functions of tight junctions. *Trends Cell Biol* 20: 142-149.
3. Zlokovic, B. V. 2008. The blood-brain barrier in health and chronic neurodegenerative disorders. *Neuron* 57: 178-201.
4. Bennett,J., J. Basivireddy,, A.Kollar, K.E.Biton, P.Reickmann, W.A.Jefferies, and McQuaid. 2010. Blood-brain barrier disruption and enhanced vascular permeability in the multiple sclerosis model EAE. *J Neuroimmunol* 229: 180-191.
5. Dussurget, O., J. Pizarro-Cerda, and P. Cossart. 2004. Molecular determinants of Listeria monocytogenes virulence. *Annual review of microbiology* 58: 587-610.
6. Masocha, W., and K. Kristensson. 2012. Passage of parasites across the blood-brain barrier. *Virulence* 3: 202-212.
7. Bonazzi, M., M. Lecuit, and P. Cossart. 2009. Listeria monocytogenes internalin and E-cadherin: from structure to pathogenesis. *Cellular microbiology* 11: 693-702.
8. Connolly, S. A., J. O. Jackson, T. S. Jardetzky, and R. Longnecker. 2011. Fusing structure and function: a structural view of the herpesvirus entry machinery.*Nature reviews. Microbiology* 9: 369-381.
9. Miller, F., H. Lecuyer, O. Join-Lambert, S. Bourdoulous, S. Marullo, X. Nassif, and M. Coureuil. 2012. Neisseria meningitidis colonization of the brain endothelium and cerebrospinal fluid invasion. *Cellular microbiology.*
10. Anderton, J. M., G. Rajam, S. Romero-Steiner, S. Summer, A. P. Kowalczyk, G. M. Carlone, J. S. Sampson, and E. W. Ades. 2007. E-cadherin is a receptor for the common protein pneumococcal surface adhesin A (PsaA) of Streptococcus pneumoniae. *Microbial pathogenesis* 42: 225-236.
11. Koppe, U., N. Suttorp, and B. Opitz. 2012. Recognition of Streptococcus pneumoniae by the innate immune system. *Cellular microbiology* 14: 460-466.
12. Arima, Y., M. Harada, D. Kamimura, J. H. Park, F. Kawano, F. E. Yull, T. Kawamoto, Y. Iwakura, U. A. Betz, G. Marquez, T. S. Blackwell, Y. Ohira, T. Hirano, and M. Murakami. 2012. Regional neural activation defines a gateway for autoreactive T cells to cross the blood-brain barrier. *Cell* 148: 447-457.

13. Mori, Y., M. Murakami, Y. Arima, D. Zhu, Y. Terayama, Y. Komai, Y. Nakatsuji, D. Kamimura, and Y. Yoshioka. 2014. Early pathological alterations of lower lumbar cords detected by ultrahigh-field MRI in a mouse multiple sclerosis model. *International immunology* 26: 93-101.

14. Atsumi, T., R. Singh, L. Sabharwal, H. Bando, J. Meng, Y. Arima, M. Yamada, M. Harada, J. J. Jiang, D. Kamimura, H. Ogura, T. Hirano, and M. Murakami. 2014. Inflammation amplifier, a new paradigm in cancer biology. *Cancer research* 74: 8-14.

15. Ogura, H., M. Murakami, Y. Okuyama, M. Tsuruoka, C. Kitabayashi, M. Kanamoto, M. Nishihara, Y. Iwakura, and T. Hirano. 2008. Interleukin-17 promotes autoimmunity by triggering a positive-feedback loop via interleukin-6 induction. *Immunity* 29: 628-636.

16. Murakami, M., Y. Okuyama, H. Ogura, S. Asano, Y. Arima, M. Tsuruoka, M. Harada, M. Kanamoto, Y. Sawa, Y. Iwakura, K. Takatsu, D. Kamimura, and T. Hirano.2011 Local microbleeding facilitates IL-6- and IL-17-dependent arthritis in the absence of tissue antigen recognition by activated T cells. *The Journal of experimental medicine* 208: 103-114.

17. Lee, J., T. Nakagiri, T. Oto, M. Harada, E. Morii, Y. Shintani, M. Inoue, Y. Iwakura, S. Miyoshi, M. Okumura, T. Hirano, and M. Murakami. 2012. IL-6 amplifier,NF-kappaB-triggered positive feedback for IL-6 signaling, in grafts is involved in allogeneic rejection responses.*Journal of immunology* 189: 1928-1936.

18. Atsumi, T., K. Ishihara, D. Kamimura, H.Ikushima, T. Ohtani, S. Hirota, H. Kobayashi, S. J. Park, Y. Saeki, Y. Kitamura, and T. Hirano. 2002. A point mutation of Tyr-759 in interleukin 6 family cytokine receptor subunit gp130 causes autoimmune arthritis. *The Journal of experimental medicine* 196: 979-990.

19. Lee, J., T. Nakagiri, D. Kamimura, M. Harada, T. Oto, Y. Susaki, Y. Shintani, M. Inoue, S. Miyoshi, E. Morii, T. Hirano, M. Murakami, and M. Okumura. 2013. IL-6 amplifier activation in epithelial regions of bronchi after allogeneic lung transplantation. *International immunology* 25: 319-332.

20. Murakami, M., M. Harada, D. Kamimura, H. Ogura, Y. Okuyama, N. Kumai, A. Okuyama, R. Singh, J. J. Jiang, T. Atsumi, S. Shiraya, Y. Nakatsuji, M. Kinoshita, H. Kohsaka, M. Nishida, S. Sakoda, N. Miyasaka, K. Yamauchi-Takihara, and T. Hirano.

2013. Disease-association analysis of an inflammation-related feedback loop. *Cell Rep* 3: 946-959.

21. Tracey, K. J. 2012. Immune cells exploit a neural circuit to enter the CNS. *Cell* 148: 392-394.
22. Andersson, U., and K. J. Tracey. 2012. Neural reflexes in inflammation and immunity. *The Journal of experimental medicine* 209: 1057-1068.
23. Deutschman, C. S., and K. J. Tracey. 2014. Sepsis: current dogma and new perspectives. *Immunity* 40: 463-475.
24. Ohira, Y., F. Kawano, J. L. Stevens, X. D. Wang, and A. Ishihara. 2004. Load-dependent regulation of neuromuscular system. *J Gravit Physiol* 11: P127-128.
25. Shen, J., H. Y. Wang, J. Y. Chen, and B. L. Liang. 2006. Morphologic analysis of normal human lumbar dorsal root ganglion by 3D MR imaging. *AJNR. American journal of neuroradiology* 27: 2098-2103.

Title: A novel regulatory mechanism for virus-induced activation of pattern recognition receptors

Akinori Takaoka

Division of Signaling in Cancer and Immunology, Institute for Genetic Medicine, Hokkaido University, Sapporo, Hokkaido, 060-0815

Introduction

Dioxins are found as persistent environmental organic pollutants throughout the world, which is a serious concern owing to its highly toxic potential. A number of studies have shown that these chemically related compounds can cause developmental, reproductive and endocrine problems, and are also potent tumor promoters and oncogenic substances. In addition, it has been reported that this group of compounds adversely affects the immune system including Treg cells and TH17 cell differentiation and that signaling pathways mediated by the aryl hydrocarbon receptor (AHR), which serves as a receptor of dioxins, have modulatory roles in immune cell development/maturation and inflammatory responses. The molecular mechanisms underlying the biological activity of dioxins, however, remain largely unexplored, particularly in the innate immune signalings mediated by pattern-recognition receptors (PRRs) during viral infection.

Materials and Methods

Cells, antibodies and reagents

HEK293T, A549 and HeLa cells were purchased from American Type Culture Collection and cultured in DMEM with 10% heat-inactivated fetal bovine serum (FBS). MonoMac6 cells were purchased from German Research Centre for Microorganisms and Cell Cultures and cultured in RPMI medium 1640 (Sigma) with 10% heat-inactivated FBS, OPI Media Supplement (Sigma) and non-essential amino acids (Sigma). Immortalized SCI5+/+ and SCI5-/- mouse embryonic fibroblasts (MEFs) were previously established and were grown in DMEM with 10 % heat-inactivated FBS. Antibodies were used as follows: anti-Flag (M2; Sigma), anti-hemagglutinin (5D8; MBL, 3F10; Roche), anti-IRF3 (IRF35I218-2; MBR, FL-425; Santa Cruz), anti-IRF3(pS396) (4D4G; Cell Signaling), anti-TBK1(EP611Y;Abcam),anti-TBK1(pS172) (D52C2; Cell Signaling, J133-1171; BD Pharmingen), anti-MAVS (ab25084; Abcam) and anti-β-actin (AC-15; Sigma). 3MC was purchased from SUPELCO or Toronto Research Chemical and BaP was from Sigma. TCDD dissolved in DMSO was kindly provided by H. Ariga. The 3pRNA and dsVACV 70 mer

Table S1. Sequences of primers used for qPCR

Species	Gene	Forward (5'→3')	Reverse (5'→3')
Human	*IFNA1*	GCCTCGCCCTTTGCTTTACT	CTGTGGGTCTCAGGGAGATCA
	IFNB	ATGACCAACAAGTGTCTCCTCC	GCTCATGGAAAGAGCTGTAGTG
	ACTB	CATGTACGTTGCTATCCAGGC	CTCCTTAATGTCACGCACGAT
Mouse	*Ifna1*	CTGAGCCAAAGTGTAGAGGACTC	TGAATTGAAAGAGAACAAGTGCC
	Ifnb	GAGCTCCAAGAAAGGACGAAC	GGCAGTGTAACTCTTCTGCAT
	Actb	AGTGTGACGTTGACATCCGTA	GCCAGAGCAGTAATCTCCTTCT

oligonucleotides were prepared as reported (10, 35). The poly(rI:rC) and c[G(2',5')pA(3',5')p] (cGAMP) were purchased from GE healthcare and Biolog, respectively. Cycloheximide (CHX) was purchased from Sigma. Lipofectamine 2000 (Invitrogen) was used for transfection of nucleic acid ligands into the cytoplasm. FuGENE6 (Roche) reagent was used for gene transfer with lipid transfection.

Plasmids and molecular cloning

The cDNAs for human SCI5, N-terminal RIG-I, MAVS and TBK1 were obtained by RT-PCR of total RNAs from HeLa, HEK293T cells or MEFs. The cDNA was then cloned into a pTA2 vector with the Target Clone-Plus-TA cloning kit (TOYOBO). For YFP-, Flag- and HA-tagged proteins, cDNA was cloned into the *Xho*I and *Not*I sites of the pCAGGS-YFP, pCXN2-Flag or pIRM-3HA vector. The nucleotide sequence of each cDNA was confirmed with the BigDye Terminator v3.1 sequencing kit (Applied Biosystems). The vectors pCAGGS and Venus (called 'YFP' here) were provided by J. Miyazaki and A. Miyawaki, respectively.

qRT-PCR analysis

Total RNAs were isolated from culture cells or mouse organs by using ISOGEN (Nippon Gene), and were treated with DNase I (Invitrogen). cDNAs were prepared from total RNAs using ReverTra Ace (TOYOBO). Quantitative PCR was performed using SYBR Premix Ex Taq (TAKARA) and analyzed on a StepOnePlus real-time PCR system (Applied

Biosystems). Detailed information about the primers used here is shown in table S1. Data were normalized to the expression levels of *ACTB/Actb* for each sample.

AHR ligands and their treatments

3MC (SUPELCO), BaP (Sigma) and TCDD (kindly provided by H. Ariga) were dissolved in DMSO. For qRT-PCR analysis, cells were pretreated with TCDD or BaP for 8 h, or 3MC for 6 h and subjected to further experiment. As a control, DMSO was used. For immunoblotting analysis, cells were treated with TCDD or 3MC at the same time with transfection, and cultured for 48 h.

3MC exposure and viral infection in vivo

C57BL/6NJcl mice were obtained from CLEA Japan. 3MC (Toronto Research Chemical) was dissolved in corn-oil (Sigma) to 10 mg/ml. Mice were exposed to 3MC (80 mg/kg body weight) by intraperitoneal injection. At 24 h after exposure to 3MC, mice were intraperitoneally infected with VSV (2×10^6 p.f.u. per mouse).

Viral infection in cells and measurement of viral titers

A549 cells were infected with FluV (strain A/Puerto Rico/8/34) (1 multiplicity of infection (m.o.i.)), NDV (40 hemagglutinating units (HAU) per 2×10^5 cells), VSV (0.1 m.o.i.), SeV (40 HAU per 2×10^5 cells) or HSV-1 (1 m.o.i.). *SCI5*$^{+/+}$ and *SCI5*$^{-/-}$ MEFs were infected with NDV (80 HAU per 2×10^5 cells), FluV (0.1 m.o.i.), VSV (0.1 m.o.i.), EMCV (1 m.o.i.) or HSV-1 (1 m.o.i.). Cells were infected for 1 h at 37 ˚C with FluV in serum-free MEM containing amino acids and trypsin or with NDV, VSV, SeV or HSV-1 in serum-free DMEM. Plaque-forming assay with Madin-Darby canine kidney cells was conduced to measure the titers of FluV. Vero cells were used for plaque-forming assay to determine the titers of VSV, EMCV and HSV-1.

Luciferase assay

HEK293T cells seeded on 24-well plates were cotransfected with 100 ng of p-125Luc luciferase reporter plasmid (provided by T. Fujita) together with 200 ng of the expression vectors (N-RIG-I, MAVS or TBK1) and/or 100 ng of SCI5 expression vector. Luciferase activity was measured with the Dual-Luciferase Reporter Assay system (Promega). The renilla luciferase reporter plasmid (10 ng) was used as an internal control.

Cycloheximide (CHX) treatment

2×10^5 cells of A549 cells were seeded on 24-well plates and pretreated with 10 μg /ml CHX in DMEM for 1 h.

siRNA-mediated gene silencing

Chemically synthesized 21-nucleotide

Table S2. siRNA sequences

Target gene	Sequence (5'→3')
AHR	CUACAGAUGCUUUGGUCUUTT
ARNT	CAGUUUCUGUGAAUAGGCUTT

siRNAs, including control siRNA (siPerfect Negative Control), were obtained from Sigma or Hokkaido system science (sequence information, table S2). Cells were transfected with 50 nM siRNA in 2.0 μl Lipofectamine 2000 or Lipofectamine RNAiMAX (Invitrogen), and 48 h later, the cells were used for further experiments.

Fluorescence analysis

HeLa cells transfected with 1.0 μg of the YFP-tagged SCI5 expression vector were stimulated with 3pRNA for 4 h. Endogenous TBK1 was visualized with anti-TBK1 antibody and the appropriate secondary antibody conjugated to Alexa Fluor 594 (Molecular Probes). Hoechst 33342 (Invitrogen) was used for the counterstaining of nuclei. The localization of SCI5 and TBK1 was examined with an IX-81S confocal microscope (Olympus).

Statistical analysis

Values are shown as mean ± s.d. Statistical significance between two samples was determined with the Student's *t*-test.

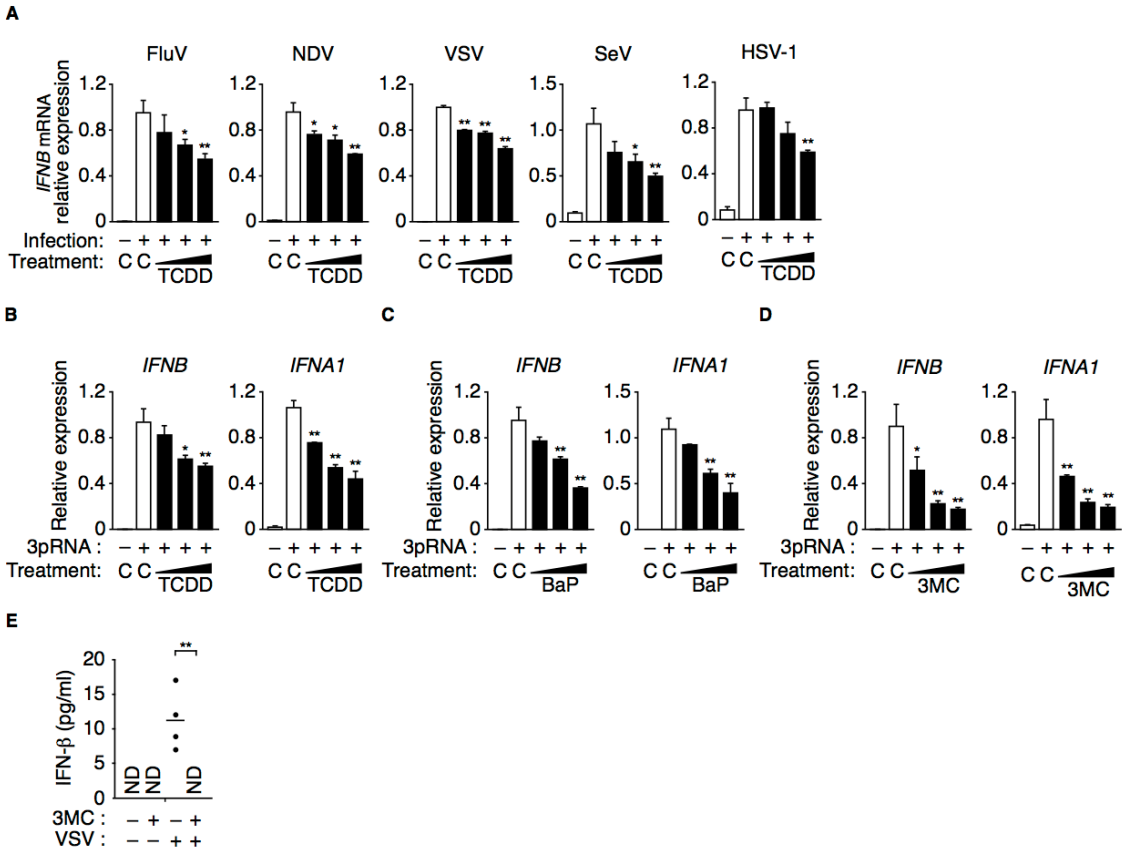

Fig. 1. Type I IFN response during viral infection is suppressed by TCDD and other AHR ligands. (A) A549 cells were pretreated with DMSO (C) or the increasing concentrations of TCDD (0.4, 2, and 10 nM) for 8 h, and then infected with the indicated viruses for 16 h. Induction of *IFNB* mRNA was measured by quantitative RT-PCR (qRT-PCR). **(B)** A549 cells were pretreated with DMSO (C) or TCDD as described in (A), and stimulated with 3pRNA (1 μg/ml) for 16 h. Induction of *IFNB* and *IFNA1* mRNAs was assessed by qRT-PCR. **(C)** MonoMac6 cells were treated with DMSO (C) or BaP (0.8, 4, and 20 μM) for 8 h, and stimulated with 3pRNA. The levels of *IFNB* and *IFNA1* mRNA were measured by qRT-PCR. **(D)** Induction of *IFNB* and *IFNA1* mRNAs by 3pRNA stimulation was evaluated by qRT-PCR in A549 cells pretreated with DMSO (C) or 3MC (0.04, 0.2, and 1 μM) for 6 h. **(E)** At 24 h after intraperitoneal injection with corn-oil or 3MC (80 mg/kg body weight), mice were intraperitoneally infected with VSV for 24 h. The levels of IFN-β in sera from these mice were measured by ELISA. The mean value is represented by a horizontal bar. Data are presented as mean and s.d. and are representative of at least two independent experiments. $*P < 0.05$ and $**P < 0.01$ as compared with control. $n = 3$ in (A to D), $n = 4$ in (E). ND, not detected.

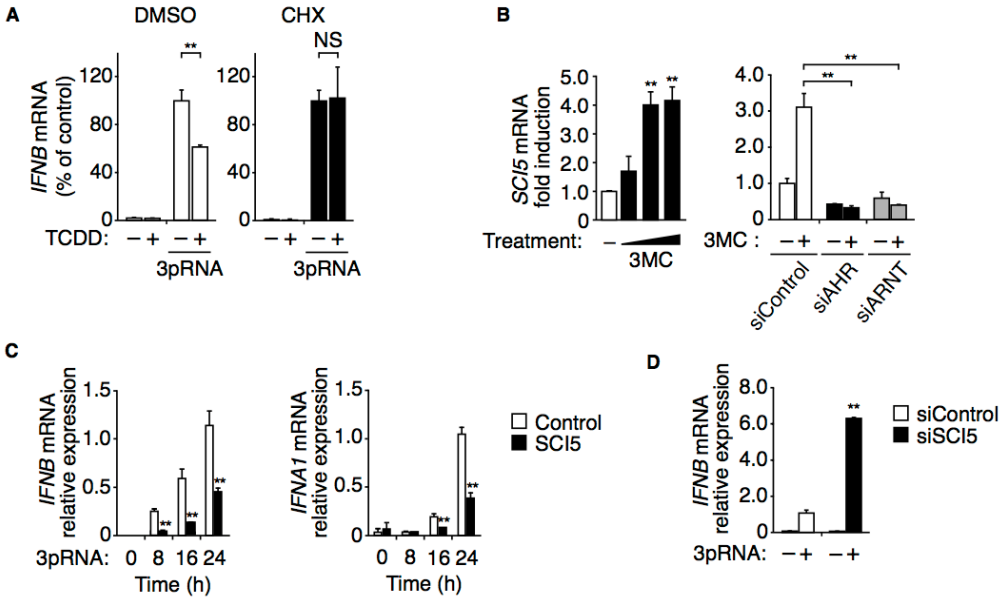

Fig. 2. SCI5 downregulates type I IFN response.

(A) Quantitative RT-PCR analysis of 3pRNA-induced *IFNB* mRNA expression in A549 cells pretreated with TCDD for 8 h in the absence (DMSO; left) or presence of cycloheximide (CHX; right). Data are shown as the percentage of control.

(B) Induction of *SCI5* mRNA was analyzed by qRT-PCR in A549 cells treated with DMSO (–) or 3MC (0.04, 0.2, and 1 μM) for 24 h (left). This was also evaluated in A549 cells treated with siRNAs for AHR or ARNT (right). (C) HEK293T cells expressing control plasmid (Control) or SCI5 were treated with 3pRNA for the indicated time periods, and then assayed for *IFNB* and *IFNA1* mRNA expression by qRT-PCR. (D) Quantitative RT-PCR analysis of *IFNB* mRNA induction by 3pRNA stimulation in HEK293T cells treated with siRNAs for control or SCI5 (siControl or siSCI5). Data are presented as mean and s.d. and are representative of at least two independent experiments. $*P < 0.05$ and $**P < 0.01$ as compared with control. $n = 3$.

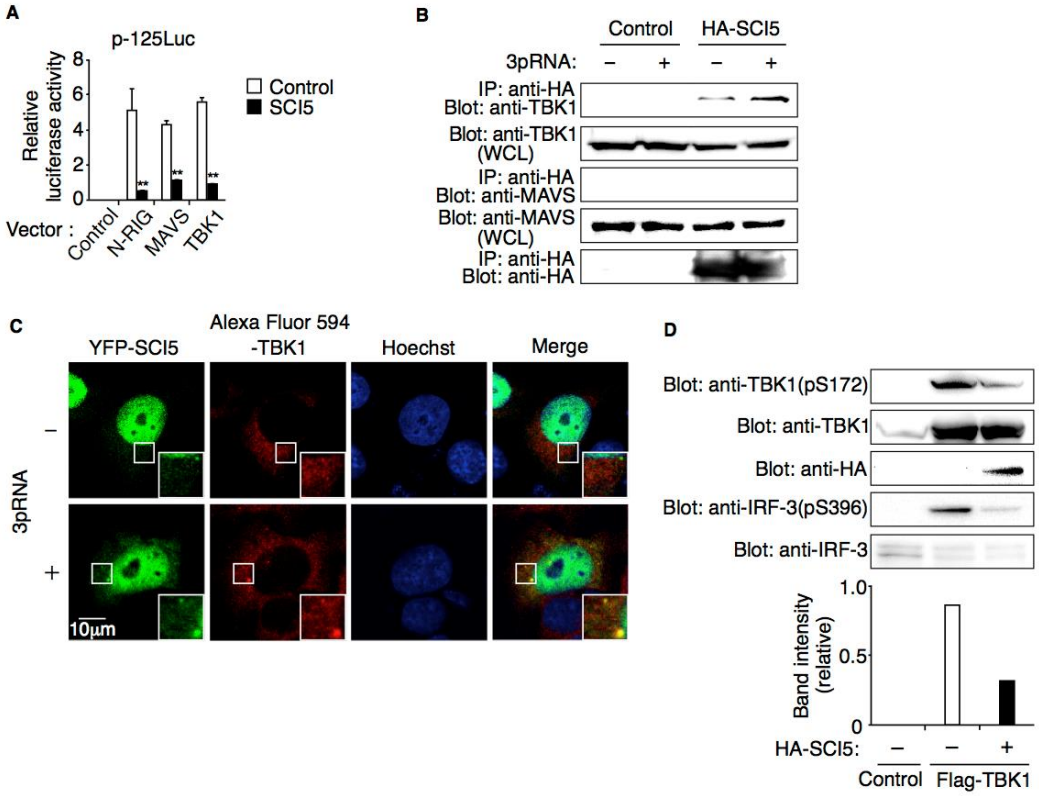

Fig. 3. SCI5 interferes with TBK1 activation. (A) Luciferase activity of a p-125Luc reporter plasmid in HEK293T cells transfected with the indicated expression vectors along with control or SCI5 expression vector. (B) After 48 h of transfection with control or HA-tagged SCI5 expression vector, HEK293T cells were stimulated with 3pRNA (10 μg/ml) for 4 h, and then were subjected to immunoprecipitation with anti-HA antibody, followed by immunoblotting with anti-TBK1, anti-MAVS or anti-HA antibody. Whole cell lysates (WCL) were also immunoblotted by anti-TBK1 or anti-MAVS. (C) Fluorescence confocal microscopy of HeLa cells transfected with YFP-tagged SCI5 and immunostained with anti-TBK1 (secondarily visualized with Alexa Fluor 594) following 3pRNA stimulation for 4 h. Nuclei were counterstained with Hoechst 33342. (E) HEK293T cells were transfected with control or Flag-tagged TBK1 along with HA-tagged SCI5, and the phosphorylation levels of TBK1-S172 and IRF-3-S396 were assessed by immunoblotting with anti-specific antibodies. Bottom, band intensities of the phosphorylated TBK1 (pS172) to that of total TBK1, quantified by a densitometer.

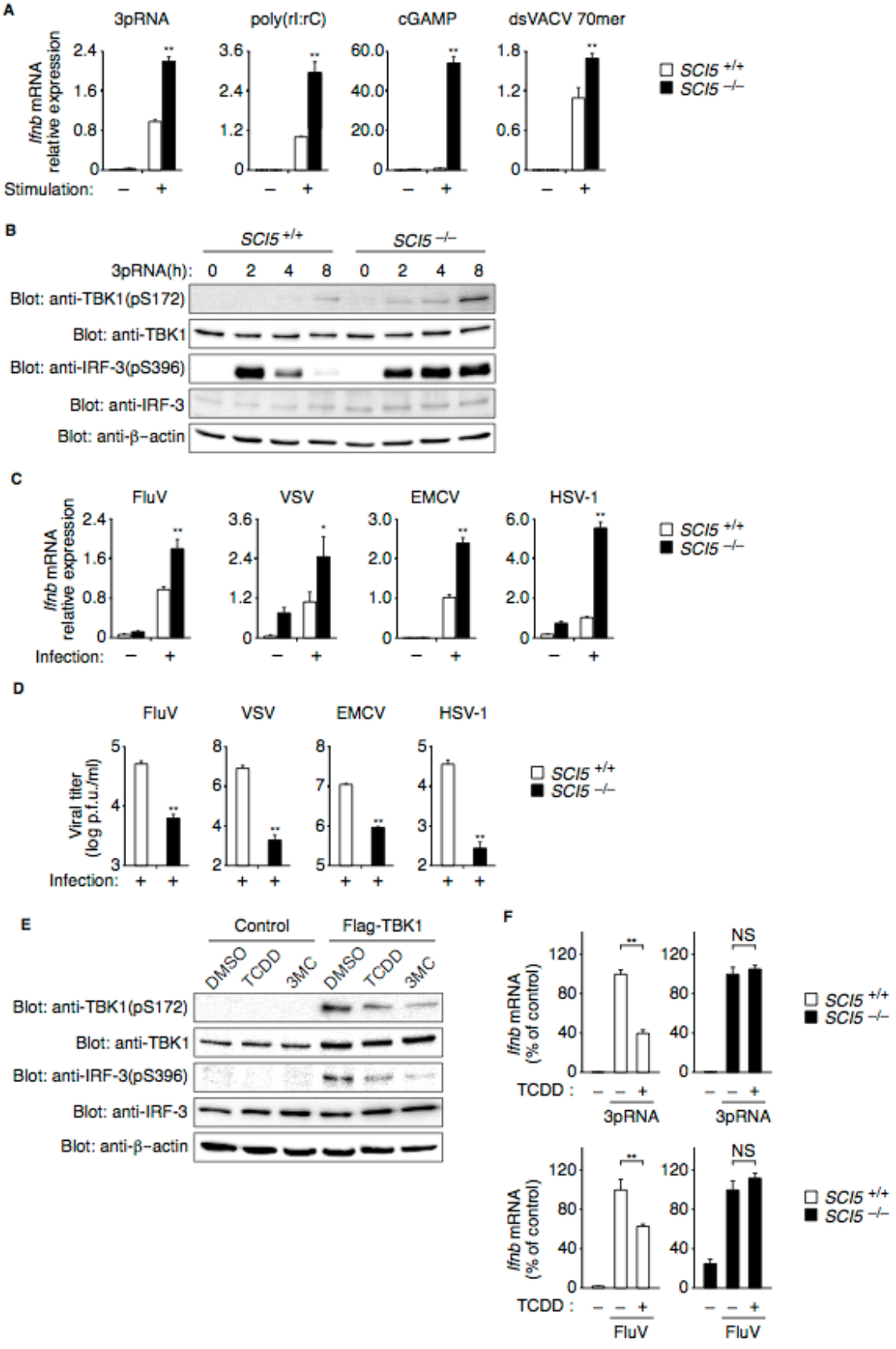
A
3pRNA
poly(rI:rC)
cGAMP
dsVACV 70mer
Ifnb mRNA relative expression
Stimulation:
SCI5 +/+
SCI5 −/−
B
SCI5 +/+
SCI5 −/−
3pRNA(h): 0 2 4 8 0 2 4 8
Blot: anti-TBK1(pS172)
Blot: anti-TBK1
Blot: anti-IRF-3(pS396)
Blot: anti-IRF-3
Blot: anti-β−actin
C
FluV
VSV
EMCV
HSV-1
Ifnb mRNA relative expression
Infection:
SCI5 +/+
SCI5 −/−
D
FluV
VSV
EMCV
HSV-1
Viral titer (log p.f.u./ml)
Infection:
SCI5 +/+
SCI5 −/−
E
Control
Flag-TBK1
DMSO
TCDD
3MC
DMSO
TCDD
3MC
Blot: anti-TBK1(pS172)
Blot: anti-TBK1
Blot: anti-IRF-3(pS396)
Blot: anti-IRF-3
Blot: anti-β−actin
F
Ifnb mRNA (% of control)
NS
TCDD :
3pRNA
3pRNA
FluV
FluV
SCI5 +/+
SCI5 −/−

Fig. 4. SCI5 is a key negative regulator of IFN response as well as an AHR target that abrogates antiviral responses. (A) Quantitative RT-PCR analysis of *Ifnb* mRNA induction in response to viral PAMPs in *SCI5*$^{+/+}$ or *SCI5*$^{-/-}$ MEFs. (B) 3pRNA-induced phosphorylation levels of TBK1 and IRF-3 in *SCI5*$^{+/+}$ or *SCI5*$^{-/-}$ MEFs were measured by immunoblotting with anti-specific antibodies. (C) Quantitative RT-PCR analysis of *Ifnb* mRNA induction by infection with the indicated viruses in *SCI5*$^{+/+}$ or *SCI5*$^{-/-}$ MEFs. (D) Plaque-forming assay of viral titers after 24 h of infection with the indicated viruses in *SCI5*$^{+/+}$ or *SCI5*$^{-/-}$ MEFs. (E) A549 cells were transfected with control or Flag-tagged TBK1 and treated with the indicated AHR ligands. At 24 h later, the phosphorylation levels of TBK1 and IRF-3 were assessed by immunoblotting with anti-specific antibodies. (F) Quantitative RT-PCR analysis of *Ifnb* mRNA induction by 3pRNA stimulation (top) or by FluV infection (bottom) in *SCI5*$^{+/+}$ or *SCI5*$^{-/-}$ MEFs with or without pretreatment with TCDD. Data are shown as the percentage of control. Data are presented as mean and s.d. and are representative of at least two independent experiments. $^{**}P < 0.01$ as compared with the wild-type MEFs. $n = 3$ in (A, C, D, and F). NS, not significant. ND, not detected.

Results

We first found that IFN-β mRNA induction in response to infection with RNA/DNA viruses, including influenza virus (FluV), Newcastle disease virus (NDV), vesicular stomatitis virus (VSV), Sendai virus (SeV) and herpes simplex virus-1 (HSV-1) was significantly suppressed following pretreatment with 2,3,7,8-tetrachrolodibenzo-p-dioxin (TCDD) in a dose-dependent manner (Fig. 1A). Since viral RNAs, which are derived from the first four types of viruses mentioned above, are sensed by RIG-I to induce the type I IFN response, we next examined the effect of TCDD on RIG-I activation by stimulation with 5'-triphosphate RNA (3pRNA), a synthetic RIG-I ligand. Treatment with TCDD resulted in a remarkable dose-dependent suppression of both IFN-β and -α1 mRNA inductions (Fig. 1B). A similar result was obtained upon pretreatment with two other AHR ligands, benzo[a]pyrene (BaP) and 3-methylcholanthrene (3MC) (Fig. 1, C and D). Additionally, the intraperitoneal pretreatment with 3MC in C57BL/6 mice resulted in a marked reduction in the protein levels of IFN-β 24 h after VSV infection (Fig. 1E). These results indicate that TCDD, BaP and 3MC, which are environmental toxins that activate AHR-mediated signalings likely adversely affect type I IFN induction by virus infection.

To clarify whether this suppressive effect is directly or indirectly mediated through dioxin-triggered activation of AHR signaling, we used cycloheximide (CHX) as a protein synthesis inhibitor. As a result, we found that TCDD failed to suppress 3pRNA-induced IFN-β mRNA induction (Fig. 2A), suggesting that this AHR ligand negatively regulates the

IFN response possibly via its induction of some target gene(s) of AHR signaling. AHR functions as a ligand-binding transcriptional factor in concert with the AHR nuclear translocator (ARNT), and this AHR-ARNT heterodimer binds to specific xenobiotic-responsive elements (XREs) found in the promoter of target genes, which thus induces the expression of a typical set of AHR target genes including *CYP1A1*, *CYP1A2*, *CYP1B1* and *SCI5*. Among these AHR-inducible genes, we focused on *SCI5*. Actually, we observed the upregulation of SCI5 mRNA in A549 cells after treatment with AHR ligands, which was dependent on both AHR and ARNT (Fig. 2B). To next examine the functional role of SCI5 in the 3pRNA-induced type I IFN pathway, we exogenously expressed SCI5 in HEK293T cells, resulting in a remarkable suppression of the 3pRNA-induced activation of both IFN-β and -α 1 mRNA expressions (Fig. 2C). On the other hand, IFN-β induction following 3pRNA treatment was strongly upregulated by knockdown of SCI5 expression in HEK293T (Fig. 2D). These results indicate that SCI5, which is inducible by dioxins, may negatively regulate nucleic-acid-sensor-mediated innate signaling pathways for type I IFN induction, suggesting that SCI5 is a candidate target of the AHR signaling pathway for the dioxin-mediated suppression of the IFN response. Activation of IFN-β gene by overexpression of not only N-terminal RIG-I and its adaptor MAVS/IPS-1/Cardif but also the downstream IRF-3 kinase TBK1 was markedly suppressed in SCI5-expressing HEK293T cells (Fig. 3A). Therefore, we focused on the involvement of SCI5 in TBK1 activation to further determine the molecular mechanism underlying the SCI5-involved regulation of nucleic-acid-triggered signalings. In this respect, the interaction of endogenous TBK1 but not MAVS with HA-tagged SCI5 was enhanced 4 h after 3pRNA stimulation (Fig. 3B). This was also confirmed by confocal microscopic analysis, showing that YFP-tagged SCI5 colocalized with endogenous TBK1 in the perinuclear region in a ligand-dependent manner (Fig. 3C). These results suggest that SCI5 may interact with TBK1 to regulate its activity. We next determined whether SCI5 regulates the autophosphorylation of TBK1 at the serine 172 residue (S172), which is crucial for its activation. Exogenous expression of SCI5 impaired the phosphorylation of TBK1-S172, which was supported by the finding that the phosphorylation (S396) of IRF-3 was significantly suppressed (Fig. 3D). These data suggest that SCI5 modifies TBK1 activity, resulting in the suppression of IRF-3-mediated type I IFN induction.

To show that SCI5 plays a critical role in the modulation of nucleic acid-triggered type I IFN expression, we evaluated the effect of SCI5 deficiency on the IFN response to various types of ligand for nucleic acid sensors. In this study, we used SCI5-deficient mouse embryonic fibroblasts (*SCI5*$^{-/-}$ MEFs). As shown in Fig. 4A, the induction of both type I IFN mRNAs and their proteins was

considerably upregulated in *SCI5*$^{-/-}$ MEFs upon stimulation with all of the nucleic acid ligands tested, as compared with the WT MEFs. Time-course analysis showed that both TBK1-S172 and IRF-3-S396 were phosphorylated after 3pRNA stimulation in WT MEFs, whereas the phosphorylation levels of these residues were significantly higher and more persistent in *SCI5*$^{-/-}$ MEFs (Fig. 4B), suggesting that SCI5 negatively regulates the TBK1-IRF-3 pathway for type I IFN gene induction. Consistent with these results, the IFN-β response was remarkably enhanced in *SCI5*$^{-/-}$ MEFs, as compared with WT MEFs, following infection with various types of virus including NDV, FluV, VSV, EMCV, and HSV-1 (Fig. 4C), which activate RIG-I (NDV, FluV, VSV), MDA5 (EMCV), and cGAS (HSV-1) (8, 21). These findings are in line with the observation that viral titers at 24-h postinfection with any of these viruses in *SCI5*$^{-/-}$ MEFs were much lower than those in WT MEFs (Fig. 4D). Taken together, these findings indicate that SCI5 functions as a critical regulator to suppress the nucleic-acid-sensor-activated IFN antiviral response to infection with a wide range of viruses, at least through the blockade of the TBK1-IRF-3 pathway.

As for the inhibitory effect of AHR ligands on the type I IFN pathway against viral infection (Fig. 1), the serine phosphorylation levels of both TBK1 and IRF-3 in A549 cells were significantly diminished in response to treatment with TCDD and 3MC (Fig. 4E). In accordance to the above findings for *SCI5*$^{-/-}$ MEFs, TCDD-induced suppression of IFN-β mRNA expression could not be observed in *SCI5*$^{-/-}$ MEFs (Fig. 4F). Thus, AHR ligands can dampen the activation of the nucleic-acid-senor-mediated IFN pathway during viral infection possibly by inducing a negative regulator(s) such as SCI5 and modifying the TBK1 activity to phosphorylate IRF-3.

Discussion

In this study, we first demonstrated that exposure to AHR agonists such as TCDD affects antiviral innate immune defense, and identified SCI5 as a possible target induced by AHR-mediated signaling, which was found to be responsible for the innate immune-suppression induced by these chemicals. Further detailed analyses revealed that SCI5 functions as a critical regulator that suppresses the TBK1-mediated pathway, a cardinal pathway for IFN induction. TBK1 has also been reported to be involved in other signaling pathways, such as PDGF-mediated signalings, autophagy, anti-apoptosis and oncogenesis. Moreover, TBK1 has been shown to be a target for immune evasion by several viruses such as hepatitis C virus, vaccinia virus, poxvirus and foot-and-mouth disease virus, to circumvent the IFN responses. The present study addresses the next interesting issue about the role of SCI5 in the modulation of TBK1 activity in these processes, and manipulating the SCI5 activity would be

useful in developing therapeutic interventions to control viral infection, innate inflammation, and possibly other diseases. Given the regulatory role of SCI5 in the virus-induced IFN pathway, we consider that this SCI5-mediated regulatory process in innate immune signalings may be disturbed following exposure to xenobiotic AHR ligands, resulting in the downregulation of the innate IFN response to viral infection. This might be supported in part by several previous reports showing that TCDD exposure leads to enhanced mortality and susceptibility to FluV, wherein it has been assumed that this may be caused by the immunotoxic effects of dioxins mainly on the adaptive immunity. Therefore, our findings has advanced our understanding of the molecular mechanism, whereby xenobiotic-mediated activation of AHR signaling leads to immunosuppression in the innate immunity. In addition, this study may also provide a novel linkage between AHR-mediated xenobiotic signaling and nucleic-acid-sensor-mediated innate signaling, which is dependent on SCI5. Further investigation will be needed to elucidate the effect of dioxin-induced modulation of innate immune function on other aspects, such as tumor progression or oncogenesis, the relevance of AHR signaling induced by endogenous ligands, such as the tryptophan metabolites 6-formylindolo[3,2-b]carbazole (FICZ) and kynurenine, and how these would impact human health and the burden of diseases.

Conclusion

Xenobiotic-induced SCI5 abrogates nucleic acid sensor-mediated IFN response against viral infection through modifying of TBK1.

The C-terminal domain of glyceraldehyde 3-phosphate dehydrogenase plays an important role in suppression of tRNALys3 packaging into human immunodeficiency virus type-1 particles

Naoki Kishimoto[a], Ayano Onitsuka-Kishimoto[a], Nozomi Iga[a], Nobutoki Takamune[b], Shozo Shoji[a], Shogo Misumi[a],

[a] *Department of Environmental and Molecular Health Sciences, Faculty of Medical and Pharmaceutical Sciences, Kumamoto University, Kumamoto 8620973, Japan*

[b] *Innovative Collaboration Organization, Kumamoto University, Kumamoto 860-8555, Japan*

ABSTRACT

Human immunodeficiency virus type-1 (HIV-1) requires the packaging of human $tRNA^{Lys3}$ as a primer for effective viral reverse transcription. Previously, we reported that glyceraldehyde 3-phosphate dehydrogenase (GAPDH) suppresses the packaging efficiency of $tRNA^{Lys3}$. Although the binding of GAPDH to $Pr55^{gag}$ is important for the suppression mechanism, it remains unclear which domain of GAPDH is responsible for the interaction with $Pr55^{gag}$. In this study, we show that Asp^{256}, Lys^{260}, Lys^{263} and Glu^{267} of GAPDH are important for the suppression of $tRNA^{Lys3}$ packaging. Yeast two-hybrid analysis demonstrated that the C-terminal domain of GAPDH (151–335) interacts with both the matrix region (MA; 1–132) and capsid N-terminal domain (CANTD; 133–282). The D256R, K263E or E267R mutation of GAPDH led to the loss of the ability to bind to wildtype (WT) MA, and the D256R/K260E double mutation of GAPDH resulted in the loss of detectable binding activity to WT CA-NTD. In contrast, R58E, Q59A or Q63A of MA, and E76R or R82E of CA-NTD abrogated the interaction with the C-terminal domain of GAPDH. Multiple-substituted GAPDH mutant (D256R/K260E/ K263E/E267R) retained the oligomeric formation with WT GAPDH in HIV-1 producing cells, but the incorporation level of the hetero-oligomer was decreased in viral particles. Furthermore, the viruses produced from cells expressing the D256R/K260E/K263E/E267R mutant restored $tRNA^{Lys3}$ packaging efficiency because the mutant exerted a dominant negative effect by preventing WT GAPDH from binding to MA and CA-NTD and improved the reverse transcription. These findings indicate that the amino acids Asp^{256}, Lys^{260}, Lys^{263} and Glu^{267} of GAPDH is essential for the mechanism of $tRNA^{Lys3}$-packaging suppression and the D256R/K260E/ K263E/E267R mutant of GAPDH acts in a dominant negative manner to suppress $tRNA^{Lys3}$ packaging.

1. Introduction

It has recently been shown that cellular proteins regulate HIV-1 replication. Interestingly, several studies of purified HIV-1 virions have shown that, in addition to proteins encoded by the virus, cellular proteins are taken into the virions [1]. Some of these proteins, such as cyclophilin A and lysyl-tRNA synthetase (LysRS), are packaged into virions as a result of their interaction with $Pr55^{gag}$ or $p160^{gag\text{-}pol}$ proteins during assembly [2–5]. These cellular proteins play an important role in viral precursor protein folding and $tRNA^{Lys3}$ packaging. Thus, understanding the packaging mechanism of cellular proteins is one way to elucidate the viral replication capacity.

One of the critical events in HIV-1 replication is reverse transcription. Cellular $tRNA^{Lys3}$ is required for the efficient initiation of reverse transcription and is selectively incorporated into viral particles during its assembly because the 3′ terminal 18 nucleotides must be hybridized to the primer-binding site of HIV-1 genome RNA as a replication primer [6]. Gabor et al. [7] reported that the elevated amount of packaged $tRNA^{Lys3}$ increases viral infectivity. Efficient packaging of $tRNA^{Lys3}$ is facilitated by interaction between $Pr55^{gag}$ or $p160^{gag\text{-}pol}$ and LysRS, which act as carriers of $tRNA^{Lys3}$ [8,9].

Although GAPDH was initially identified as a glycolytic enzyme, it has been known as a "moonlighting" protein. Several studies have shown that GAPDH is related to apoptosis, the exportation of nuclear RNA, and DNA repair. [10]. Furthermore, GAPDH regulates viral replication by binding to *cis*-acting viral RNAs, such as the hepatitis A virus, hepatitis C virus and human parainfluenza virus [11–13]. Similarly, we previously reported that GAPDH also plays a role in negatively regulating HIV-1 infection [14]. GAPDH is incorporated into virions via its interaction with $Pr55^{gag}$ [14]. Increased GAPDH packaging efficiency decreases reverse transcription efficiency owing to the suppression of LysRS and $tRNA^{Lys3}$ packaging [14]. Thus, the binding of GAPDH to $Pr55^{gag}$ has an important role in the suppression of HIV-1 replication. These findings indicate that GAPDH negatively regulates HIV-1 replication and provide insights into a new host defense mechanism against HIV-1 infection. However, it is remains unclear which amino acid residues of GAPDH are important for the recognition of $Pr55^{gag}$.

In this study, we show that amino acids Asp^{256}, Lys^{260}, Lys^{263} and Glu^{267} of GAPDH interact with MA and CA-NTD domain of $Pr55^{gag}$ and the D256R/K260E/K263E/E267R mutant of GAPDH acts as a dominant negative inhibitor of $tRNA^{Lys3}$ packaging. These findings provide a new insight into $tRNA^{Lys3}$ packaging mechanism and indicate a novel regulatory step of HIV-1 replication.

2. Materials and methods

2.1. Cell culture

TZM-bl cells, which were obtained from

the NIH AIDS Research and Reference Reagent Program, and HEK293 cells were maintained at 37 °C in DMEM supplemented with 10% fetal calf serum (FCS) containing 100 IU/ml penicillin and 100 μg/ml streptomycin in 5% CO2.

2.2. Viruses

The infectious molecular clone pNL-CH [15], derived from the pNL4-3 clone of HIV-1, and each mutated GAPDH expression vector (cloned into the pcDNA3.1D/V5-His-TOPO® vector) were cotransfected into HEK293 cells to prepare various GAPDH-mutant-packaging viruses. At 48 h post-cotransfection, the virus-containing supernatant was collected and clarified by filtration using 0.45-μm-pore-size filters [14].

2.3. Plasmid

The coding region of the HIV-1_{NL-CH} protein and GAPDH was amplified by PCR using the following primers. $Pr55^{gag}$: $Pr55^{gag}$ UP(5-AGAATTCATGGGTGCGAGAGCGTCGGTATTA-3) and $Pr55^{gag}$ DN (5-TGGATCCTTATTGTGACGA-GGGGTCGCTGCC-3′); MA: $Pr55^{gag}$ UP and MA DN (5′ -TGGATCCTTAGTAATTTTGGC-TGACCTG-3′); CA: CA UP (5′ -AGAATTCC-CTATAGTGCAGAACCTCCAG-3′) and CA DN (5-TGGATCCTTACAAAACTCTTGCTTT-ATGGCC-3′); CA-NTD: CA UP and CA-NT-D DN (5′ -TGGATCCTTAAATGCTGGTAGG-GC-TATACAT-3′); CACTD: CA-CTD UP (5′ -AGAATTCCTGGACATAAGACAAGGACCA-3′) and CA DN; NC: NC UP (5′ -AGAATTCA-TACAGAAAGGCAATTTTAGG-3′) and NC DN (5′ -TGGATCCTTAATTAGCCTGTCTCT-CAGTACA-3′); p6: p6 UP (5′ -AGAATTCCT-TCAGAGCAGACCAGAGCCA-3′) and $Pr55^{gag}$ DN; $p160^{gag-pol}$: $p160^{gag-pol}$ UP (5′ -ACTAGTCATATGGATGAATTCATGGGTGC-GAGAGCGTCGGTATTA-3′) and $p160^{gag-pol}$ DN (5′ -ACCCGGGGATCCGATGGATCCTT-AATCCTCATCCTGTCTACTTGC-3′); Pol: Pol UP (5′ -GGAGGCCAGTGAATTCCCTCA-GATCACTCTTTGGCAG-3′) and $p160^{gag-pol}$ DN; GAPDH: GAPDH UP (5′ -AGAATTCAT-GGGGAAGGTGAAGGTCGGAGTCAAC-3′) and GAPDH DN (5′ -TGGATCCTTACTCCT-TGGAGGCCATGTGGGC-3′); GAPDH-n: GAPDH UP and GAPDH-n DN (5′ -TGGATC-CTTAGCAGGAGGCATTGCTGAT-3′); GAP DH-c: GAPDH-c UP (5′ -AGAATTCTCCTGC-ACCACCAACTGCTTA-3′) and GAPDH DN. For the yeast-two-hybrid (Y2H) analysis, the HIV-1 protein or GAPDH coding regions were cloned into the *Eco*RI and *Bam*HI sites of pGBKT7 or pGADT7, respectively (Clontech Laboratories, Inc.). The fulllength GAPDH coding regions were also cloned into the *Eco*RV and *Bam*HI sites of the pcDNA™ 3.1D/V5-His-TOPO® vector (Thermo Fisher Scientific, Inc.). Each mutated GAPDH construct was obtained by sitedirected mutagenesis. All of the mutations were verified by sequencing.

2.4. Yeast two-hybrid analysis

The Matchmaker™ Gold Yeast Two-hybrid

System (Clontech Laboratories, Inc.) was used in accordance with manufacturer's recommendations to analyze the interaction between several reconstructed GAPDH and HIV-1 proteins. Briefly, the bait (cloned into pGBKT7) and prey (cloned into pGADT7) constructs were cotransformed into Y2HGold and plated on QDO/X/A plates (without tryptophan leucine, adenine, and histidine and with aureobasidin A and X-α-Gal). As a positive or negative control, pGADT7-T and pGBKT7-53 or pGADT7 AD and pGBKT7 DNA-BD were cotransformed, respectively. To validate transformed protein expression, each yeast strain was lysed and detected using an anti-HA antibody (Wako Pure Chemical Industries, Ltd.) or an anti-c-Myc antibody (Clontech Laboratories, Inc.).

2.5. Coimmunoprecipitation

HEK293 cells transfected with each GAPDH expression vector were lysed and the lysate was used for coimmunoprecipitation, as a previously described [14]. Briefly, the precleaned lysate was incubated with an anti-V5 antibody (Thermo Fisher Scientific Inc.) or an isotype control mouse IgG antibody (R&D SYSTEMS, Inc.), and further incubated with μMACS™ Protein G MicroBeads (Miltenyi Biotec K.K.). The separated proteins were detected by western immunoblot analysis using the anti-GAPDH antibody (Santa Cruz Biotechnology, Inc.). To detect GAPDH interacting $Pr55^{gag}$, pNL-CH and WT or M6 GAPDH expression vector were cotransfected into HEK293 and the resulting lysate was incubated with an anti-GAPDH antibody before incubating with μMACS™ Protein G MicroBeads.

2.6. Measurement of $tRNA^{Lys3}$ packaging levels in virions and reverse transcription products

$tRNA^{Lys3}$ was prepared from various GAPDH mutants packaging viruses, as a previously described [14]. Briefly, $tRNA^{Lys3}$ was collected from each virus and reverse-transcribed using a SuperScript™ III Firststrand Synthesis System (Thermo Fisher Scientific, Inc.). The packaging level of $tRNA^{Lys3}$ was normalized by incorporated viral genomic RNA. The reverse transcription products were analyzed using previously described methods [14]. Total DNA from each virus infected TZM-bl cells was subjected to quantitative real-time PCR with primer pair specific for the R/U5 (early) region.

3. Results

3.1. C-terminal domain of GAPDH interacts with HIV-1 MA and CA

We previously demonstrated that GAPDH, which is expressed in HIV-1 producer cells, is incorporated into viral particles via its

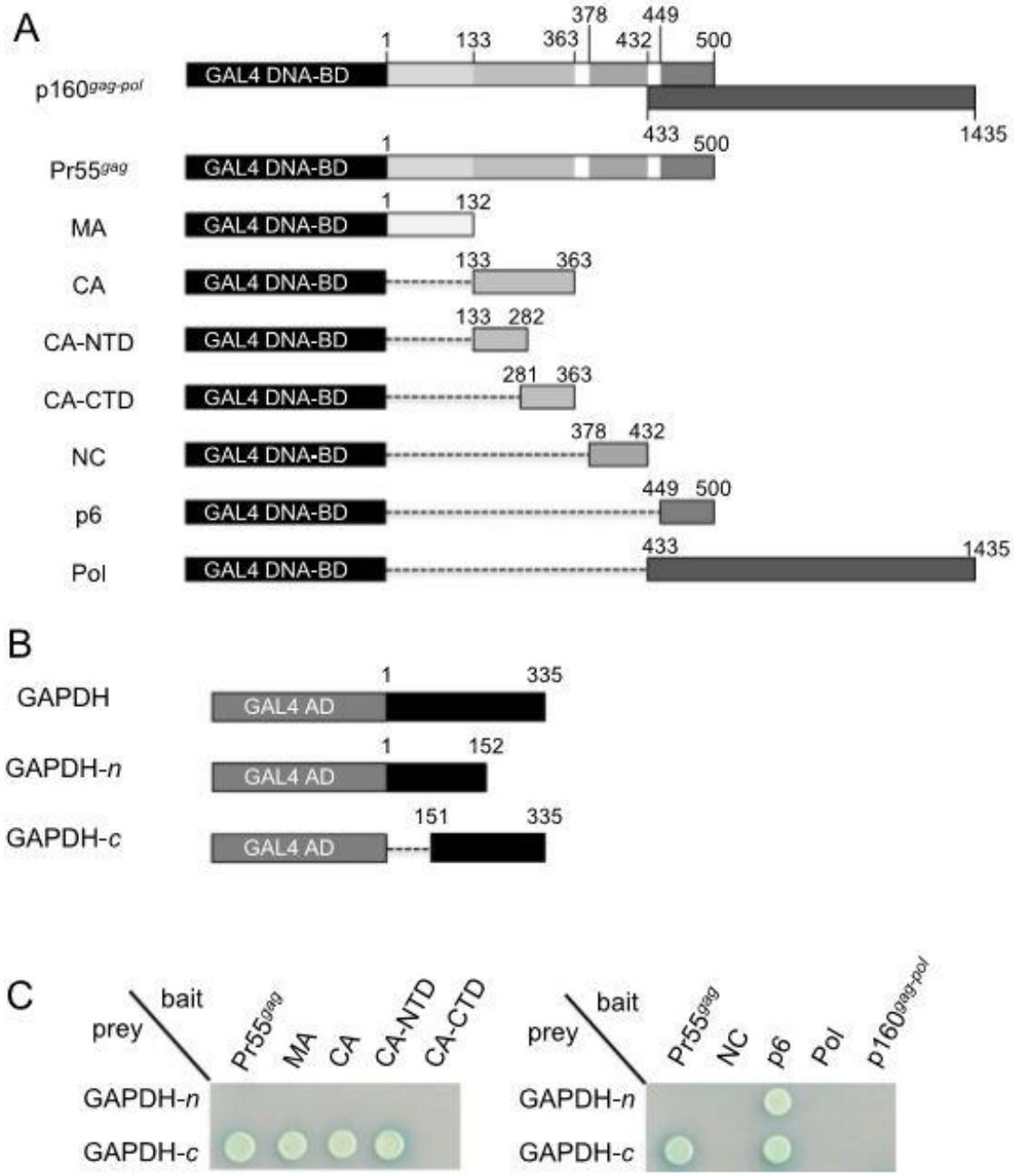

Fig. 1. *Y2H analysis of interaction between GAPDH and HIV-1 precursor proteins*. (A) Bait constructs obtained from pNL-CH and (B) prey constructs obtained from human GAPDH are illustrated. (C) Y2H analysis of N-terminal domain of GAPDH (GAPDH-n) orC-terminal domain of GAPDH (GAPDH-c) with p160$^{gag\text{-}pol}$, Pr55^{gag}, MA, CA, CA-NTD, CA-CTD, NC, p6 or Pol. The Y2HGold strain was cotransformed with the constructs-expressing bait (as indicated in Fig. 1A) and prey proteins (as indicated in Fig. 1B). Growth on QDO/X/A plates indicates the positive interaction.

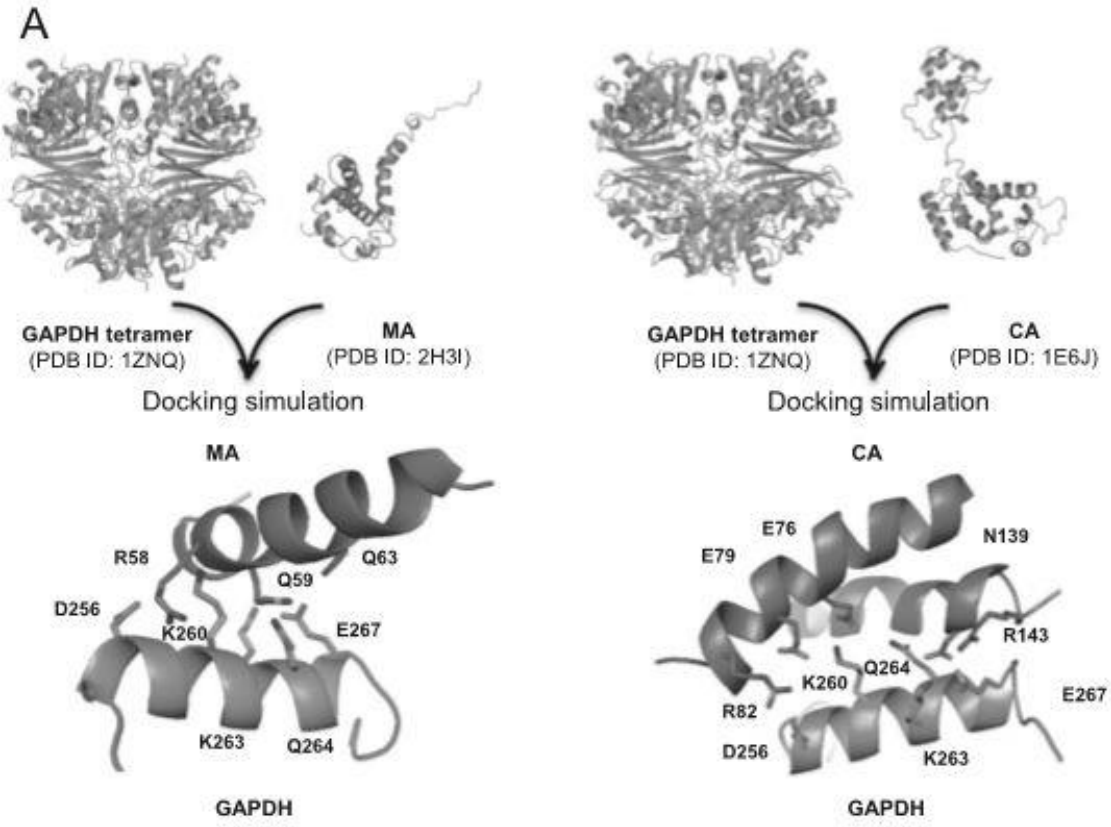

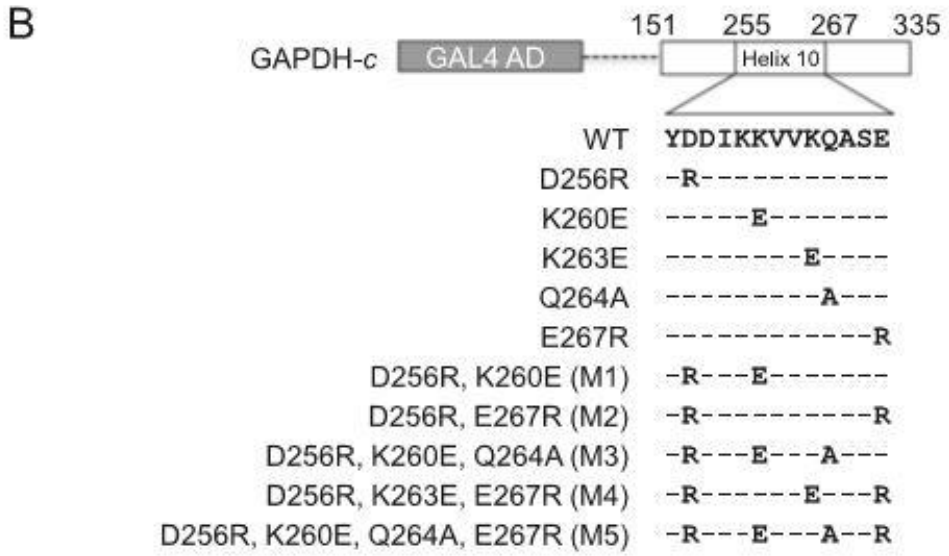

Fig. 2. *Deduced interaction between GAPDH and MA or CA.* (A) Proposed models for the interaction of GAPDH with MA (left) or CA (right). (B) GAPDH constructs mutated in GAPDH-c in Y2H analysis.

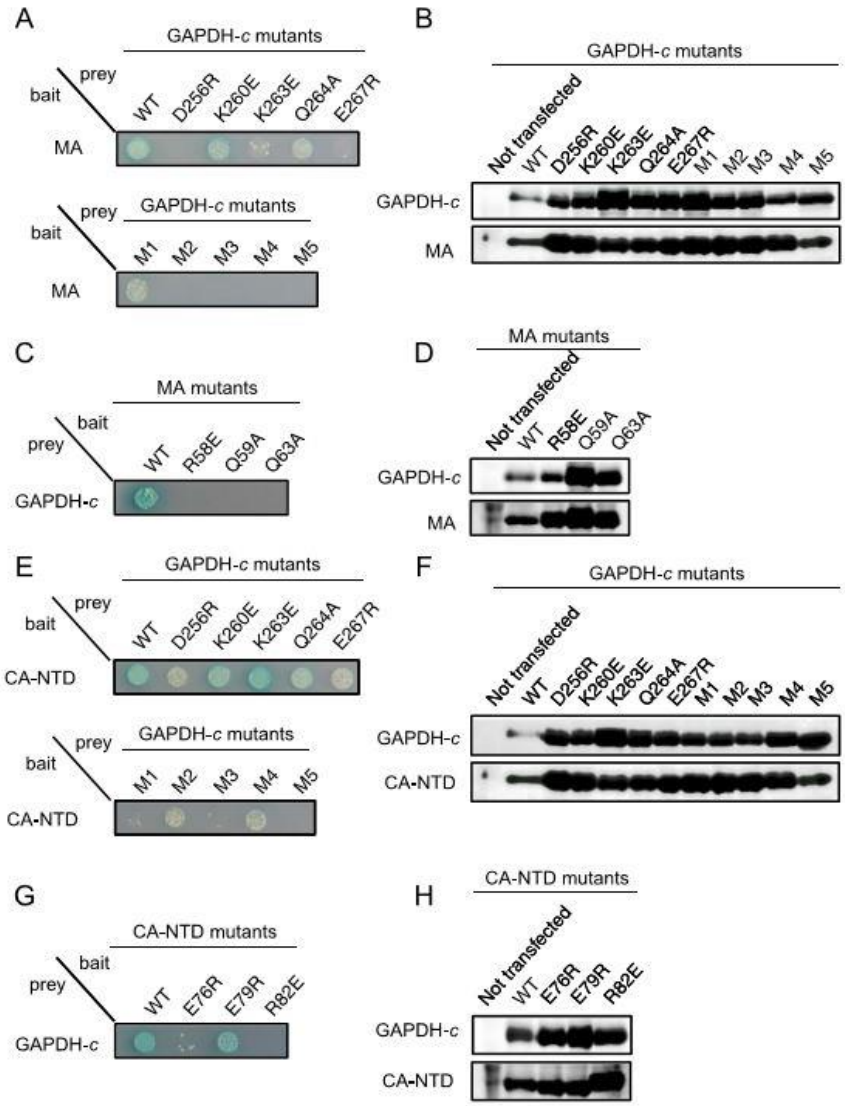

Fig. 3. *Y2H analysis of the interaction between C-terminal domain of GAPDH (GAPDH-c) and MA or CA-NTD.* (A) The C-terminal domain of WT or GAPDH mutants was used as prey proteins, and WT MA was used as the bait protein. (B) Bait and prey proteins expression level in Y2HGold strain using Fig. 3A. (C) WT or MA mutants were used as bait proteins, and WT GAPDH-c was used as the prey protein. (D) Bait and prey proteins expression level in Y2HGold strain using Fig. 3C. (E) The C-terminal domain of WT or GAPDH mutants was used as prey proteins, and WT CA-NTD was used as the bait protein. (F) Bait and prey proteins expression level in Y2HGold strain using Fig. 3E. (G) WT or CA-NTD mutants were used as bait proteins, and WT GAPDH-c was used as the prey protein. (H) Bait and prey proteins expression level in Y2HGold strain using Fig. 3G. Western immunoblot analysis of total protein extracts from each transformed Y2HGold strain was performed using the anti-HA antibody (against prey proteins) and the anti-c-Myc antibody (against bait proteins), respectively.

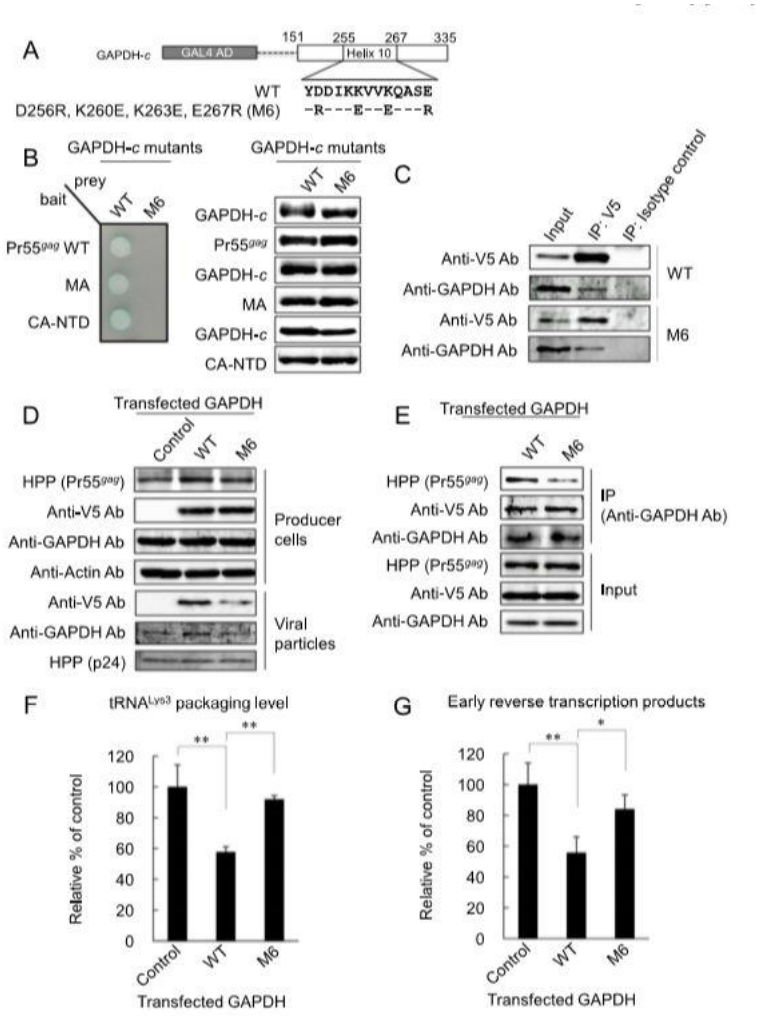

Fig. 4. *Effect of mutations of Asp^{256}, Lys^{260}, Lys^{263} and Glu^{267} in GAPDH on HIV-1 replication.* (A) To validate the critical residues of GAPDH, D256R/K260E/K263E/E267R mutation (M6) was introduced in GAPDH. (B) Y2H analysis of interaction between M6 GAPDH and MA or CA-NTD. The M6 GAPDH prey and MA or CA-NTD bait vector were cotransfected into Y2HGold. M6 GAPDH abrogated the GAPDH interaction with MA and CA-NTD (left panel), although each protein was expressed (right panel). (C) Coimmunoprecipitation assay of endogenous and exogenous GAPDH (V5-tagged WT or M6 GAPDH). (D) GAPDH expression in HIV-1 producer cells and incorporation level of GAPDH in viral particles. V5-tagged WT or M6 GAPDH was used to distinguish between endogenous and exogenous GAPDH. HEK293 cells were cotransfected with pNL-CH and V5tagged WT, M6 GAPDH or empty (indicated as control) expression vector. Pr55^{gag} and p24 were detected by HIV-1-positive plasma (HPP). (E) Coimmunoprecipitation assay of GAPDH and Pr55^{gag}. (F) Packaging level of tRNA^{Lys3}. The amount of tRNA^{Lys3} in the control virus was set as 100%. (G) Effects of each virus that is produced from cells transfected with WT or M6 GAPDH vector on early reverse transcription products in TZM-bl cells. The value in the control experiment was set as a 100%. The significance of difference (Nonrepeated measures ANOVA and Dunnett's test versus WT) is indicated as follows: **, $p<0.01$; *, $p<0.05$. The error bars denote the standard deviation. The mean values of at least three independent experiments are shown.

interaction with viral precursor proteins [14]. To further investigate which domain is required for the interactions, we prepared viral proteins- or GAPDH-expression vectors, and performed Y2H analysis. The Y2HGold yeast strain was cotransformed with the constructed bait (Fig. 1A) and prey (Fig. 1B) vectors and grown on the QDO/X/A plates. As shown in Fig. 1C, the growth of blue colonies on the QDO/X/A plates signifies the positive interaction between the C-terminal domain of GAPDH (GAPDH-c) and $Pr55^{gag}$. Furthermore, Y2H analysis using processing forms of $Pr55^{gag}$ indicated that MA and CA-NTD interact with GAPDH-c. In contrast, the Y2HGold yeast strain cotransformed with GAPDH-c and $p160^{gag\text{-}pol}$ did not grow on the QDO/X/A plates, despite sufficient protein expression levels, because the GAL4-activation domain (GAL4 AD) fused to $p160^{gag\text{-}pol}$ could not translocate to the nucleus [16]. Although the p6 bait protein also indicated positive interaction with GAPDH-c, this result reflected its autoactivity, which was confirmed by transforming only the bait vector into Y2HGold in the absence of the prey vector (Supplementary Fig. 1). These results suggest that MA and CA-NTD are essential for specific binding via the multiple-site binding of GAPDH to $Pr55^{gag}$.

3.2. Asp^{256}, Lys^{263} and Glu^{267} of GAPDH interact with HIV-1 MA and Asp^{256} and Lys^{260} of GAPDH are essential for the interaction between GAPDH and CA-NTD

To explore the MA- or CA-NTD-interacting domain of GAPDH, we performed docking simulation of interaction between GAPDH (PDB ID: 1ZNQ) [17] and MA (PDB ID: 2H3I) [18] or CA (PDB ID: 1E6J) [19] with a software system molecular operating environment (MOE)Dock (Docking software). The docking simulation proposed one possible model that the GAPDH helix 10 (255–267), which is located at the surface of GAPDH, plays a role in the interaction between GAPDH-c and MA or CA-NTD (Fig. 2A). Because GAPDH actually exists as a stable tetramer, which is in equilibrium with a metastable dimer, it is possible that GAPDH tetramer interacts with more than two proteins using same region. Therefore, on the basis of these deduced interaction domains, 5 single-point and 5 multiple-point mutants of the helix 10 domain of GAPDH were prepared to perform mutagenesis study (Fig. 2B).

In Y2H analysis using GAPDH mutants and WT MA, as shown in the Fig. 3A, the K260E and Q264A of GAPDH mutants retained their ability to interact with WT MA. In contrast, the D256R, K263E or E267R of GAPDH mutants showed the loss of the ability to bind to WT MA. In addition, combined mutations except for D256R/K260E (M1) caused the loss of interaction. Western immunoblot analysis indicated that these effects were apparently not due to the low expression levels of the bait and prey proteins (Fig. 3B). On the other hand, the docking simulation predicted that residues Arg^{58}, Gln^{59} and Gln^{63} of MA formed an ion or a hydrogen bond network with Asp^{256}, Lys^{263} and Glu^{267} of

GAPDH. As shown in the Fig. 3C, the R58E, Q59A and Q63A of MA mutants did not interact with GAPDH-c. These effects were also not due to the low protein expression levels of the bait and prey proteins (Fig. 3D). These findings suggest that $Asp^{256,}$ Lys^{263} and Glu^{267} of GAPDH are crucial for the interaction between GAPDH and MA.

Since the docking simulation proposed that GAPDH helix 10 is also required for the interaction with CA-NTD, Y2H analysis focusing on the interaction GAPDH and CA-NTD was carried out. The D256R, K260E, K263E, Q264A and E267R of GAPDH single-point mutants maintained the interaction between GAPDH and CA-NTD (Fig. 3E). In contrast, the multiple-point mutations of GAPDH, D256R/K260E (M1), D256R/ K260E/Q264A (M3) and D256R/K260E/Q264A/ E267R (M5) lacked the binding ability to the WT CA-NTD. These results suggest that both of Asp^{256} and Lys^{260} of GAPDH play an important role in GAPDH interaction with CA-NTD. Furthermore, the docking simulation predicted that Asp^{256} and Lys^{260} of GAPDH interact with Arg^{82}, Glu^{79} and Glu^{76} of CA-NTD. Therefore, we prepared the E76R, E79R and R82E of CA-NTD mutants and coexpressed them with GAPDH-c. As shown in the Fig. 3G, the E79R of CA-NTD mutant retained its ability to interact,but the E76R and R82E mutants lost their ability to interact with GAPDH-c. These effects were apparently not due to the low expression levels of the bait and prey proteins (Fig. 3F and H). These results suggest that GAPDH-c requires Asp256 and Lys260 to bind to CA-NTD.

3.3. Asp^{256}, Lys^{260}, Lys^{263} and Glu^{267} of GAPDH are critical residues for $tRNA^{Lys3}$-packaging suppression effect

The Y2H analysis demonstrated that GAPDH helix 10 contributes to the interaction of GAPDH with both MA and CA-NTD. Because MA and CA exist as the precursor protein $Pr55^{gag}$ in HIV-1 producer cells, we next prepared the D256R/K260E/K263E/E267-R mutant (M6) of GAPDH (Fig. 4A). To examine whether M6 GAPDH interacts with WT $Pr55^{gag}$, M6 GAPDH and $Pr55^{gag}$ were coexpressed in the Y2HGold strain. M6 GAPDH did not show interaction with WT $Pr55^{gag}$, MA or CA-NTD (Fig. 4B, left panel), despite the expression levels being sufficient for examining protein-protein interaction (Fig. 4B, right panel), suggesting that Asp^{256}, Lys^{260}, Lys^{263} and $Glu2^{67}$ of GAPDH are important for the interaction between GAPDH and $Pr55^{gag}$.

We previously reported that viruses produced from GAPDH-overexpressing cells enhanced GAPDH packaging and suppressed $tRNA^{Lys3}$ packaging [14]. Therefore, V5-tagged WT or M6 GAPDH expression vectors were prepared and cotransfected into HEK293 cells with pNLCH to investigate whether the viruses produced from M6-GAPDHexpressing cells showed suppressed GAPDH packaging and restored $tRNA^{Lys3}$ packaging efficiency. We first performed coimmunoprecipitation assay to validate whether endogenous GAPDH and exogenous V5tagged GAPDH retained

oligomatic formation, because GAPDH exists primarily as a homotetramer in the cytoplasm [17]. The assay showed that both V5-tagged WT and M6 GAPDH retained oligomatic forma tion with endogenous GAPDH in HIV-1 producer cells (Fig. 4C), suggesting that M6 did not affect the oligomatic formation of GAPDH. Furthermore, overexpression of V5-tagged WT GAPDH in HIV-1 producer cells (Fig. 4D, WT lane of producer cells) increased the endogenous and V5-tagged WT GAPDH incorporation levels in viruses (Fig. 4D, WT lane of viral particles) as previously described [14]. However, as expected, a similar level of expression of M6 GAPDH (Fig. 4D, M6 lane of producer cells) decreased the incorporation levels of both endogenous and V5-tagged M6 GAPDH (Fig. 4D, M6 lane of viral particles) in comparison with that of WT GAPDH. To address whether the decreased incorporation level of V5-tagged M6 GAPDH depended on the poorer interaction of GAPDH with $Pr55^{gag}$ than V5tagged WT GAPDH, we examined the interaction level in the virus producer cells by coimmunoprecipitation assay. As a result, the interaction between oligomatic GAPDH, which was composed of endogenous GAPDH and V5-tagged WT or M6 GAPDH, and Pr55gag was found to be weaker in V5-tagged M6 GAPDH-expressing cells (Fig. 4E, M6 lane of IP) than in V5-tagged WT GAPDH-expressing cells (Fig. 4E, WT lane of IP). This finding suggests that the amino acid residues Asp^{256}, Lys^{260}, Lys^{263} and Glu^{267} of GAPDH play critical roles in the interaction of GAPDH with $Pr55^{gag}$ and GAPDH packaging into virions. Finally, we examined the effects of M6 GAPDH on the viral replication by measuring $tRNA^{Lys3}$ packaging level and reverse transcription products. Although the expression of WT GAPDH suppressed packaging of $tRNA^{Lys3}$ as previously described, the expression of M6 GAPDH rescued packaging of $tRNA^{Lys3}$ (Fig. 4F). Furthermore, the levels of early reverse transcription products were also recovered by M6 GAPDH expression in virus producer cells (Fig. 4G). These findings indicate that the Asp^{256}, Lys^{260}, Lys^{263} and Glu^{267} residues within GAPDH are critical for the mechanism of $tRNA^{Lys3}$-packaging suppression and that M6 GAPDH acts as a dominant negative regulator of HIV-1 replication.

4. Discussion

During HIV-1 assembly, the selective cellular $tRNA^{Lys3}$ packaging is required for the effective reverse transcription [6]. Thus, the disruption of the interaction between the $Pr55^{gag}$/$p160^{gag\text{-}pol}$/viral genome RNA complex and the $tRNA^{Lys3}$/LysRS complex likely provides a novel therapeutic strategy. Interestingly, we previously identified cellular GAPDH inside virions as a $tRNA^{Lys3}$ packaging inhibitor and demonstrated that the inhibitory mechanism is dependent on the interaction between cellular GAPDH and HIV-1 precursor proteins ($Pr55^{gag}$ and $p160^{gag\text{-}pol}$) [14]. However, it remained unclear how GAPDH interacts with these proteins. Our findings indicate that $tRNA^{Lys3}$ packaging is interrupted by the interaction of GAPDH with MA and CA-NTD

translated as part of viral precursor proteins. The GAPDH mutagenesis assay indicated that Asp^{256}, Lys^{260}, Lys^{263} and Glu^{267} of GAPDH are important residues in the interaction of GAPDH with MA and CA-NTD. Importantly, the crystal structure of GAPDH tetramer (PDB ID: 1ZNQ) [17] shows that all of these amino acids in helix 10 are exposed on four each of monomer GAPDH, suggesting that two subunits of the GAPDH tetramer simultaneously interact with MA and CA-NTD, respectively (Supplementary Fig. 2A and B). On the other hand, Y2H analysis demonstrated that the R58E, Q59A or Q63A of MA, and E76R or R82E of CA-NTD mutants abrogated their interaction with the C-terminal domain of GAPDH. MA (Arg^{58}, Gln^{59} and Gln^{63}) or CA (Glu^{76} and Arg^{82}) residues, which contribute to ionic or hydrogen bond interaction with Asp^{256}, Lys^{260}, $Lys^{263}$and Glu^{267} of GAPDH, are also exposed on the surface of MA or CA and located on the same side of MA helix 3 or CA helix 4 (Supplementary Fig. 2A). Interestingly, a MOE candidate model (Fig. 2A) conferred a somewhat different helix orientation between GAPDH-MA or GAPDH-CA-NTD (Supplementary Fig. 2C) and was supported by Y2H analysis and data regarding oligomatic formation, $tRNA^{Lys3}$ packaging level and reverse transcription using M6 GAPDH. Furthermore, we tried to prepare mutant pNL-CH proviral clones encoding R58E/Q59A/ Q63A in MA and E76R/R82E in CA to clarify the effects of these mutations on tRNALys3 incorporation. The mutated pNL-CH expressed a similar level of the virus precursor protein in HIV-1 producer cells to WT pNL-CH. However, we did not examine whether the $tRNA^{Lys3}$ incorporation level inside virions was increased because the mutational introduction within the capsid-coding gene (E76R, R82E) impaired HIV-1 budding (data not shown).

Many studies have denoted how $tRNA^{Lys3}$ is incorporated into virions. The findings of such studies demonstrated that the tRNALys3/ LysRS complex interacts with the $Pr55^{gag}$/$p160^{gag\text{-}pol}$/viral genome RNA complex and is efficiently packaged into virions [4,5,9,20,21]. Javanbakht et al. [5] demonstrated that the domains critical for the $Pr55^{gag}$-LysRS interaction are mapped to include the dimerization domains of both LysRS and CA. Kovaleski et al. [20] more specifically reported that the interaction between LysRS and $Pr55^{gag}$ is dependent on the helix 7 of LysRS and the helix 4 of CA-CTD of $Pr55^{gag}$. In addition, Khorchid et al. [21] reported that the interaction between $tRNA^{Lys3}$ and $p160^{gag\text{-}pol}$ is involved in the thumb domain sequence of reverse transcriptase (RT). However, the amounts of all $tRNA^{Lys}$s ($tRNA^{Lys1,2}$ and $tRNA^{Lys3}$) and non-$tRNA^{Lys}$s incorporated into virions are significantly increased when $p160^{gag\text{-}pol}$ is present with $Pr55^{gag}$ [22]. Thus, Kleiman et al. [23] reviewed that $p160^{gag\text{-}pol}$ probably increases the incorporation of all tRNAs into $Pr55^{gag}$ virus-like particles through the nonspecific binding of tRNAs to RT sequences within $p160^{gag\text{-}pol}$. Since there is no evidence that RT sequences in $p160^{gag\text{-}pol}$ show a preference for

interacting with $tRNA^{Lys3}$ and not with other tRNAs, $Pr55^{gag}$ does specifically interact with LysRS to play an important role in concentrating $tRNA^{Lys3}$ in the virions. These findings suggest that by sterically inhibiting the interaction between the $Pr55^{gag}$ and $tRNA^{Lys3}$/LysRS complex, the GAPDH tetramer efficiently suppresses the incorporation of $tRNA^{Lys3}$ into the virions. Taken together, these findings indicate that increasing the stability of the GAPDH tetramer or shifting the equilibrium toward the tetramer by increasing the expression level of GAPDH in HIV-1-infected cells might provide an effective approach to interrupt the $tRNA^{Lys3}$ packaging into virions.

Acknowledgements

We thank Dr. Swanstrom (Lineberger Comprehensive Cancer Center, University of North Carolina at Chapel Hill) for providing pNL-CH and helpful discussions. We thank Dr. Shuzo Matsushita (AIDS Research Institute, Kumamoto University, Kumamoto, Japan) for providing the HIV-1-positive plasma. We thank Dr. Morikawa (Kitasato Institute for Life Sciences and Graduate School of Infection Control, Kitasato University, Japan) for providing the $p160^{gag\text{-}pol}$ plasmid [pNL/FS Pol-HA PR(-)]. We thank Dr. Nakamura (Graduate School of Pharmaceutical Sciences, Kumamoto University) for helpful discussions. TZM-bl cells were obtained from the AIDS Research and Reference Reagent Program, Division of AIDS, NIAID, NIH. Funding: This work was supported by a grant from the Waksman Foundation of Japan Inc. and JSPS KAKENHI Grant Number 25670062, 15H04659 and 16K18922.

References

[1] D.E. Ott, Cellular proteins in HIV virions, Rev. Med. Virol. 7 (1997) 167–180.

[2] E.K. Franke, H.E. Yuan, J. Luban, Specific incorporation of cyclophilin A into HIV1 virions, Nature 372 (1994) 359–362.

[3]M. Thali, A. Bukovsky, E. Kondo, et al., Functional association of cyclophilin A with HIV-1 virions, Nature 372 (1994) 363–365.

[4] S. Cen, A. Khorchid, H. Javanbakht, et al., Incorporation of lysyl-tRNA synthetase into human immunodeficiency virus type 1, J. Virol. 75 (2001) 5043–5048.

[5] H. Javanbakht, R. Halwani, S. Cen, et al., The interaction between HIV-1 Gag and human lysyl-tRNA synthetase during viral assembly, J. Biol. Chem. 278 (2003) 27644–27651.

[6] X. Li, J. Mak, E.J. Arts, et al., Effect of alterations of primer-binding site sequences on human immunodeficiency virus type 1 replication, J. Virol. 68 (1994) 6198–6206.

[7] J. Gabor, S. Cen, H. Javanbakht, et al., Effect of altering the tRNA(Lys)(3) concentration in human immunodeficiency virus type 1 upon its annealing to viral RNA, GagPol incorporation, and viral infectivity, J. Virol. 76 (2002) 9096–9102.

[8] L. Kleiman, S. Cen, The tRNALys packaging complex in HIV-1, Int. J. Biochem. Cell Biol. 36 (2004) 1776–1786.

[9] L. Kleinman, C. Jones, K. Musier-Forsyth, Formation of the tRNAlys packaging complex in HIV-1, FEBS Lett. 584 (2010) 359–365.

[10] M.A. Sirover, On the functional diversity of glyceraldehyde-3-phosphate dehydrogenase: biochemical mechanisms and regulatory control, Biochim. Biophys. Acta 2011 (1810) 741–751.

[11] D.E. Schultz, C.C. Hardin, S.M. Lemon, Specific interaction of glyceraldehyde 3phosphate dehydrogenase with the 5′ -nontranslated RNA of hepatitis A virus, J. Biol. Chem. 271 (1996) 14134–14142.

[12] B.P. De, S. Gupta, H. Zhao, et al., Specific interaction in vitro and in vivo of glyceraldehyde-3-phosphate dehydrogenase and LA protein with cis-acting RNAs of human parainfluenza virus type 3, J. Biol. Chem. 271 (1996) 24728–24735.

[13] J. Petrik, H. Parker, G.J. Alexander, Human hepatic glyceraldehyde-3-phosphate dehydrogenase binds to the poly(U) tract of the 3′ non-coding region of hepatitis C virus genomic RNA, J. Gen. Virol. 80 (1999) 3109–3113.

[14] N. Kishimoto, A. Onitsuka, K. Kido, et al., Glyceraldehyde 3-phosphate dehydrogenase negatively regulates human immunodeficiency virus type 1 infection, Retrovirology 9 (2012) 107.

[15] S.K. Lee, J. Harris, R. Swanstrom, A strongly transdominant mutation in the human immunodeficiency virus type 1 gag gene defines an Achilles heel in the virus life cycle, J. Virol. 83 (2009) 8536–8543.

[16] L. Kobbi, G. Octobre, J. Dias, et al., Association of mitochondrial Lysyl-tRNA synthetase with HIV-1 GagPol involves catalytic domain of the synthetase and transframe and integrase domains of Pol, J. Mol. Biol. 410 (2011) 875–886.

[17] S.A. Ismail, H.W. Park, Structural analysis of human liver glyceraldehyde-3pho- sphate dehydrogenase, Acta Crystallogr. D. Biol. Crystallogr. 61 (2005) 1508–1513.

[18] J.S. Saad, J. Miller, J. Tai, et al., Structural basis for targeting HIV-1 Gag proteins to the plasma membrane for virus assembly, Proc. Natl. Acad. Sci. U. S. A. 103 (2006) 11364–11369.

[19] S. Monaco-Malbet, C. Berthet-Colominas, A. Novelli, et al., Mutual conformational adaptations in antigen and antibody upon complex formation between an Fab and HIV-1 capsid protein p24, Structure 8 (2000) 1069–1077.

[20] B.J. Kovaleski, K.A. Khorchid, L. Kleiman, et al., Critical role of helix 4 of HIV-1 capsid C-terminal domain in interactions with human lysyl-tRNA synthetase, J. Biol. Chem. 282 (2007) 32274–32279.

[21] A. Khorchid, H. Javanbakht, M.A. Parniak, et al., Sequences within Pr160gag–pol affecting the selective packaging of tRNALys into HIV-1, J. Mol.

Biol. 299 (2000) 17–26.

[22] M. Pavon-Eternod, M. Wei, T. Pan, et al., Profilling non-lysyl tRNAs in HIV-1, RNA 16 (2010) 267–273.

[23] J. Saadatmand, L. Kleiman, Aspects of HIV-1 assembly that promote primer tRNA (Lys3) annealing to viral RNA, Virus Res. 169 (2012) 340–348.

Analysis of T cell exhaustion observed in tumor suppressor Menin KO mice.

Takeshi Yamada, Ph.D.

Department of Infection and Host Defenses, Graduate School of Medicine, Ehime University Shitsukawa, Toon, Ehime 791-0295, Japan

Introduction

The main functions of antigen-experienced $CD8^+$ T cells are to eliminate tumors and cells infected with intracellular pathogens (1, 2). The goal of our vaccine and immunotherapeutic strategies is to gain a better understanding of the immune response of $CD8^+$ T cells. In response to infection, naïve $CD8^+$ T cells are activated by specific antigen-stimulation, and then antigen-experienced $CD8^+$ T cells undergo robust proliferation, giving rise to effector and immunological memory subsets (3, 4). The effector $CD8^+$ T cells exhibit antiviral and antibacterial activities, including cytotoxic activity against infected cells; therefore they are defined as the cells that produce functional molecules such as interferon-γ (IFN-γ) and granzyme B (GzmB), important for protection against infections (5). To acquire these functions, $CD8^+$ T cells need to differentiate from naïve T cells into effectors. The fate of activated $CD8^+$ T cells is determined by the T cell receptor (TCR) signal strength, co-stimulation, transcription factors, inflammatory cytokines and metabolic regulators (6, 7). In particular, a number of transcriptional activators and repressors have been reported to be involved in the proliferation and differentiation of $CD8^+$ T cells upon infection (4, 6, 8-12). There appears to be a delicate balance in the proliferation, differentiation, exhaustion and survival regulated by transcription factors, indicating that a lack of balance could be harmful for the homeostasis of activated T cells. However, precisely which molecules contribute to the adequate immune response of antigen-experienced $CD8^+$ T cells for the maximal function of effectors still remains to be clearly elucidated.

Antigen-specific effector $CD8^+$ T cells highly express the lectin-like NK receptor KLRG1 in response to infection, while memory $CD8^+$ T cells highly express cytokine interleukin-7 receptorα (IL-7Rα)for long-term protection (4). $CD8^+$ T cells with a high expression of KLRG1, referred to as short-lived effector cells, represent terminally differentiated effector cells with a lower survival than memory $CD8^+$ T cells (13). It is known that the differentiation into short-lived effector cells is regulated by inflammatory

conditions, followed by an increased expression of transcription factors such as Blimp-1 and T-bet (14). Besides the well-known regulatory function of these transcription factors, recent data indicate that transcriptional repressors including Bcl-6 are also involved in the regulation of differentiation in $CD8^+$ T cells, suggesting there is a network of transcriptional regulation rather than a single master regulator for cell fate determination (15). The identification of the molecules that play a role in the differentiation and maintenance of effector $CD8^+$ T cells is important to improve immunological protection against infections. However, the detailed mechanism behind this process remains unclear.

We focused on a transcriptional repressor, menin, which is also known as a tumor-suppressor (16-19). We recently reported that menin is a critical regulator of $CD4^+$ T cell senescence and cytokine homeostasis (20). Despite the importance of menin for the maintenance of $CD4^+$ T cells, its role in other lymphocytes remains to be elucidated. Thus, we hypothesized that menin is also involved in the regulation of differentiation and homeostasis in antigen-stimulated $CD8^+$ T cells. The goal of this study is to investigate how menin is involved in the immune response of $CD8^+$ T cells. We herein demonstrated that tumor-suppressor menin is critical for the primary immune response to infections using T cell-specific Menin-deleted mice. Menin-deficient $CD8^+$ T cells showed a severe defect in proliferation and the survival during expansion upon Listeria infection in a cell-intrinsic manner. Since Menin-deficiency enhanced the expression of effector lineage-specific transcription factors, Blimp-1 and T-bet, menin could play a role in the differentiation checkpoint for cell fate determination and homeostasis of activated $CD8^+$ T cells by controlling the expression of transcription factors. Taken together, our findings could provide important targets within this novel control pathway of the immune response to enhance the response to vaccination and immunotherapy.

Materials and Methods

Mice and cells

Menin$^{flox/flox}$ mice, *CD4*-Cre transgenic (Tg) mice, *Rosa26*-Cre-ER^{T2} Tg (*Rosa*-Cre) mice, C 57BL/6 $Thy1.1^+$ mice, and OT-1 Tg mice were purchased from The Jackson Laboratory. *Menin*$^{flox/flox}$ mice were crossed with *CD4*-Cre Tg mice to generate T cell-specific gene-deleted (*Menin* KO) mice. Next, we crossed wild-type (WT) or *Menin* KO mice with OT-1 Tg mice to generate WT OT-1 Tg or *Menin* KO OT-1 Tg mice. For tamoxifen-inducible gene-deletion, *Menin*$^{flox/flox}$ OT-1 Tg mice were crossed with *Rosa*-Cre Tg mice. The mice were genotyped by PCR using genomic DNA isolated from tails. All mice were used at 6-12 weeks of age, and both sexes were included in the experiments. All experiments using mice were performed with the approval of the Ehime University

Administrative Panel for Animal Care. All animal care was conducted in accordance with the guidelines of Ehime University.

Flow cytometry

The cell suspensions were prepared by manual disruption of spleens and lymph nodes with frosted glass slides, followed by lysis of erythrocytes with an ammonium chloride/potassium solution. The livers and lungs were perfused with ice-cold PBS as previously described (12). Both tissues were homogenized and incubated in PBS containing collagenase III (400 U/ml, Funakoshi, Japan) for 37oC for 30 min. Then digested tissues were applied to a Percoll gradient (GE Healthcare Life Sciences) to collect the lymphocytes, according to the manufacturer's protocol. Cells were then stained with reagents as described below the OVA-specific $CD8^+$ T cells were detected using MHC-class I Pentamer H-2Kb SIINFEKL (#F093-0A-G, PROIMMUNE) and Fluorotag R-PE label (#K2A, PROIMMUNE) according to the manufacturer's protocol. The following antibodies were used for cell surface staining and intracellular staining: anti-Thy1.1 FITC (HIS51, eBioscience), anti-Thy1.1 Alexa 647 (OX-7, BioLegend), anti-Thy1.2 APC-Cy7 (30-H12, BioLegend), anti-Thy1.2 PE (53-2.1, BD Biosciences), anti-CD3 VioletFluor450 (17A2, TONBO Biosciences), anti-CD8 VioletFluor450 (2.43, TONBO Biosciences), anti-CD8Alexa488 (53-6.7, BioLegend), anti-CD4 eFluor780 (RM4-5, eBioscience), anti-CD62L FITC (MEL-14, BD Biosciences), anti-CD62L APC (MEL-14, TONBO Biosciences), anti-CD44 PE (IM7, TONBO Biosciences), anti-CD27 PE (LG.3A10, BD Biosciences), anti-CD127 Alexa488 (SB/199, BioLegend), anti-CD25 PE (3C7, BD Biosciences), anti-CD69 PE (H1.2F3, BD Biosciences), anti-KLRG1 PE (2FI/KLRG1, BD Biosciences), anti-Granzyme B Alexa647 (GB11, BD Biosciences), anti-IFN-γ PE (XMG11.2, BD Biosciences), anti-PD-1 PE (J43, BD Biosciences), anti-2B4 PE (m2B4.B6.458.1, BioLegend), anti-LAG-3 PE (C9B7W, BioLegend), anti-CTLA-4 PE (UC10-4B9, BioLegend), anti-CD160 PE (7H1, BioLegend), anti-Tim-3 PE (8B.2C12, eBioscience), anti-Blimp-1 PE (C-21, Santa Cruz Biotechnology) anti-T-bet PE (4B10, BioLegend), anti-Eomes PE (Dan11mag, eBioscience), anti-pStat1 Alexa647 (58D6, Cell Signaling Technology), anti-pStat4 Alexa647 (38/p-Stat4, BD Biosciences), and anti-pStat5 Alexa647(47/Stat5-pY694, BD Biosciences). For IFN-γ and Granzyme B staining, intracellular staining was performed as previously described (21). Briefly, the splenocytes were isolated and stimulated with 1 μg/ml of $H\text{-}2K^b$ OVA peptide SIINFEKL (MBL, Nagoya, Japan) in the presence of monensin (2 μM) in a 96-well culture plate for 6 h, then stained with anti-Thy1.1, anti-Thy1.1 and anti-CD8α, and fixed and permeabilized, followed by intracellular staining of anti-IFN-γ or Granzyme B. For intracellular staining of Blimp-1, T-bet, Eomes, pStat1, pStat4 and pStat5, the cell surface was

stained as described above, then fixed and permeabilized using a Transcription Factor Staining Buffer Kit (TONBO Biosciences), followed by intracellular staining. For the analysis of apoptosis, the cell surface was stained with anti-CD8α, anti-Thy1.1, and anti-Thy1.2, and then incubated with 7-AAD and AnnexinV-PE using an AnnexinV Apoptosis Detection Kit (#556422, BD Biosciences) according to the manufacturer's protocol. Flow cytometry was performed using a Gallios instrument (Beckman Coulter), and data were analyzed with the FlowJo software program (Tree Star).

Adoptive transfer of CD8$^+$ T cells and Listeria infection

Naïve CD44^{lo}CD8$^+$ T cells were purified from the spleens of WT OT-1 Tg (Thy1.1$^+$ or Thy1.2$^+$) and *Menin* KO OT-1 Tg (Thy1.2$^+$) mice using a Naïve CD8a$^+$ T cell Isolation Kit and an autoMACS Pro Separator (Miltenyi Biotec), and their purities were checked by flow cytometry (> 95% purity). The purified cells were mixed at a 1:1 ratio (WT: *Menin* KO) and adoptively transferred to double congenic (Thy1.1$^+$Thy1.2$^+$) mice (1 x 10^4 cells/mouse, i.v.). Next, the mice were infected with a recombinant OVA-expressing *Listeria monocytogenes* (*Lm*-OVA) strain at 5 x 10^3 colony-forming units (CFU) i.v. 18-24 h later. For the analysis or purification of donor cells, the splenocytes isolated from recipient mice were stained with anti-CD3, anti-CD8, anti-CD4, anti-Thy1.1, and anti-Thy1.2 antibodies. The donor cells were then analyzed or purified using a Gallios instrument or a BD FACSAria II cell sorter (BD Biosciences) by gating on CD3$^+$CD4$^-$CD8$^+$Thy1.1$^+$Thy1.2$^-$ (WT) cells or CD3$^+$CD4$^-$CD8$^+$Thy1.1$^-$Thy1.2$^+$ (*Menin* KO) cells. All experiments using *Lm*-OVA were performed according to the protocols approved by the Ehime University Institutional Biosafety Committee.

Measurement of the bacterial burden

WT and *Menin* KO mice were infected with *Lm*-OVA (4 x 10^5 CFU, i.v.). The bacterial burden in the spleen, liver, and lung was determined on day 7 after *Lm*-OVA infection in culture with BHI bacterial plates as previously described (22).

Induction of gene deletion with tamoxifen

Naïve CD8$^+$ T cells from Rosa-Cre OT-1 Tg (Thy1.2$^+$) mice were purified and mixed with naïve OT-1 CD8$^+$ T cells at a 1:2 ratio (WT: *Rosa*-Cre) and then adoptively transferred into double congenic (Thy1.1$^+$Thy1.2$^+$) mice (1 x 10^4 cells/mouse, i.v.). Mice were infected with *Lm*-OVA (5 x 10^3 CFU, i.v.) 18-24 h later. For the induction of gene deletion, we used tamoxifen (#T5648-1G, Sigma-Aldrich) resolved in corn oil (#23-0320-5, Sigma-Aldrich). Tamoxifen was administered to the mice (3 mg/mouse, i.p.) on day 4 after *Lm*-OVA infection.

In vivo proliferation assay by eFluor670

staining and BrdU incorporation

For eFluor670 staining, OT-1 $CD8^+$ T cells were incubated with 5 μM Cell Proliferation Dye eFluor670 (#65-0840, eBioscience), according to the manufacturer's protocol. The eFluor670-labeled cells were adoptively transferred into recipient mice, which were infected with *Lm*-OVA (5 x 10^3 CFU, i.v.). At different time points after infection, splenocytes from the recipients were stained with anti-CD8, anti-Thy1.1 and anti-Thy1.2, and the dilution of eFluor670 was measured by flow cytometry to evaluate cell proliferation. The proliferation index (PI) was calculated using the FlowJo software program to compare between WT and *Menin* KO $CD8^+$ T cells. For BrdU incorporation, BrdU (Sigma-Aldrich) was injected into mice (2 mg/mouse, i.p.) on day 5 after *Lm*-OVA infection, then the spleens were harvested 14 h later. Splenocytes were stained with anti-CD8α VioletFluor450, anti-Thy1.1 Alexa647 and anti-Thy1.2 APC-Cy7, and BrdU incorporation was measured by flow cytometry with a FITC BrdU flow kit (#559619, BD Biosciences) according to the manufacturer's protocol.

In vitro proliferation assay by stimulation with OVA altered peptide ligands

OT-1 $CD8^+$ T cells were labeled with eFluor670 as described above. Splenocytes were pulsed with OVA altered peptide Q4 (SIIQFEKL) (#AS-64402, AnaSpec Inc.) at 37 oC for 60 min. Then, OT-1 $CD8^+$ T cells were co-cultured with peptide-pulsed splenocytes. After 3 days of stimulation, the dilution of eFluor670 in OT-1 $CD8^+$ T cells was analyzed by flow cytometry.

RNA isolation and quantitative RT-PCR

Total RNA was isolated using TRIzol Reagent (Life Technologies) or NucleoSpin RNA XS (Takara Bio) according to the manufacturer's protocols. Then, cDNA was synthesized using the Superscript VILO cDNA synthesis kit (Life Technologies). Quantitative PCR (qPCR) was performed using the Step One Plus Real-Time PCR System (Life Technologies). The levels of gene expression were normalized to that of CD3e. Specific primers and Roche Universal Probes (Roche) used were as follows: *Hprt* : 5' TCCTCCTCAGACCGCTTTT 3' (forward), 5' CCTGGTTCATCATCGCTAATC 3'(reverse), probe #95; *Menin*: 5' ACCCACTCACCCTTTA-TCACA 3' (forward), 5' ACATTTCGGTTGCGA-CAG T 3' (reverse), probe #20; *Bach2:* 5'CAGT-GAGTCGTGTCCTGTGC 3' (forward), 5' TTC-CTGGGAAGGTCTGTGAT 3'(reverse),probe #79; *Pmaip1(Noxa)*: 5' CAGATGCCTGGGAA-GTCG 3' (forward), 5'TGAGCACACTCGTCC-TTCAA 3' (reverse), probe #15; *Perp*: 5'GACC-CCAGATGCTTGTTTTC 3' (forward), 5' ACCA-GGGAGATGATCTGGAA 3'(reverse), probe#-71; *Cdkn1a (p21)*: 5'-TCCACAGCGATATCCA-GACA-3' (forward), 5'GGACATCACCAGGAT-TGGAC 3' (reverse), probe #21;*Cdkn2d (p19)*: 5' GGGTTTTCTTGGTGAAGTTCG 3' (forward), 5'TTGCCCATCATCATCACCT 3' (reverse), probe #106; *Cdkn2a (p16)*: 5'AATCTCCGCGA-GGAAAGC 3' (forward), 5' GTCTGCAGCCGA-

CTCCAT 3'(reverse), probe #91; *Cdkn2b (p15)*: 5' GGCTGGATGTGTGTGACG 3' (forward), 5' GCAGATACCTCGCAATGTCA 3' (reverse), probe #41; *Cdkn2a (p16)*: 5'AATCTCCGCGAG-GAAAGC 3' (forward), 5' GTCTGCAGCGGAC-TCCAT 3'(reverse), probe #91; *Bim*: 5' GGAG-ACGAGTTCAACGAAACTT 3' (forward), 5' A-ACAGTTGTAAGATAACCATTTGAGG 3' (reverse), probe #41; *Puma*: 5' TTCTCCGGAGTG-TTCATGC 3' (forward), 5' TACAGCGGAGGG-CATCAG 3' (reverse), probe #79; *Bcl-2*: 5' GTACCTGAACCGGCATCTG 3' (forward), 5'GGGGCCATATAGTTCCACAA 3' (reverse), probe #75; *Bcl-xL*: 5' TGACCACCTAGAGCCT-TGGA 3' (forward), 5'GCTGCATTGTTCCCGT-AGA 3' (reverse), probe #2; Mcl-1: 5' GGTATT-TAAGCTAGGGTCATTTGAA 3' (forward), 5'T-GCAGCCCTGACTAAAGGTC 3' (reverse), probe #41; *Prdm1*: 5' TGCGGAGAGAGGCTC-CACTA 3' (forward), 5'TGGGTTGCTTTCCGT-TTG 3' (reverse), probe #80; *Tbx21*: 5' AAACATCCTGTAATGGCTTGTG 3' (forward), 5'TCAACCAGCACCAGACAGAG 3' (reverse), probe #19; *Bcl6*: 5' CTGCAGATGGAGCATGT-TGT 3' (forward), 5' GCCATTTCTGCTTCACT-CG3' (reverse), probe #4; *Id3*: 5' GAGGAGCTT-TTGCCACTGAC 3' (forward), 5' GCTCATCC-ATGCCCTCAG 3' (reverse), probe #19; *Bax*: 5' GTGAGCGGCTGCTTGTCT 3' (forward), 5'GGTCCCGAAGTAGGAGAGGA 3' (reverse), probe #83; *Cdkn6 (p18)*: 5' AAATGGATTTGG-GAGAACTGC 3' (forward), 5'AAATTGGGATT-AGCACCTCTGA 3' (reverse), probe #79; *Cdkn1b (p27)*: 5' GAGCAGTGTCCAGGGATG-AG 3' (forward), 5'TCTGTTCTGTTGGCCCTT-TT 3' (reverse), probe #62; CD3ε: 5' CCAGCCTCAAATAAAAACACG 3' (forward), 5'GATGATTATGGCTACTGCTGTCA 3' (reverse), probe #10; β-actin: 5' CTAAGGCCAACC-GTGAAAAG 3' (forward), 5'ACCAGAGGCAT-ACAGGGACA 3' (reverse), probe #64. Specific reagents for Tcf7 were purchased from Applied Biosystems (#Mm00493445-ml). The gene expression levels were calculated as the relative expression, normalized to the expression of HPRT or CD3ε.

Results

Menin-deficiency impairs the immune response of antigen-specific CD8$^+$ T cells.

T cell-specific *Menin*-deleted mice were generated by crossing *Menin*-floxed mice with CD4-promoter derived Cre-recombinase transgenic (Tg) mice. An efficiently reduced expression of menin was observed in peripheral CD8$^+$ T cells from *Menin*$^{flox/flox}$ *CD4*-Cre Tg (*Menin* KO) mice by quantitative RT-PCR (qRT-PCR) (Fig. 1A). Before the infection study, an immunophenotypic analysis of CD8$^+$ T cells was performed at the steady state. There was no significant difference with respect to the CD44^{hi}CD62L^{hi} population among CD8$^+$ T cells in the thymus between WT and *Menin* KO mice (Fig. 1B). However, *Menin* KO mice had a larger CD44^{hi}CD62L^{hi} population among CD8$^+$ T cells in the spleen, blood, inguinal lymph node (iLN), mesenteric lymph node (mLN), liver, and lung (Fig. 1C), although the total number of CD8$^+$ T cells was lower than in the wild-type (WT) (Fig.

1D). Naïve $CD8^+$ T cells from WT and *Menin* KO expressed no activation markers CD69 and CD25, and no GzmB in steady state without stimulation (Fig. 2A). Intriguingly, naïve *Menin* KO OT-1 $CD8^+$ cells showed enhanced proliferation upon stimulation with low-affinity OVA peptides, and a more rapid increase of activation markers CD69 and CD25, compared to the WT, suggesting a reduced activation threshold in naïve *Menin* KO cells (Fig. 2B-F). Next, we infected the mice with the intracellular pathogen *Lm*-OVA to determine the impact of *Menin*-deficiency in the immune response of $CD8^+$ T cells, as previously described (23). We investigated the primary immune response of endogenous $CD8^+$ T cells to *Lm*-OVA infection by flow cytometry using a pentamer for the detection of OVA-specific $CD8^+$ T cells. While there were no significant differences between WT and *Menin* KO mice on day 3 and day 5 after *Lm*-OVA infection, *Menin* KO $CD8^+$ T cells showed a much lower frequency of OVA-specific pentamer-positive ($Pent^+$) cells in the spleen on day 7 at the peak of the immune response of WT cells (Fig. 3A). The kinetics showed a significantly lower frequency and absolute number of $Pent^+$ cells in *Menin* KO cells after day 7 of infection (Fig. 3B). Other tissues including the liver, lung, iLN and mLN also showed a significantly lower percentage and absolute number of $Pent^+$ cells amongst *Menin* KO $CD8^+$ T cells, compared to WT, indicating that the lower level of antigen-specific $CD8^+$ T cells in the spleen was not due to a difference in tissue distribution (Fig. 3C). Correlated with these results, *Menin* KO mice showed a significantly lower clearance of *Lm*-OVA than the WT mice in the spleen, liver and lung (Fig. 3D). On the other hand, heterozygous *Menin*-deleted ($Menin^{flox/+}$ *CD4*-Cre Tg) mice showed a comparable expansion in the spleen to the WT mice (Fig. 3E).

Immune response of Menin KO $CD8^+$ T cells is impaired in a cell-intrinsic manner.

In the T cell-specific gene deletion system with *CD4*-Cre Tg mice, menin is absent in $CD4^+$ T cells as well as $CD8^+$ T cells. This raises the possibility that the immune response of *Menin*-deleted $CD8^+$ T cells was impaired due to functional defects in *Menin*-deleted $CD4^+$ T cells, that is, in a cell-extrinsic manner. To exclude this possibility, we used an adoptive transfer approach by transferring donor cells from OT-1 transgenic (Tg) mice into congenic recipient mice. We confirmed the presence of more than 90% of $Pent^+$ cells in naïve $CD8^+$ T cells from both WT OT-1 Tg and *Menin* KO OT-1 Tg mice by flow cytometry (data not shown). We purified naïve $CD44^{lo}CD8^+$ cells from the spleens of WT OT-1 Tg ($Thy1.1^+$) and Menin KO OT-1 Tg ($Thy1.2^+$) mice, and then adoptively transferred a 1:1 mixture of WT and *Menin* KO OT-1 Tg cells into the double-congenic ($Thy1.1^+Thy1.2^+$) recipient mice to distinguish cells by flow cytometry with cell surface staining, as shown in Fig. 4A (1). Consistent with the results of the endogenous immune response, donor *Menin*

KO cells were outcompeted by the WT cells in the spleen, liver and lung on day 7 after *Lm*-OVA infection (Fig. 4B). It appears to be clear that menin plays a critical role in the immune response of antigen-specific $CD8^+$ T cells to infection in a cell-intrinsic manner.

Next, we induced gene deletion using a drug, tamoxifen, after *Lm*-OVA infection. For tamoxifen-induced *Menin*-deletion, we crossed *Menin*$^{flox/flox}$ OT-1 Tg mice with *Rosa26*-promoter-derived Cre-ER^{T2} recombinase Tg mice to generate Meninflox/flox *Rosa*26-Cre-ER^{T2} (*Rosa*-Cre) OT-1 Tg mice for the analysis of the role of menin during expansion following infection. Naïve $CD44^{lo}CD8^+$ T cells were purified from WT OT-1 Tg ($Thy1.1^+$) mice and *Rosa*-Cre OT-1 Tg ($Thy1.2^+$) mice, and then mixed at a 1:2 ratio (WT: *Rosa*-Cre) to compare the expansion of antigen-specific activated $CD8^+$ T cells in the same recipient host. The day after adoptive transfer, recipient mice were infected with *Lm*-OVA (5 x 103 CFU, i.v.) and then administered tamoxifen (3 mg/ mouse) or control vehicle (corn oil) by intraperitoneal injection (i.p.) on day 4 after infection, as shown in Fig. 4A (2). A high rate of gene deletion was observed in donor $CD8^+$ T cells from *Rosa*-Cre OT-1 Tg mice by genomic PCR (data not shown). The results showed a much lower percentage and absolute number of tamoxifen-treated *Rosa*-Cre OT-1 $CD8^+$ T cells compared to the WT or vehicle-treated Rosa-Cre OT-1 $CD8^+$ T cells in the spleen, liver and lung (Fig. 4C). However, donor *Menin* KO OT-1 $CD8^+$ T cells showed comparable proliferation with the WT cells in the early time points (day 3 and day 4) after infection with a slightly higher proliferation index (PI) in the Menin KO cells on day 3 (Fig. 4D). These observations suggest that a key change related to an impaired expansion occurs in *Menin* KO cells after day 4 of infection.

Menin enhances proliferation and inhibits apoptosis in activated $CD8^+$ T cells.

We compared proliferation in antigen-specific $CD8^+$ T cells on day 5 after infection by BrdU incorporation. BrdU was injected i.p. 14 h before spleen harvest and detected by flow cytometry with anti-BrdU. *Menin* KO $CD8^+$ T cells showed a significantly lower percentage of BrdU-positive cells than the WT cells (Fig. 5A). Next, we isolated donor $CD8^+$ T cells from recipient mice on day 5 after infection by cell sorting and then isolated total RNA to compare the gene expression of cell cycle inhibitors between WT and *Menin* KO cells. The results revealed that *Menin* KO cells proliferated less, with a higher expression of cell cycle inhibitor genes (*p15, p16, p19,* and *p27*) than the WT cells on day 5 after infection (Fig. 5B).

Next, we compared apoptosis in antigen-specific $CD8^+$ T cells between WT and Menin KO cells by flow cytometry with AnnexinV staining on day 5 after *Lm*-OVA infection. *Menin* KO $CD8^+$ T cells showed a significantly higher percentage of Annexin V-positive cells than the WT cells (Fig. 5C). We then measured the expression of pro-apoptotic

genes (Fig. 5D, upper) and anti-apoptotic genes (Fig. 5D, lower) in donor CD8$^+$ T cells on day 5 after infection by a qRT-PCR analysis, as in Fig. 3B. The qRT-PCR analysis showed a higher expression of pro-apoptotic genes (*Bim and Puma*) and lower expression of an anti-apoptotic gene (*Bcl-xL*) in Menin KO than the WT cells. To identify the factors for these defects in *Menin* KO cells, we analyzed cytokine responsiveness by the measurement of phosphorylated Stats upon cytokine stimulation. The response to cytokines IL-2, IL-12 and IFN-α were normal in *Menin* KO cells (Fig. 6A and 6B).

Menin-deficiency enhances differentiation into terminal effectors in activated CD8$^+$ T cells during expansion.

Next, we focused on the analysis of differentiation from naïve T cells into effectors and memory precursor cells by comparing immunophenotypes using flow cytometry. We examined phenotypic markers of antigen-specific activated CD8$^+$ T cells in the spleen on day 3 to 30 after *Lm*-OVA infection to compare differentiation during primary expansion and memory development. The populations of activated CD8$^+$ T cells can be divided into short-lived effectors and memory precursors according to the expression of KLRG1 and CD127 (IL-7 receptor α) (13). The time course study revealed enhanced differentiation of *Menin* KO CD8$^+$ T cells into short-lived effectors during expansion, compared to the WT cells before the peak of expansion on day 7 (Fig. 7A). *Menin* KO CD8$^+$ T cells showed a significantly higher percentage of CD127^{lo}KLRG1^{hi} cells than the WT on day 5 (Fig. 7D left). WT CD8$^+$ T cells showed a gradual increase in percentage of CD127^{hi}KLRG1^{lo} memory precursors after day 7. On the other hand, *Menin* KO CD8$^+$ T cells did not show an increase of memory precursors, and sustained a high percentage of CD127^{lo}KLRG1^{hi} terminal effectors. Surprisingly, we could only rarely detect *Menin* KO CD8$^+$ T cells due to a large decrease in cell number after 14 days (Fig. 7C). We also examined the immunophenotype of activated CD8$^+$ T cells by flow cytometry with anti-CD27 and anti-CD62L antibodies. In agreement with the CD127/KLRG1 analysis, *Menin* KO CD8$^+$ T cells showed enhanced differentiation into CD27^{lo}CD62L^{lo} terminal effectors and sustained a high percentage of terminal effectors (Fig. 7B). *Menin* KO CD8$^+$ T cells showed a significantly higher percentage of terminal effectors than the WT cells on day 5 (Fig. 7D right). Finally, we could not detect memory *Menin* KO CD8$^+$ T cells on day 60 in a co-transfer setting, suggesting there was a cell-intrinsic defect in memory development (Fig. 7E). Next, we analyzed the function of effector cells to compare the production of functional molecules granzyme B (GzmB) and IFN-γ between WT and *Menin* KO cells by comparing the mean fluorescent intensity (MFI) on day 5 after infection using flow cytometry. *Menin* KO CD8$^+$ T cells showed greater production of both GzmB and IFN-γ than the WT cells (Fig. 7F). Correlating with

an enhanced terminal differentiation, *Menin* KO CD8$^+$ T cells showed a higher expression of inhibitory receptors, including PD-1 and 2B4, compared to the WT cells, in a co-transfer setting on day 5 after infection (Fig. 7G).

Menin negatively regulates the expression of transcription factors related to terminal effector differentiation.

We compared the expression of the transcription factors related to differentiation into terminal effectors and memory precursors in activated CD8$^+$ T cells after *Lm*-OVA infection by intracellular staining. The time course study revealed rapid enhancement of Blimp-1 expression related to terminal effector differentiation in *Menin* KO CD8$^+$ T cells (Fig. 8A). *Menin* KO CD8$^+$ T cells also showed significantly higher expression levels of Blimp-1 and T-bet than the WT cells on day 5 after infection, while there was no significant difference in Eomes expression in the antigen-specific activated CD8$^+$ T cells between *Menin* KO and the WT cells, as measured by comparing MFIs and gene expression (Fig. 8B). Intriguingly, higher expression of Blimp-1 was sustained in *Menin* KO cells beyond day 7, in contrast to the WT. On the other hand, the expression of *Bcl6* and *Id3* were significantly lower in *Menin* KO cells at time points later than day 7, and the expression of Tcf7 was significantly reduced in *Menin* KO cells on day 12, compared to the WT, although there was no significant difference on day 5 after infection (Fig. 8C). These results indicate that menin inhibits terminal effector differentiation on day 5, and enhances memory development after day 7, by controlling the expression of transcription factors important for differentiation into effectors and memory.

Discussion

The understanding of differentiation and homeostasis in activated CD8$^+$ T cells upon infection is required for the development of vaccination and immunotherapeutic protocols. Transcription factors are involved in cell fate determination of antigen-experienced CD8$^+$ T cells (4). We herein demonstrated that a tumor suppressor, menin, is also involved in the regulation of differentiation, proliferation and the survival in activated CD8$^+$ T cells upon infection. In steady state without infection, *Menin* KO CD8$^+$ T cells showed a larger percentage of CD44^{hi}CD62L^{hi} cells in peripheral tissues, but not in the thymus, compared to WT cells. Interestingly, *Menin*-deficiency also lead to a reduced activation threshold upon TCR-stimulation, which suggest that *Menin* KO naïve CD8$^+$ T cells are easily activated by encountering unknown low-affinity antigens in steady state and may contribute to increase CD44^{hi} population. For the initial investigation into the impact of menin in the immune response, we infected mice and compared the response of CD8$^+$ T cells from WT and *Menin* KO mice. Notably, T cell-specific *Menin*-deficiency resulted in the dramatic decrease of antigen-specific CD8$^+$ T cells on day 7 after

Lm-OVA infection, compared with the WT cells. On the other hand, heterozygous *Menin*-deleted mice showed expansion similar to the WT mice after *Lm*-OVA infection, indicating that *Menin* is haplosufficient in the immune response of $CD8^+$ T cells. Correlated with the reduced clonal expansion in *Menin* KO $CD8^+$ T cells, *Menin* KO mice showed less effective clearance of intracellular pathogens compared to the WT mice, which could be due to the reduced number of antigen-specific $CD8^+$ T cells. Moreover, adoptive-transfer experiments using OT-1 Tg mice showed a lower number of antigen-specific *Menin* KO $CD8^+$ T cells than the WT cells on day 7 after *Lm*-OVA infection, and *Menin* KO $CD8^+$ T cells were rarely detectable later than 14 days after infection. Intriguingly, the treatment with tamoxifen for *Menin*-deletion after infection reduced the cell number on day 7, suggesting that menin is required in the expansion phase after infection in order to obtain a proper immune response.

Regarding proliferation and the survival in activated $CD8^+$ T cells, *Menin* KO $CD8^+$ cells showed increased cell cycle arrest and apoptosis on day 5 after *Lm*-OVA infection. Surprisingly, the BrdU incorporation results revealed much less proliferation in *Menin* KO $CD8^+$ T cells on day 5 compared to the WT cells, although *Menin* KO $CD8^+$ cells showed a slightly higher PI compared to the WT cells on day 3 after infection. This proliferation defect in *Menin* KO cells could not be due to cytokine IL-2, IL-12 and type-I IFN responsiveness since there were no significant differences in cytokine signaling between WT and *Menin* KO cells. Thus, *Menin*-deficiency may contribute to cell cycle arrest during expansion by enhancing the expression of cell cycle inhibitor genes (*p15, p16, p19 and p27*). Among these cell cycle inhibitors, the gene expression of p15 (Ink4b) and p16 (Ink4a) are known to be regulated by Polycomb group (PcG) (24), which indicates that cell cycle arrest could be regulated by epigenetic modifications in $CD8^+$ T cells. Trithorax group gene products can antagonize the effect of PcG gene products (25). Thus, menin could regulate the gene expression of cell cycle inhibitors in an epigenetic fashion since menin forms a Trithorax complex with mixed-lineage leukemia 1 (MLL1), a histone H3K4 methyltransferase (26, 27). Moreover, p16 is associated with cellular senescence in $CD8^+$ T cells from elderly persons (28). This may be related to senescence as observed in activated *Menin* KO $CD4^+$ T cells from *in vitro* culture by β-galactosidase staining (20), although the detailed mechanism of cell cycle arrest regulated by menin remains to be explored. In addition to proliferation, the survival of activated antigen-specific $CD8^+$ T cells has to be maintained during expansion to eliminate the pathogen. The analysis with AnnexinV demonstrated enhanced apoptosis in *Menin* KO $CD8^+$ T cells, indicating a lower survival in the absence of menin, which could be due to the increased expression of pro-apoptotic genes (*Bim* and *Puma*) and the decreased expression of an anti-apoptotic gene (*Bcl-xL*). The pro-apoptotic genes are known to be regulated

by the PcG gene *Bmi1* in $CD4^+$ T cells (29, 30), which suggests that apoptosis could be induced by epigenetic modifications in $CD8^+$ T cells by menin as well.

According to an immunophenotypic analysis, *Menin* KO $CD8^+$ T cells showed enhanced differentiation into $CD127^{lo}KLRG1^{hi}$ and $CD62L^{lo}CD27^{lo}$ terminal effectors with the higher expression levels of GzmB and IFN-γ and diminished the $CD127^{hi}KLRG1^{lo}$ long-lived memory precursor subset in the expansion phase. Therefore, our activated *Menin* KO $CD8^+$ T cells do not appear to retain sufficient plasticity to give rise to other subsets, such as effector memory T cells, and are perhaps mostly destined for death or senescence as with exhausted $CD8^+$ T cells during chronic infection (31, 32). Terminal effector differentiation is known to be enhanced by inflammatory signals produced upon infection (14, 33, 34). Regarding the reduced cell number in *Menin* KO cells, however, extrinsic environmental influences can be excluded because adoptive-transfer experiments also resulted in an impaired immune response of *Menin* KO $CD8^+$ T cells. Therefore, an important finding was the fact that menin plays a role in the differentiation and homeostasis of activated $CD8^+$ T cells during expansion, which is due to the cell-intrinsic effect of menin. In the present study, we could link the role of transcription factors to the differentiation of terminal effectors. *Menin*-deficiency increased the expression of Blimp-1 and T-bet, which are important transcription factors for differentiation into terminal effector $CD8^+$ T cells (35) (36-38). Menin could negatively regulate the expression of those factors as a transcriptional repressor of AP-1 by interacting with JunD (16, 26, 27, 39-41). On the other hand, there was no significant difference in the expression of the transcription factor Eomes, which is important for memory differentiation (42, 43), suggesting that the disrupted balance in *Menin* KO $CD8^+$ T cells predominantly leads to terminal effectors. Concomitantly with enhanced terminal effector differentiation, *Menin* KO $CD8^+$ T cells showed a higher expression of inhibitory receptors (PD-1 and 2B4) with reduced proliferation compared to the WT cells, as observed in exhausted $CD8^+$ T cells during chronic infection (44). The high expression of Blimp-1 is known to play a role in the exhaustion of activated $CD8^+$ T cells during chronic infection (45, 46). In addition, an increased T–bet expression has also been reported to be associated with senescence of virus-specific $CD8^+$ T cells (47). Thus, our results may imply that the higher expression of Blimp-1 and T-bet is likely to increase the expression of inhibitory receptors and senescence, which could also contribute to the reduced cell number in *Menin* KO cells compared to the WT cells during expansion upon infection. As is the case with *Menin* KO $CD4^+$ T cells, menin might be targeting Bach2, which is known to regulate immune homeostasis as previously reported (20). Bach2 is also known to promote memory $CD8^+$ T cell development (48). Importantly, Bach2 binds to

the *Prdm1* gene locus and represses its transcription. Indeed, *Menin* KO $CD8^+$ T cells showed a reduced expression of Bach2 (data not shown), suggesting that Bach2 could be involved in the regulation of the immune system, downstream of menin. Thus, the overexpression of Bach2 potentially rescues the impaired immune response in *Menin* KO $CD8^+$ T cells.

Conclusion

A key finding of our study is the fact that menin is required in order to obtain a proper immune response during clonal expansion, by inhibiting terminal differentiation and high expression of inhibitory receptors related with T-cell exhaustion. Our study identified that menin plays an important role in the control of $CD8^+$ T cells response to infection, although menin may also have many so far unexplored effects on immune responses, beyond the regulation of differentiation and homeostasis. As a result, these findings could be used for the optimization of immunotherapies for cancer diseases, as well as for vaccination against infectious pathogens.

References

1. Butterfield, L. H. 2015. Cancer vaccines. *BMJ (Clinical research ed.)* 350: h988.
2. Comber, J. D., and R. Philip. 2014. MHC class I antigen presentation and implications for developing a new generation of therapeutic vaccines. *Therapeutic advances in vaccines* 2: 77-89.
3. Arens, R., and S. P. Schoenberger. 2010. Plasticity in programming of effector and memory CD8 T-cell formation. *Immunol Rev* 235: 190-205.
4. Kaech, S. M., and W. Cui. 2012. Transcriptional control of effector and memory CD8+ T cell differentiation. *Nat Rev Immunol* 12: 749-761.
5. Seder, R. A., P. A. Darrah, and M. Roederer. 2008. T-cell quality in memory and protection: implications for vaccine design. *Nat Rev Immunol* 8: 247-258.
6. Chang, J. T., E. J. Wherry, and A. W. Goldrath. 2014. Molecular regulation of effector and memory T cell differentiation. *Nat Immunol* 15: 1104-1115.
7. Lee, P. H., T. Yamada, C. S. Park, Y. Shen, M. Puppi, and H. D. Lacorazza. 2015. G0S2 modulates homeostatic proliferation of naive CD8(+) T cells and inhibits oxidative phosphorylation in mitochondria. *Immunol Cell Biol* 93: 605-615.
8. Best, J. A., D. A. Blair, J. Knell, E. Yang, V. Mayya, A. Doedens, M. L. Dustin, A. W. Goldrath, and C. Immunological Genome Project. 2013. Transcriptional insights into the CD8(+) T cell response to infection and memory T cell formation. *Nat Immunol* 14: 404-412.
9. Gray, S. M., S. M. Kaech, and M. M. Staron. 2014. The interface between transcriptional and epigenetic control of effector and memory CD8(+) T-cell differentiation. *Immunol Rev* 261: 157-168.
10. Knell, J., J. A. Best, N. A. Lind, E. Yang, L. M. D'Cruz, and A. W. Goldrath. 2013. Id2

influences differentiation of killer cell lectin-like receptor G1(hi) short-lived CD8+ effector T cells. *J Immunol* 190: 1501-1509.

11. Thaventhiran, J. E., D. T. Fearon, and L. Gattinoni. 2013. Transcriptional regulation of effector and memory CD8+ T cell fates. *Current opinion in immunology* 25: 321-328.
12. Yamada, T., C. S. Park, M. Mamonkin, and H. D. Lacorazza. 2009. Transcription factor ELF4 controls the proliferation and homing of CD8+ T cells via the Kruppel-like factors KLF4 and KLF2. *Nat Immunol* 10: 618-626.
13. Kaech, S. M., J. T. Tan, E. J. Wherry, B. T. KOnieczny, C. D. Surh, and R. Ahmed. 2003. Selective expression of the interleukin 7 receptor identifies effector CD8 T cells that give rise to long-lived memory cells. *Nat Immunol* 4: 1191-1198.
14. Joshi, N. S., W. Cui, A. Chandele, H. K. Lee, D. R. Urso, J. Hagman, L. Gapin, and S. M. Kaech. 2007. Inflammation directs memory precursor and short-lived effector CD8(+) T cell fates via the graded expression of T-bet transcription factor. *Immunity* 27: 281-295.
15. Ichii, H., A. Sakamoto, M. Hatano, S. Okada, H. Toyama, S. Taki, M. Arima, Y. Kuroda, and T. Tokuhisa. 2002. Role for Bcl-6 in the generation and maintenance of memory CD8+ T cells. *Nat Immunol* 3: 558-563.
16. Agarwal, S. K., A. Lee Burns, K. E. Sukhodolets, P. A. Kennedy, V. H. Obungu, A. B. Hickman, M. E. Mullendore, I. Whitten, M. C. Skarulis, W. F. Simonds, C. Mateo, J. S. Crabtree, P. C. Scacheri, Y. Ji, E. A. Novotny, L. Garrett-Beal, J. M. Ward, S. K. Libutti, H. Richard Alexander, A. Cerrato, M. J. Parisi, A. S. Santa Anna, B. Oliver, S. C. Chandrasekharappa, F. S. Collins, A. M. Spiegel, and S. J. Marx. 2004. Molecular pathology of the MEN1 gene. *Ann N Y Acad Sci* 1014: 189-198.
17. Hory, B., and T. B. Drueke. 1998. Menin and MEN 1 gene: a model of tumour suppressor system. *Nephrol Dial Transplant* 13: 2176-2179.
18. Poisson, A., B. Zablewska, and P. Gaudray. 2003. Menin interacting proteins as clues toward the understanding of multiple endocrine neoplasia type 1. *Cancer Lett* 189: 1-10.
19. Schernthaner-Reiter, M. H., G. Trivellin, and C. A. Stratakis. 2015. MEN1, MEN4, and Carney Complex: Pathology and Molecular Genetics. *Neuroendocrinology*.
20. Kuwahara, M., J. Suzuki, S. Tofukuji, T. Yamada, M. Kanoh, A. Matsumoto, S. Maruyama, K. KOmetani, T. Kurosaki, O. Ohara, T. Nakayama, and M. Yamashita. 2014. The Menin-Bach2 axis is critical for regulating CD4 T-cell senescence and cytokine homeostasis. *Nat Commun* 5: 3555.
21. Yamashita, M., K. Hashimoto, M. Kimura, M. Kubo, T. Tada, and T. Nakayama. 1998. Requirement for p56(lck) tyrosine kinase activation in Th subset differentiation. *Int Immunol* 10: 577-591.
22. Nolz, J. C., and J. T. Harty. 2011.

Protective capacity of memory CD8+ T cells is dictated by antigen exposure history and nature of the infection. *Immunity* 34: 781-793.

23. Khan, S. H., and V. P. Badovinac. 2015. Listeria monocytogenes: a model pathogen to study antigen-specific memory CD8 T cell responses. *Semin Immunopathol* 37: 301-310.
24. Gil, J., and G. Peters. 2006. Regulation of the INK4b-ARF-INK4a tumour suppressor locus: all for one or one for all. Nature reviews. *Molecular cell biology* 7: 667-677.
25. Francis, N. J., and R. E. Kingston. 2001. Mechanisms of transcriptional memory. Nature reviews. *Molecular cell biology* 2: 409-421.
26. Huang, J., B. Gurung, B. Wan, S. Matkar, N. A. Veniaminova, K. Wan, J. L. Merchant, X. Hua, and M. Lei. 2012. The same pocket in menin binds both MLL and JUND but has opposite effects on transcription. *Nature* 482: 542-546.
27. Scacheri, P. C., S. Davis, D. T. Odom, G. E. Crawford, S. Perkins, M. J. Halawi, S. K. Agarwal, S. J. Marx, A. M. Spiegel, P. S. Meltzer, and F. S. Collins. 2006. Genome-wide analysis of menin binding provides insights into MEN1 tumorigenesis. *PLoS genetics* 2: e51.
28. Onyema, O. O., R. Njemini, L. N. Forti, I. Bautmans, J. L. Aerts, M. De Waele, and T. Mets. 2015. Aging-associated subpopulations of human CD8+ T-lymphocytes identified by their CD28 and CD57 phenotypes. *Archives of gerontology and geriatrics* 61: 494-502.
29. Nakayama, T., and M. Yamashita. 2009. Critical role of the Polycomb and Trithorax complexes in the maintenance of CD4 T cell memory. *Seminars in immunology* 21: 78-83.
30. Yamashita, M., M. Kuwahara, A. Suzuki, K. Hirahara, R. Shinnaksu, H. Hosokawa, A. Hasegawa, S. Motohashi, A. Iwama, and T. Nakayama. 2008. Bmi1 regulates memory CD4 T cell survival via repression of the Noxa gene. *J Exp Med* 205: 1109-1120.
31. Angelosanto, J. M., S. D. Blackburn, A. Crawford, and E. J. Wherry. 2012. Progressive loss of memory T cell potential and commitment to exhaustion during chronic viral infection. *J Virol* 86: 8161-8170.
32. Wherry, E. J. 2011. T cell exhaustion. *Nat Immunol* 12: 492-499.
33. Badovinac, V. P., B. B. Porter, and J. T. Harty. 2004. CD8+ T cell contraction is controlled by early inflammation. *Nat Immunol* 5: 809-817.
34. Obar, J. J., E. R. Jellison, B. S. Sheridan, D. A. Blair, Q. M. Pham, J. M. ZicKOvich, and L. Lefrancois. 2011. Pathogen-induced inflammatory environment controls effector and memory CD8+ T cell differentiation. *J Immunol* 187: 4967-4978.
35. Rutishauser, R. L., G. A. Martins, S. KalachiKOv, A. Chandele, I. A. Parish, E. Meffre, J. Jacob, K. Calame, and S. M. Kaech. 2009. Transcriptional repressor Blimp-1 promotes CD8(+) T cell terminal

differentiation and represses the acquisition of central memory T cell properties. *Immunity* 31: 296-308.

36. IntleKOfer, A. M., N. Takemoto, C. Kao, A. Banerjee, F. Schambach, J. K. Northrop, H. Shen, E. J. Wherry, and S. L. Reiner. 2007. Requirement for T-bet in the aberrant differentiation of unhelped memory CD8+ T cells. *J Exp Med* 204: 2015-2021.
37. Kallies, A., A. Xin, G. T. Belz, and S. L. Nutt. 2009. Blimp-1 transcription factor is required for the differentiation of effector CD8(+) T cells and memory responses. *Immunity* 31: 283-295.
38. Martins, G. A., L. Cimmino, M. Shapiro-Shelef, M. Szabolcs, A. Herron, E. Magnusdottir, and K. Calame. 2006. Transcriptional repressor Blimp-1 regulates T cell homeostasis and function. *Nat Immunol* 7: 457-465.
39. Agarwal, S. K., S. C. Guru, C. Heppner, M. R. Erdos, R. M. Collins, S. Y. Park, S. Saggar, S. C. Chandrasekharappa, F. S. Collins, A. M. Spiegel, S. J. Marx, and A. L. Burns. 1999. Menin interacts with the AP1 transcription factor JunD and represses JunD-activated transcription. *Cell* 96: 143-152.
40. Ikeo, Y., W. Yumita, A. Sakurai, and K. Hashizume. 2004. JunD-menin interaction regulates c-Jun-mediated AP-1 transactivation. *Endocr J* 51: 333-342.
41. Kim, H., J. E. Lee, B. Y. Kim, E. J. Cho, S. T. Kim, and H. D. Youn. 2005. Menin represses JunD transcriptional activity in protein kinase C theta-mediated Nur77 expression. *Exp Mol Med* 37: 466-475.
42. Banerjee, A., S. M. Gordon, A. M. IntleKOfer, M. A. Paley, E. C. Mooney, T. Lindsten, E. J. Wherry, and S. L. Reiner. 2010. Cutting edge: The transcription factor eomesodermin enables CD8+ T cells to compete for the memory cell niche. *J Immunol* 185: 4988-4992.
43. Cui, W., Y. Liu, J. S. Weinstein, J. Craft, and S. M. Kaech. 2011. An interleukin-21-interleukin-10-STAT3 pathway is critical for functional maturation of memory CD8+ T cells. *Immunity* 35: 792-805.
44. Blackburn, S. D., H. Shin, W. N. Haining, T. Zou, C. J. Workman, A. Polley, M. R. Betts, G. J. Freeman, D. A. Vignali, and E. J. Wherry. 2009. Coregulation of CD8+ T cell exhaustion by multiple inhibitory receptors during chronic viral infection. *Nat Immunol* 10: 29-37.
45. Shin, H., S. D. Blackburn, A. M. IntleKOfer, C. Kao, J. M. Angelosanto, S. L. Reiner, and E. J. Wherry. 2009. A role for the transcriptional repressor Blimp-1 in CD8(+) T cell exhaustion during chronic viral infection. *Immunity* 31: 309-320.
46. Welsh, R. M. 2009. Blimp hovers over T cell immunity. *Immunity* 31: 178-180.
47. Dolfi, D. V., K. D. Mansfield, A. M. Polley, S. A. Doyle, G. J. Freeman, H. Pircher, K. E. Schmader, and E. J. Wherry. 2013. Increased T-bet is associated with senescence of influenza virus-specific CD8 T cells in aged humans. *Journal of leuKOcyte biology* 93: 825-836.

48. Hu, G., and J. Chen. 2013. A genome-wide regulatory network identifies key transcription factors for memory CD8(+) T-cell development. *Nat Commun* 4: 2830.

Fig.1

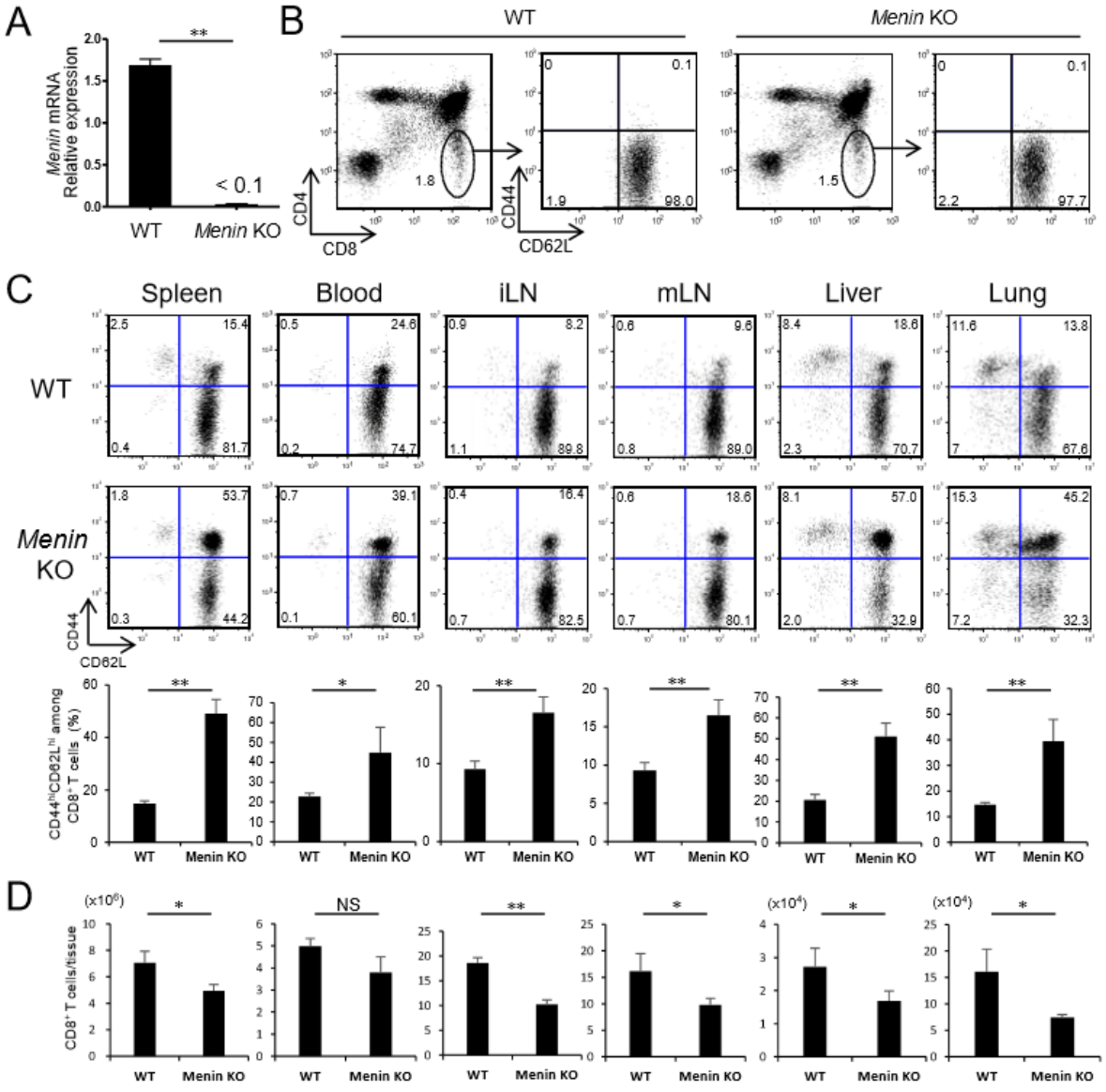

Figure 1: Expression of Menin and the immunophenotypic analysis of CD8$^+$ T cells. (A) *Menin* gene expression was measured in CD8$^+$ T cells from the spleen by qRT-PCR and compared between WT and *Menin* KO (mean ± SD, n = 3 per genotype). (B) CD44 and CD62L expression in CD8-single positive T cells from the thymus. (C) CD44 and CD62L expression in CD8$^+$ T cells were analyzed in different tissues from 10-week-old mice by flow cytometry (upper). Statistics show CD44^{hi}CD62L^{hi}CD8$^+$ T cells based on the percentage in different tissues (lower, mean ± SD, n = 3 per genotype). (D) Statistics show total CD8$^+$ T cells based on the number in different tissues (mean ± SD, n = 3 per genotype). The data in the blood, iLN, and mLN indicate the number of CD8$^+$ T cells per 1 × 10^2 total cells isolated from the tissue specimens. *, $P < 0.05$ and **, $P < 0.01$, WT versus *Menin* KO (two-tailed Student's t-test). NS, not significant. The data are representative of two independent experiments.

Fig.2

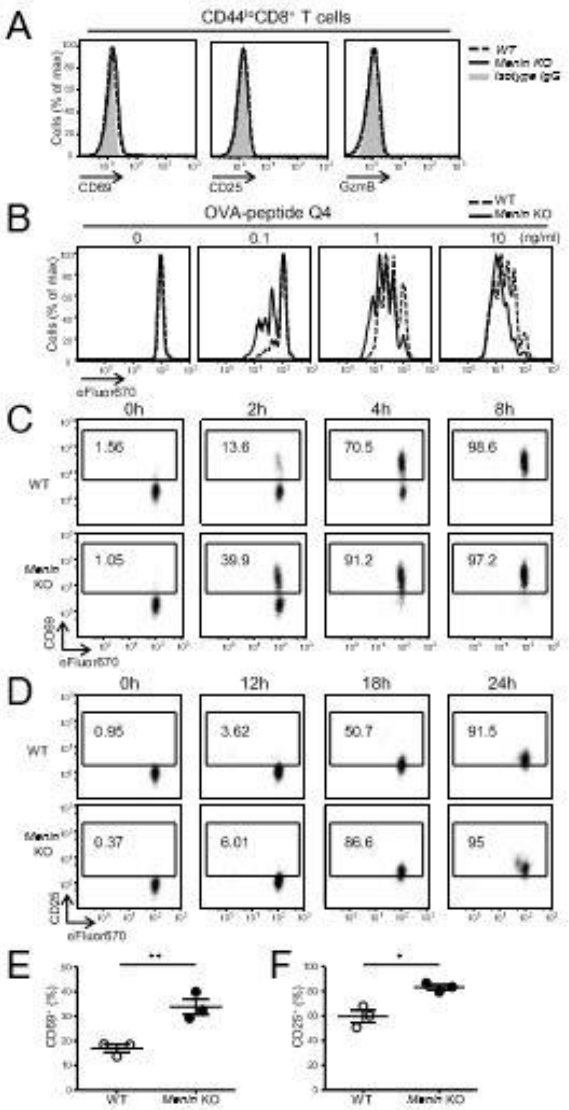

Figure 2: *Menin*-deficiency reduces the activation threshold of naïve CD8$^+$ T cells. The proliferation and expression of activation markers were analyzed by flow cytometry. (A) T-cell activation markers were analyzed in naïve CD44^{lo}CD8$^+$ T cells from the spleen. (B) The proliferation of eFluor670-labeled CD8$^+$ T cells was compared between WT and *Menin* KO upon TCR stimulation using splenocytes pulsed with mutated OVA-peptide Q4 for 3 days. Next, the expression of activation markers CD69 (C) and CD25 (D) was analyzed at different time points. The numbers indicate the percentage of CD69- or CD25-positive cells among total cells. Statistics show a comparison of the percent of CD69$^+$ cells at 2 h (E) and CD25$^+$ cells at 18 h (F) upon TCR stimulation (mean ± SD, $n = 3$ per genotype). *, $P < 0.05$, and **, $P < 0.01$ (two-tailed Student's *t*-test). The data are representative of two independent experiments.

Fig.3

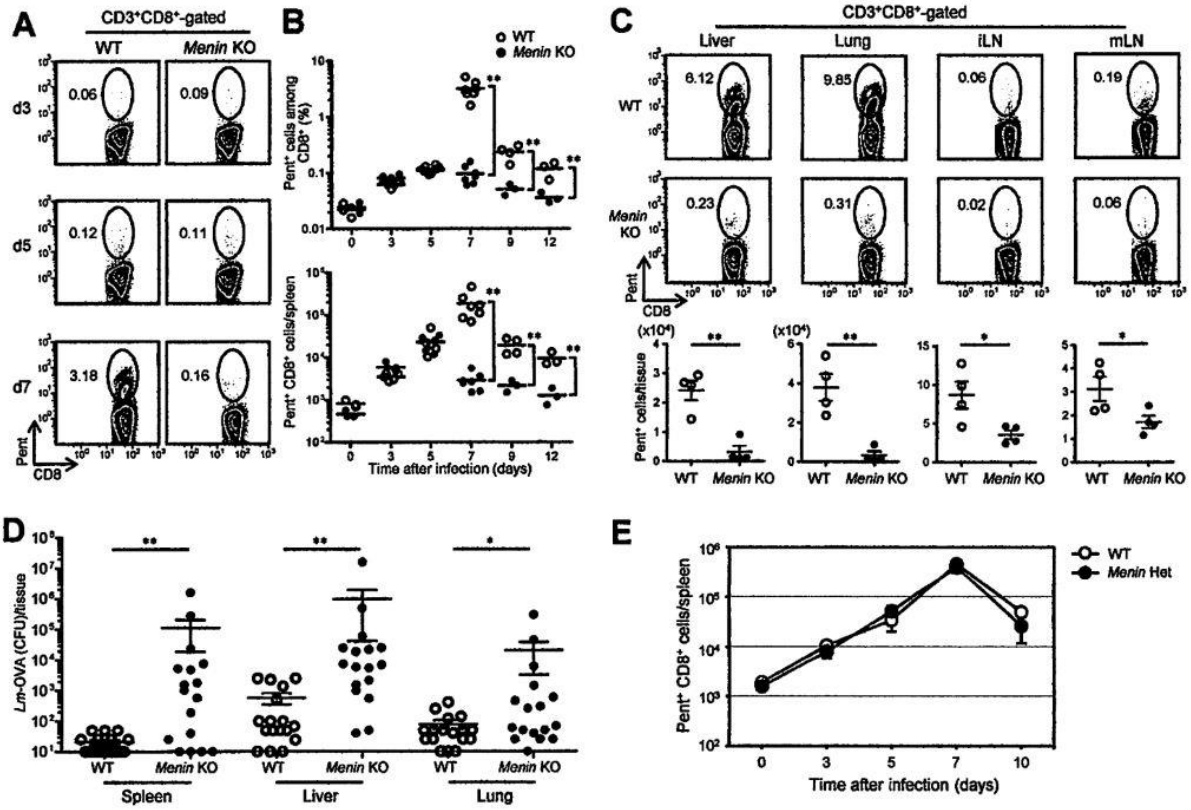

Figure 3: Lack of Menin impairs the immune response of antigen-specific CD8+ T cells upon Lm-OVA infection. The immune response of antigen-specific CD8+ T cells was analyzed at different time points after *Lm*-OVA infection by flow cytometry with an OVA-specific pentamer. (A) Numbers indicate the percentage of pentamer-positive (Pent+) cells among CD8+ T cells in the spleen at 3, 5 and 7 days after infection (d3, d5, and d7, respectively). (B) The kinetics of percent Pent+ cells among CD8+ T cells (upper) and the absolute number of Pent+ CD8+ T cells in the spleen (lower) after *Lm*-OVA infection (mean ± SD, n = 3-7 per genotype). *, $P < 0.05$ and **, $P < 0.01$ (two-tailed Student's t-test). (C) The different tissues were analyzed on day 7 after infection. Numbers indicate the percentage of Pent+ cells among CD8+ T cells (upper). The absolute number of Pent+ CD8+ T cells in the liver, lung, inguinal lymph node (iLN), and mesenteric lymph node (mLN) were compared between WT and *Menin* KO mice (lower, mean ± SD, n = 4 per genotype). The data in iLN and mLN indicate the number of Pent+ cells per 1 x 10^5 total cells isolated from the tissues. *, $P < 0.05$ and **, $P < 0.01$ (two-tailed Student's t-test). (D) The elimination of bacteria was assessed. Mice were infected with *Lm*-OVA and the bacterial titer was calculated by culturing bacteria isolated from the spleen, liver and lung on day 7 after infection (mean ± SD, n = 17 per genotype). *, $P < 0.05$ and **, $P < 0.01$ (Mann-Whitney U-test). (E) An analysis of the immune response in heterozygous *Menin*-deleted (*Menin* Het) mice. The immune response of pentamer-positive (Pent+) antigen-specific T cells was analyzed by flow cytometry. The number of Pent+ CD8+ T cells at different time points after *Lm*-OVA-infection is shown. n = 3-5 per genotype. Symbols represent individual mice. Data are representative of at least three independent experiments.

Fig.4

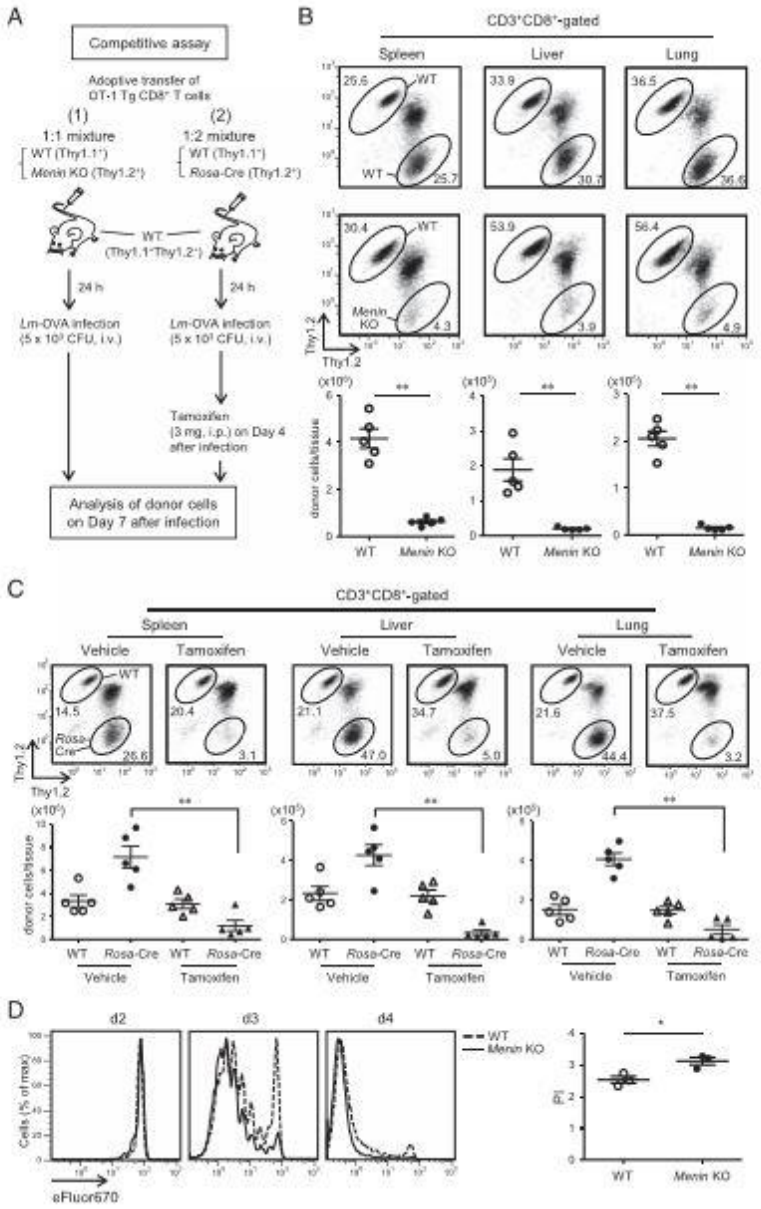

Figure 4: *Menin*-deficiency impairs the immune response of antigen-specific CD8+ T cells in a cell-intrinsic manner. (A) A schematic outline of a competitive assay of the T-cell immune response by adoptive transfer of naïve OT-1 CD44loCD8+ T cells into congenic mice. (B) A 1:1 mixture of WT OT-1 Tg CD8+ T (Thy1.1+) cells and *Menin* KO OT-1 Tg CD8+ T (Thy1.2+) cells was adoptively transferred into WT congenic (Thy1.1+Thy1.2+) mice, which were then infected with *Lm*-OVA to activate the donor cells as shown in Fig. 2A (1). The donor cells were collected from the spleen, liver and lung on day 7 after *Lm*-OVA infection and analyzed by flow cytometry (upper). The absolute number of donor cells was calculated in each tissue after *Lm*-OVA infection (lower, mean ± SD, n = 5 per genotype). Symbols represent individual mice. (C) A 1:2 mixture of WT OT-1 Tg CD8+ T (Thy1.1+) and *Rosa*-Cre OT-1 Tg CD8+ T (Thy1.2+) cells was adoptively transferred into WT congenic

(Thy1.1$^+$Thy1.2$^+$) mice, which were then infected with *Lm*-OVA to activate the donor cells. Tamoxifen was administered i.p. on day 4 after infection as shown in Fig. 2A (2). The donor cells from the spleen, liver and lung were analyzed on day 7 after infection by flow cytometry (upper). The absolute number of donor cells was calculated and compared between WT and *Rosa*-Cre in the different tissues (lower). Symbols represent individual mice (mean ± SD, $n = 5$ per genotype). (D) The eFluor670-labeled WT or *Menin* KO OT-1 Tg CD8$^+$ T (Thy1.2$^+$) cells were adoptively transferred into WT congenic (Thy1.1$^+$) mice, which were then infected with *Lm*-OVA to activate the donor cells. Splenocytes were collected from recipient mice at different time points after infection, and proliferation was compared by dilution of eFluor670 measured by flow cytometry. Statistics show a comparison of the proliferation index (PI) calculated by the FlowJo software program on day 3 after infection. Symbols represent individual mice (mean ± SD, $n = 3$ per genotype).*, $P < 0.05$, and **, $P < 0.01$ (two-tailed Student's *t*-test). Data are representative of at least two independent experiments.

Fig.5

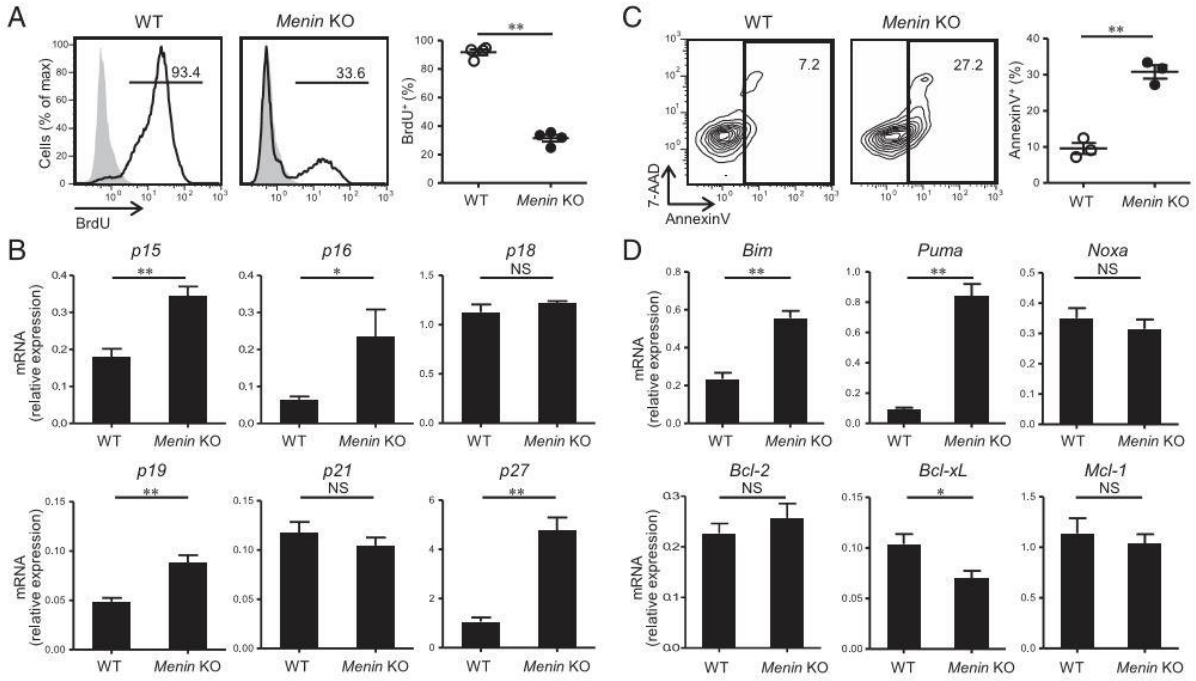

Figure 5: *Menin*-deficiency inhibits proliferation and increases apoptosis in activated CD8$^+$ T cells. OT-1 Tg CD8$^+$ T cells adoptively transferred into the WT congenic mice were analyzed on day 5 after *Lm*-OVA infection by flow cytometry. (A) BrdU was injected i.p. on day 5 after *Lm*-OVA infection, and BrdU-incorporation in the donor cells was assessed 14 h later by flow cytometry. Numbers indicate the percentage of BrdU-positive (BrdU$^+$) cells among donor cells (left). Shaded histograms indicate control without BrdU-injection. The percentage of BrdU-positive cells was compared between WT and *Menin* KO (right, mean ± SD, $n = 4$ per genotype). Symbols represent individual mice. (B) Donor cells were isolated from recipient mice on day 5 after *Lm*-OVA infection by cell sorting, and then RNA was isolated. The expression level of cell cycle inhibitor genes was analyzed by qRT-PCR. The values were normalized to the expression of the CD3ε control gene (mean ± SD, $n = 4$ per genotype). (C) Apoptosis was assessed by staining with AnnexinV and 7-AAD. Numbers in the quadrants indicate the percentage of AnnexinV-positive (AnnexinV$^{+)}$ cells (left). The percentage of AnnexinV$^+$ cells was compared between WT and *Menin* KO (right, mean ± SD, $n = 3$ per genotype). Symbols represent individual mice. (D) The expression level of apoptosis-related genes was analyzed by qRT-PCR as in Fig. 3B (mean ± SD, $n = 4$ per genotype). *, $P < 0.05$, and **, $P < 0.01$ (two-tailed Student's t-test). NS, not significant. Data are representative of at least two independent experiments.

Fig.6

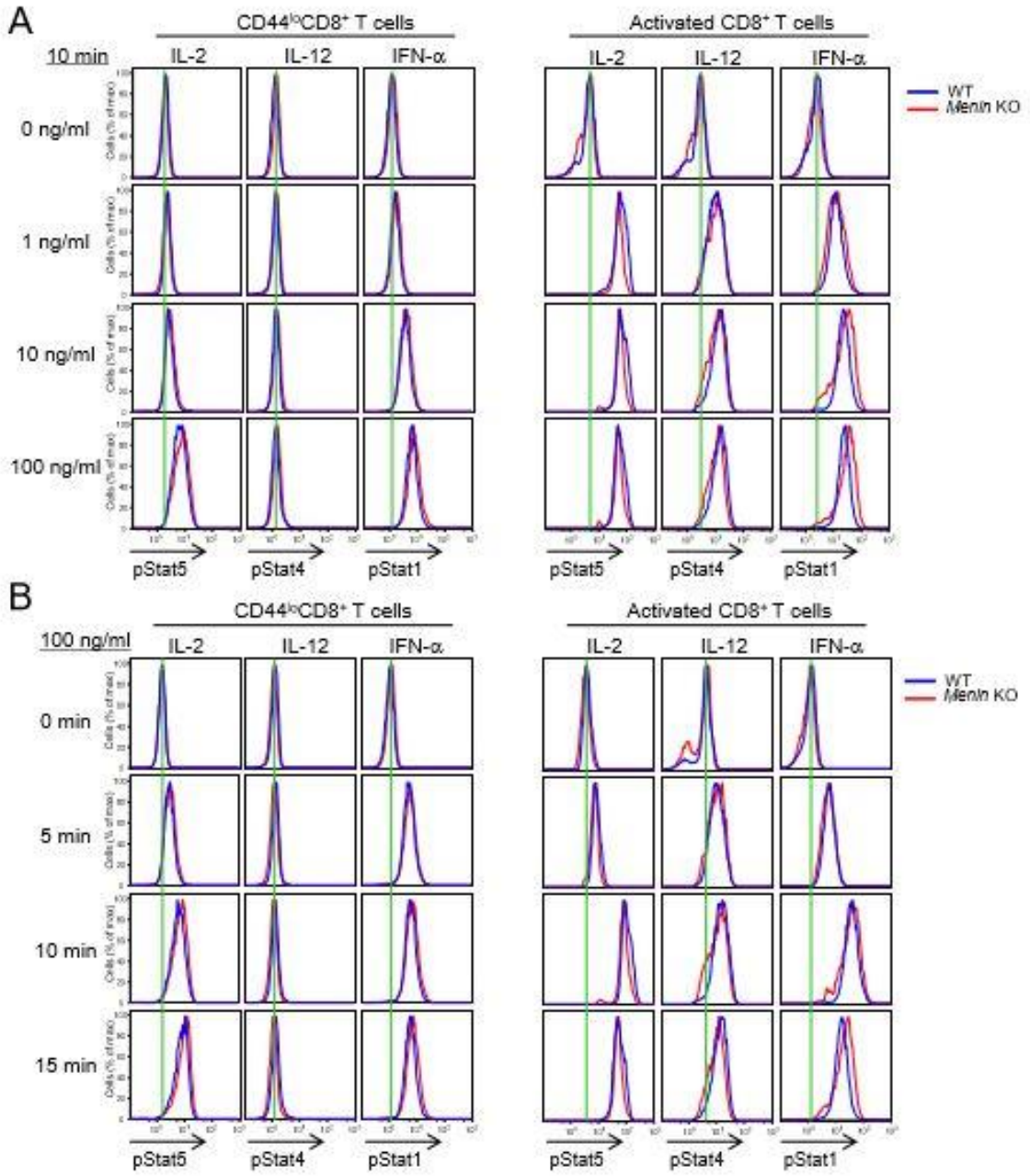

Figure 6: Normal response to cytokines in *Menin* KO CD8$^+$ T cells. Naïve CD8$^+$ T cells were activated with anti-CD3 (10 ng/ml) and anti-CD28 (2 ng/ml) antibodies for 3 days and cultured without any cytokines for 18 h. Next, naïve and activated CD8$^+$ T cells were treated with cytokines IL-2, IL-12, and IFN-α at different concentrations for 10 min (A) and at 100 ng/ml for different periods (B). The data are representative of two independent experiments.

Fig.7

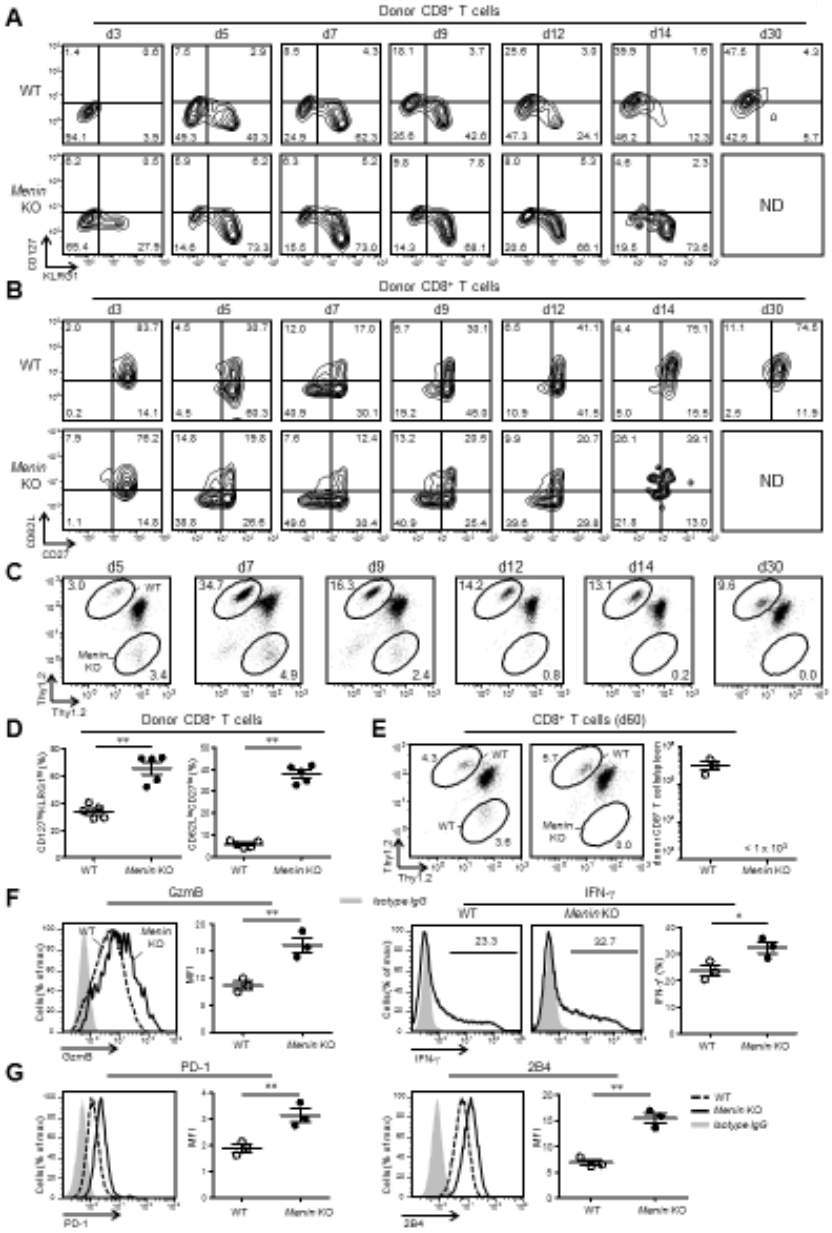

Figure 7: Menin negatively regulates differentiation into terminal effectors and decreases the expression of inhibitory receptors. An immunophenotypic analysis of antigen-specific $CD8^+$ T cells was performed by flow cytometry after *Lm*-OVA infection. OT-1 Tg $CD8^+$ T cells adoptively transferred into WT congenic mice were analyzed on different days after infection. (A) $CD127^{hi}KLRG1^{lo}$ and $CD127^{lo}KLRG1^{hi}$ populations were assessed by staining with anti-KLRG1 and anti-CD127. Numbers in the quadrants indicate the percentage of each population. (B) $CD62L^{lo}CD27^{lo}$ and $CD62L^{hi}CD27^{hi}$ populations were assessed by staining with anti-CD62L and anti-CD27 antibodies. Numbers in the quadrants indicate the percentage of each population. (C) Ratio of adoptive co-transferred cells was analyzed and compared between WT and *Menin* KO in the

spleen on different days after infection. (D) Statistics show a comparison of percent $CD127^{lo}KLRG1^{hi}$ cells (left) and $CD62L^{lo}CD27^{lo}$ cells (right) on day 5 after infection (mean ± SD, $n = 5$ per genotype). (E) Ratio of adoptive co-transferred cells was analyzed and compared between WT and *Menin* KO in the spleen on 60 days after infection. (F) The splenocytes were re-stimulated by *ex vivo* culture with an OVA peptide for 6 h. Next, the production of functional molecules in effectors was assessed by intracellular staining. Left, the production of GzmB was compared between WT (dotted line) and *Menin* KO (solid line) using the mean fluorescent intensity (MFI) calculated by the FlowJo software program. Right, the percentage of IFN-γ–positive cells was compared between WT and Menin KO (mean ± SD, $n = 3$ per genotype). (G) The expressions of inhibitory receptors were analyzed by staining with anti-PD-1 (left) and anti-2B4 (right) antibodies. MFIs were calculated using the FlowJo software program and compared between WT (dotted line) and *Menin* KO (solid line) (mean ± SD, $n = 3$ per genotype). Symbols represent individual mice. *, $P < 0.05$, and **, $P < 0.01$ (two-tailed Student's *t*-test). Data are representative of at least two independent experiments. ND, not determined.

Fig.8

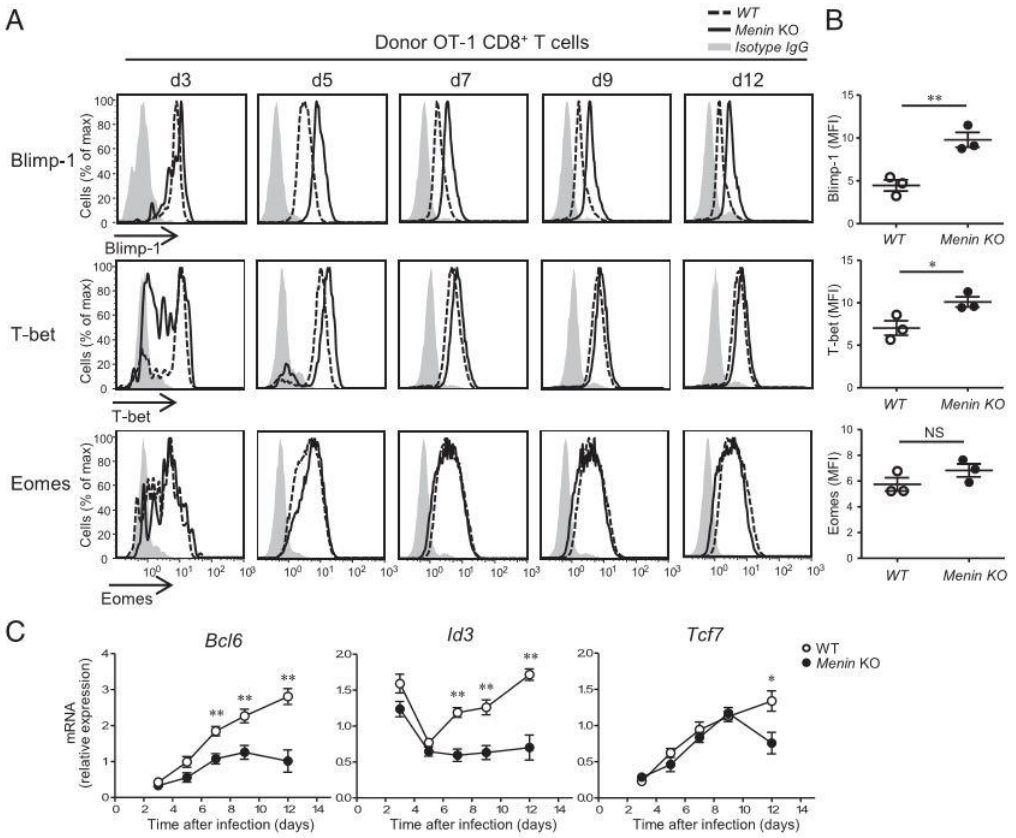

Figure 8: *Menin*-deficiency increases the expression of transcription factors related to effector differentiation. Adoptively transferred OT-1 Tg CD8$^+$ T cells were analyzed at different time points after *Lm*-OVA infection by flow cytometry. (A) The expression of transcription factors Blimp-1, T-bet and Eomes was assessed by intracellular staining on day 3-12 after infection. (B) MFIs were calculated using the FlowJo software program and compared between WT and *Menin* KO. The statistics are shown in the lower section (mean ± SD, n = 3 per genotype). Symbols represent individual mice. (C) Donor cells were isolated from recipient mice at different days after *Lm*-OVA infection by cell sorting, and then RNA was isolated. The expression level of the memory-related genes was analyzed by qRT-PCR and compared between WT and *Menin* KO (as in Fig. 3B, mean ± SD, n = 4 per genotype).*, $P < 0.05$, and **, $P < 0.01$ (two-tailed Student's t-test). NS, not significant. Data are representative of at least three independent experiments.

Identification of a new marker and its pathogenesis in pulmonary tuberculosis、

Sub title: Combined analysis of IFN-γ, IL-2, IL-5, IL-10, IL-1RA and MCP-1 in QFT supernatant is useful for distinguishing active tuberculosis from latent infection

Maho Suzukawa,1 Shunsuke Akashi,1 Hideaki Nagai,1 Hiroyuki Nagase,2 Hiroyuki Nakamura,3 Hirotoshi Matsui,1 Akira Hebisawa1 and Ken Ohta1

1National Hospital Organization Tokyo National Hospital, Tokyo, Japan 204-8585; 2Division of Respiratory Medicine and Allergology, Department of Medicine, Teikyo University School of Medicine, Tokyo, Japan 173-8605; 3Department of Environmental and Preventive Medicine, Graduate School of Medical Science, Kanazawa University, Ishikawa, Japan 920-1192.

Introduction

Tuberculosis is still among the most dangerous communicable infectious diseases in the world. Although the incidence of tuberculosis is slowly declining every year, WHO estimated that there were 9.0 million new cases of tuberculosis in 2013 [1]. Since interferon-γ release assays (IGRAs), including QuantiFERON®-TB Gold In-Tube test (QFT) (Cellestis Inc., Victoria, Australia), became readily available to clinical practitioners, diagnosis of *Mycobacterium tuberculosis* (*M. tuberculosis*) infection has become much easier and faster compared to when diagnosis relied on microbiologic methods such as mycobacterial culture, acid-fast smear and the Mantoux tuberculin skin test (TST).

Today, despite Japan's high level of social health care, active tuberculosis is still seen. Another problem is that new cases are often (multi-)drug-resistant. Other complicating factors include increased prescription of immune-suppressive medications for specific diseases such as cancer and rheumatic diseases, increased numbers of immigrants and travelers from developing countries with a higher incidence of active TB, and increased prevalence of acquired immune disorders such as HIV infection. These multiple factors make diagnosis and management of M. tuberculosis infection even more complex and challenging than before. Thus, there is a need for more accurate, faster and easier diagnosis of M. tuberculosis, which would permit early treatment.

A profound concern of physicians with regard to IGRAs, including QFT, is their inability to discriminate active TB from LTBI. Moreover, QFT quite often gives a positive

result for patients with a past history of tuberculosis infection, even if they received curative therapy for the disease. When a patient is QFT-positive, he/she is diagnosed as infected with tuberculosis and may be started on treatment even in the absence of other clinical data and symptoms. If the patient shows no other evidence of active TB, then he/she may be put on a single-drug regimen using isoniazid (INH) for at least 6 months, with monthly visits to the clinic. If the patient has no clinical symptoms, compliance may decrease due to psychological, economic or physical reasons [2]. In addition, daily use of INH may cause unnecessary side effects such as liver injury or allergic reactions, as well as select for drug-resistant mycobacteria [3]. Therefore, it would be useful to be able to identify other cytokines besides IFN-γ that could be measured in QFT supernatants, thereby increasing the sensitivity and specificity of QFT and making it easier to discriminate active TB from LTBI. Here, we report the results of our performance of multiplex cytokine analysis of QFT supernatants of samples from 31 patients with active TB and 29 patients with LTBI. We identified IL-2, IL-5, IL-10, IL-1RA and MCP-1 as new candidates to be measured in QFT supernatants for better differentiation of active TB from LTBI.

Study population and methods

Study Population

The protocol for this study was reviewed and approved by the National Hospital Organization Tokyo National Hospital Institutional Ethical Review Board (IRB). Informed verbal consent was obtained from all the study participants and documented in the medical records. The IRB approved this verbal informed consent procedure for this study because the participants needed to undergo QFT as part of their requisite clinical examinations or routine medical checkups, regardless of participation in this study, and leftover specimens were used for this study. The study population comprised 31 patients diagnosed as active TB, 29 patients with LTBI and 10 healthy control subjects. Patients and subjects who were examined by QFT at Tokyo National Hospital from February 2010 to December 2012 and were QFT-positive, 21 to 55 years of age, HIV-negative and not using immunosuppressive medications, and had no clinical complications, were consecutively enrolled in this study. The population was then further specified into active TB or LTBI. The control patients were examined by QFT as part of routine annual examinations of healthcare workers at Tokyo National Hospital. All the active TB and LTBI patients underwent QFT at the time of diagnosis, prior to initiation of therapy.

Active TB patients were defined as patients with abnormal radiologic findings suggestive of active pulmonary tuberculosis with microbiologic confirmation of infection with *M. tuberculosis* by mycobacterial culture, acid-fast smear examination and transcription

reverse transcription concerted amplification (TRC) of sputa. All the active TB patients were untreated cases. LTBI is conventionally defined as presence of signs of infection with M. tuberculosis but with no evidence of active disease. In this study, the LTBI patients were QFT-positive, but had no clinical or physical findings, no symptoms of active TB and no abnormal chest X-ray findings. No sputum specimens were examined for LTBI or control subjects because they had almost no sputum. All TLBI and control subjects were selected from our hospital workers.

QFT

QFT was performed according to the manufacturer's instructions. Briefly, blood was drawn by venipuncture. Blood aliquots were then incubated at 37˚C for 16-24 hours with either a mixture of ESAT-6, CFP-10 and TB7.7 as tuberculosis-specific antigens (TBAg) or a mitogen as a positive control, or without stimulation as a negative control (Nil). The culture supernatants were collected and used to quantitate IFN-γ by enzyme-linked immunosorbent assay using the QFT system. QFT was judged according to the manufacturer's instructions.

Multiple Cytokine Assay

Supernatants remaining from QFT were frozen at -20°C for as long as 5 years at Tokyo National Hospital and subsequently used for this study. The levels of cytokines in the TBAg supernatants and Nil supernatants were analyzed using a Bio-Plex Pro Human Cyokine Panel, 27-Plex (BioRad) and LUMINEX 200 (Luminex, Austin, TX) according to the manufacturers' instructions. The analyzed cytokines were basic FGF, eotaxin, G-CSF, GM-CSF, IFN-γ, IL-1β, -1RA, -2, -4, -5, -6, -7, -8, -9, -10, -12, -13, -15 and -17A, IP-10, MCP-1, MIP-1α, MIP-1ß, PDGF-BB, RANTES, TNF-α and VEGF. Prior to measuring the samples, the supernatants were diluted 4x according to the manufacturers' instructions, or diluted 40x for measuring IL-8, IP-10, MCP-1, MIP-1α, MIP-1ß and RANTES because those 6 cytokines were above the detection limit of Luminex kit when measured for 4x-diluted supernatants.

Statistical Analysis

Continuous variables were expressed as medians with interquartile ranges. Overall comparisons between the three groups were done with 1-way ANOVA. Then post hoc Bonferroni comparisons were performed between the groups and P values were determined. P values of less than 0.05 were considered significant. We constructed receiver operating characteristic (ROC) curves, and the area under each ROC curve (AUC) was calculated.

We selected the top four cytokines based on their TBAg – Nil AUCs, i.e., IL-10, IFN-γ, MCP-1 and IL-1RA, and then we selected the cytokine value with the highest Youden Index as the cut-off value for the level of each

cytokine in the supernatant. We assigned a score of 0 or 1 to each assay result depending on whether it was below or above the cut-off value for the cytokine. Then the sum of the four cytokine scores (total score) was calculated [4] and the percentages of active TB were calculated to see the accuracy of distinguishing active TB from LTBI.

Next, stepwise Wilk's lambda discriminant analyses were performed as general discriminant analyses (GDA) to determine the candidate cytokines that contributed the most to the discrimination between active TB and LTBI. The stepwise procedures were guided by an F value probability of 0.05 for inclusion and 0.20 for exclusion. The coefficients for the cytokines included in the last step were calculated.

All statistical analyses were performed using GraphPad Prism version 5.0 (GraphPad Software, San Diego, CA) and SPSS version 23.0 (IBM, Armonk, NY).

Results

Study Subjects

All 70 enrolled subjects, consisting of 31 active TB patients, 29 LTBI patients and 10 healthy control subjects, were analyzed. Table 1 shows the demographic and clinical characteristics of all subjects. All the active TB patients had been diagnosed with pulmonary TB by pulmonologists on the basis of positive chest X-ray results and positive microbial examinations. We selected the active TB and LTBI patients from among QFT-positive subjects, and all the control subjects were QFT-negative. None of the LTBI or healthy control participants had comorbidities or a history of active TB. None of the participants were infected with HIV. The active TB and LTBI patients included more male patients and older patients compared to the healthy control subjects, but there was no statistical difference between the active TB and LTBI patients in regard to gender or age.

Differences in QFT supernatant cytokine levels between active TB and LTBI patients

TBAg – Nil supernatant

The cytokine levels in the QFT TBAg and Nil supernatants were measured by Luminex assay. Since QFT in the clinical setting is always judged on the basis of TBAg – Nil, we also determined that value (Table 2 and Fig 1). IFN-γ, IL-1RA, IL-8 and MCP-1 were significantly higher in the active TB patients compared to LTBI patients. Interestingly, IL-5 and IL-10 were significantly lower in the active TB patients compared to the LTBI patients, although the actual differences in their values are quite small. The TBAg – Nil data also found that several cytokines (IL-2, IP-10 and PDGF) showed a significant difference between the LTBI patients and the healthy control subjects.

Table 1. Patient characteristics.

Group	All	Active	LTBI	Control	p-value
N (%)	70 (100)	31 (44)	29 (42)	10 (14)	
Male, N (%)	31 (45)	18 (58)	12 (41)	1 (10)	n.s.
Age (y) (range)	37 (21-55)	37 (21-48)	42 (23-55)	29 (25-35)	n.s.
Presence of TB history, N (%)	0 (0)	0 (0)	0 (0)	0 (0)	
QFT positive, N (%)	60 (86)	31 (100)	29 (100)	0 (0)	

p-value: active TB patients vs. LTBI patients.

Table 2. Concentrations of cytokines in the three groups (TBAg – Nil).

Cytokine	Median Concentration (IQR)				p-value	
	Active	LTBI	Control	Active vs LTBI	Active vs Control	LTBI vs Control
Basic	-2.03 (-23.63-9.00)	-3.87 (-19.38-6.30)	-10.96 (-25.29--2.49)	N.S.	N.S.	N.S.
FGF						
Eotaxin	-28.32 (-40.46--15.82)	-27.30 (-49.23--2.75)	-23.78 (-28.01--13.52)	N.S.	N.S.	N.S.
G-CSF	25.82 (-10.05-54.47)	-5.19 (-20.75-24.99)	27.52 (-15.04-45.74)	N.S.	N.S.	N.S.
GM-CSF	-15.50 (-30.80-7.80)	-16.65 (-32.20--5.64)	-31.83 (-44.24--7.24)	N.S.	N.S.	N.S.
IFN-γ	724.91 (321.78-1166.55)	224.73 (45.34-476.84)	-77.59 (-139.85--62.44)	0.003	<0.001	N.S.
IL-1β	-4.94 (-102.05-189.63)	4.21 (-97.46-80.62)	16.30 (-141.18-130.32)	N.S.	N.S.	N.S.
IL-1RA	707.23 (444.68-1184.28)	336.58 (176.53-592.04)	-117.08 (-199.78--78.61)	0.031	0.002	N.S.
IL-2	83.61 (43.71-185.37)	116.20 (23.44-311.57)	2.38 (-4.29-5.46)	N.S.	N.S.	0.047
IL-4	0.28 (-0.38-1.13)	0.53 (-0.12-1.83)	0.58 (-0.77-1.89)	N.S.	N.S.	N.S.
IL-5	-15.08 (-24.89--12.62)	-10.00 (-15.69--5.53)	-3.91 (-11.33-0.23)	0.014	0.01	N.S.
IL-6	176.55 (-48.81-1097.84)	31.12 (-96.44-738.96)	167.65 (65.80-951.83)	N.S.	N.S.	N.S.
IL-7	2.18 (-1.36-7.21)	2.18 (2.18-8.45)	4.66 (2.18-7.60)	N.S.	N.S.	N.S.
IL-8	20890.78 (7327.91-28423.52)	7415.39 (2365.61-15300.97)	13256.78 (6566.29-20347.51)	0.007	N.S.	N.S.
IL-9	-118.84 (-165.08--92.39)	-101.21 (-130.48--70.55)	-115.88 (-152.37--73.32)	N.S.	N.S.	N.S.
IL-10	-4.28 (-10.66-3.11)	6.07 (1.37-8.14)	5.15 (0.33-7.98)	0.023	N.S.	N.S.
IL-12	-11.01 (-27.53-3.68)	-0.29 (-9.47-9.71)	7.61 (1.45-10.06)	N.S.	N.S.	N.S.
IL-13	0.85 (-1.79-4.23)	-0.17 (-2.38-6.05)	-0.28 (-2.72-1.16)	N.S.	N.S.	N.S.
IL-15	-10.06 (-27.04--4.23)	1.55 (-9.55-1.55)	-1.92 (-9.94-1.55)	N.S.	N.S.	N.S.
IL-17A	-195.68 (-235.40--163.17)	-154.06 (-213.78--111.84)	-193.69 (-215.66--139.76)	N.S.	N.S.	N.S.
IP-10	52277.85 (31097.49-90807.68)	33045.90 (23854.53-71496.1)	559.11 (-382.88-1967.80)	N.S.	<0.001	0.009
MCP-1	27929.10 (10770.41-48038.45)	10299.09 (1293.56-23234.76)	-429.70 (-683.82--84.31)	0.001	<0.001	N.S.
MIP-1α	-382.65 (-882.75--76.53)	-150.39 (-793.64--37.93)	-302.47 (-825.80--137.43)	N.S.	N.S.	N.S.
MIP-1β	3250.81 (780.23-8292.59)	1520.92 (-82.31-6873.52)	1694.73 (1034.85-2106.29)	N.S.	N.S.	N.S.
PDGF-BB	3671.89 (2067.81-6657.97)	2443.54 (1195.44-4426.76)	-1600.84 (-1885.38--1314.11)	N.S.	<0.001	<0.001
RANTES	15836.36 (2136.57-35205.30)	440.27 (-20413.57-11500.78)	-30840.99 (-60681.70--14263.16)	N.S.	0.045	N.S.
TNF-α	-37.03 (-259.98-736.27)	-20.67 (-219.56-94.27)	-497.81 (-819.28--300.54)	N.S.	0.032	N.S.
VEGF	2.56 (-25.07-41.47)	0.93 (-8.45-17.91)	57.39 (18.15-93.38)	N.S.	N.S.	N.S.

Table 3. AUCs for discriminating active tuberculosis from LTBI (TBAg–Nil).

Cytokine	AUC (95% CI)	p-value	Cut-off	Sensitivity, % (95% CI)	Specificity, % (95% CI)
Basic FGF	0.50 (0.35-0.65)	N.S.	-2.2	51.61 (33.06-69.85)	58.62 (38.94-76.48)
Eotaxin	0.51 (0.35-0.66)	N.S.	-14.9	80.65 (62.53-92.55)	41.38 (23.52-61.06)
G-CSF	0.62 (0.48-0.77)	N.S.	14.7	61.29 (42.19-78.15)	72.41 (52.76-87.27)
GM-CSF	0.56 (0.42-0.71)	N.S.	-2.7	38.71 (21.85-57.81)	82.76 (64.23- 94.15)
IFN-γ	0.78 (0.67-0.90)	<0.001	256.9	90.32 (74.25-97.96)	58.62 (38.94-76.48)
IL-1β	0.51 (0.36-0.66)	N.S.	179.4	25.81 (11.86-44.61)	93.1 (77.23-99.15)
IL-1RA	0.74 (0.61-0.86)	0.002	631.9	64.52 (45.37-80.77)	79.31 (60.28-92.01)
IL-2	0.55 (0.40-0.70)	N.S.	333.2	96.77 (83.30-99.92)	24.14 (10.30-43.54)
IL-4	0.58 (0.44-0.73)	N.S.	0.3	51.61 (33.06-69.85)	68.97 (49.17-84.72)
IL-5	0.70 (0.57-0.83)	0.007	-11.3	87.1 (70.17-96.37)	51.72 (32.53-70.55)
IL-6	0.54 (0.39-0.69)	N.S.	53.2	61.29 (42.19-78.15)	55.17 (35.69-73.55)
IL-7	0.60 (0.45-0.74)	N.S.	5.2	70.97 (51.96-85.78)	48.28 (29.45-67.47)
IL-8	0.71 (0.58-0.85)	0.005	16088	66.67 (47.19-82.71)	82.76 (64.23-94.15)
IL-9	0.6352 (0.493-0.78)	N.S.	-154.1	32.26 (16.68-51.37)	93.1 (77.23-99.15)
IL-10	0.81 (0.70-0.92)	<0.001	-0.8	64.52 (45.37-80.77)	89.66 (72.65-97.81)
IL-12	0.70 (0.56-0.83)	0.009	-10.3	54.84 (36.03-72.68)	79.31 (60.28-92.01)
IL-13	0.51 (0.36-0.66)	N.S.	0.1	54.84 (36.03-72.68)	55.17 (35.69-73.55)
IL-15	0.73 (0.60-0.86)	0.002	0.3	83.87 (66.27-94.55)	65.52 (45.67-82.06)
IL-17	0.66 (0.52-0.80)	0.03	-155.3	87.1 (70.17-96.37)	51.72 (32.53-70.55)
IP-10	0.62 (0.48-0.76)	N.S.	33082	73.33 (54.11-87.72)	51.72 (32.53-70.55)
MCP-1	0.74 (0.62-0.87)	0.001	26573	51.61 (33.06-69.85)	86.21 (68.34-96.11)
MIP-1α	0.60 (0.46-0.75)	N.S.	-300.3	60.0 (40.60-77.34)	68.97 (49.17-84.72)
MIP-1β	0.57 (0.42-0.72)	N.S.	1686	70.0 (50.60-85.27)	51.72 (32.53-70.55)
PDGF-BB	0.65 (0.51-0.79)	0.042	1516	90.32 (74.25-97.96)	37.93 (20.69-57.74)
RANTES	0.69 (0.56-0.83)	0.011	13836	53.33 (34.33-71.66)	79.31 (60.28-92.01)
TNF-α	0.53 (0.38-0.68)	N.S.	660.6	29.03 (14.22-48.04)	93.1 (77.23-99.15)
VEGF	0.50 (0.35-0.65)	N.S.	-23.4	25.81 (11.86-44.61)	93.1 (77.23-99.15)
95% CI = 95% confidence interval.					

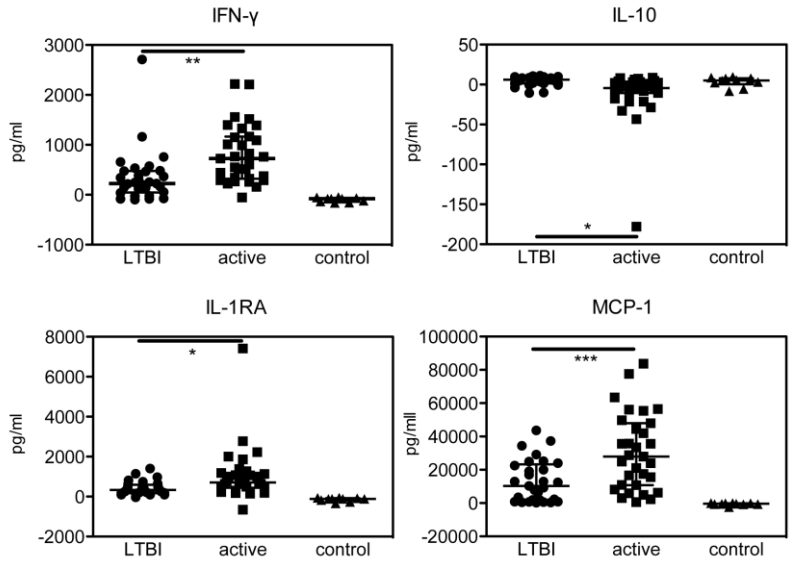

Fig 1. Major cytokines in TBAg – Nil supernatants of patients with active TB, LTBI and healthy controls. *** $P < 0.001$ and ** $P < 0.01$
between active TB vs. LTBI. Bars represent means, and error bars represent the SEM.

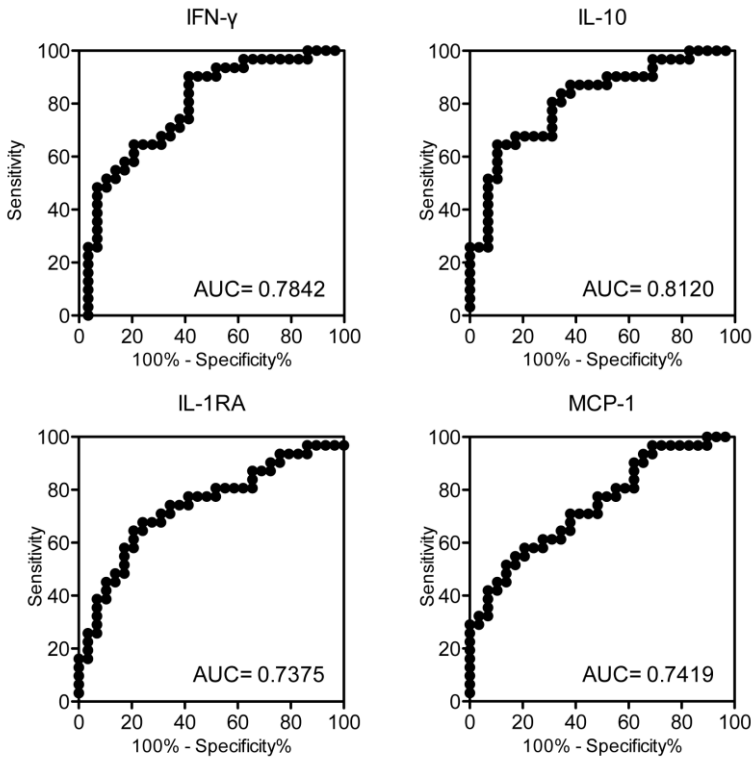

Fig 2. Major ROC curves comparing the diagnostic accuracy of cytokines in TBAg – Nil supernatants for differentiating active TB from LTBI. AUCs for each cytokine are shown in the graph.

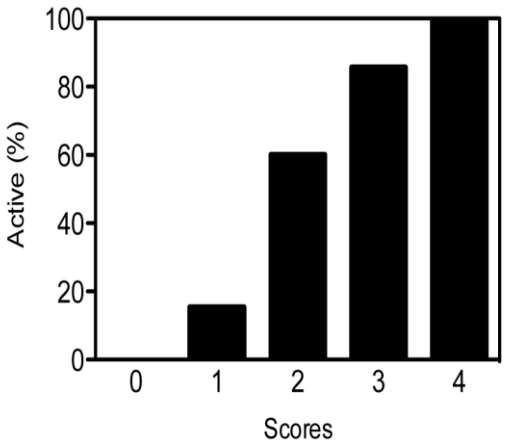

Fig 3. Rates of identification of active TB on the basis of the total score for combination of four cytokines (IL-10, IFN-γ, MCP-1 and IL-1RA) in TBAg – Nil supernatant.

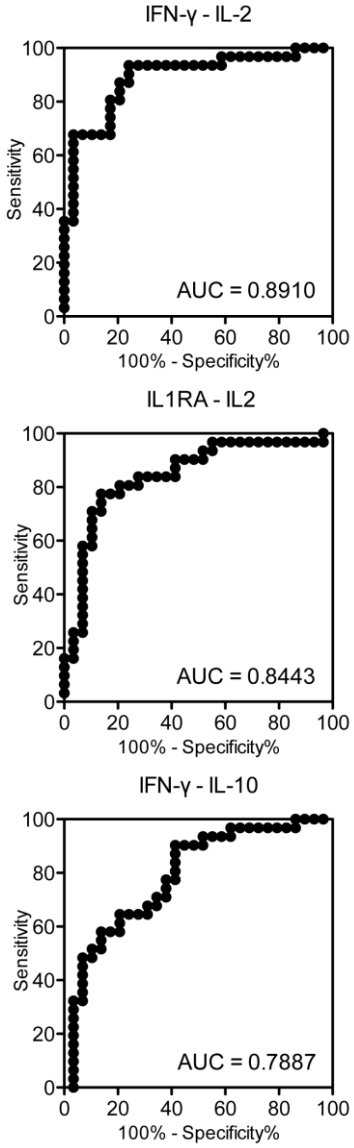

Fig 4. ROC curves comparing the diagnostic accuracy of differences between two cytokines in TBAg – Nil supernatants for differentiating active TB from LTBI. The AUCs are shown

Nil supernatant

Unlike the case of TBAg – Nil (Table 2 and Fig 1), Nil supernatants showed bigger differences between active TB and LTBI patients in terms of the number of cytokines that showed statistical significance (S1 Table and S1 Fig). Interestingly even in the Nil supernatants, many of the cytokines were significantly increased in the active TB patients compared to LTBI patients (S1 Table and S1 Fig). Among the 25 cytokines tested, Basic FGF, G-CSF, IFN-γ, IL-1β, IL-1RA, IL-2, -4, -5, -10, -12, -13, -15, -17A, MCP-1, PDGF, TNF-α and VEGF were significantly elevated in the active TB patients compared to the LTBI patients. On the other hand, none of the cytokines showed a significant difference between the LTBI patients and the healthy

control subjects.

Accuracy of each cytokine marker in differentiating between active TB and LTBI

TBAg – Nil supernatant

To elucidate the accuracy of these markers in diagnosing active TB, ROC curves were created, and their AUCs were calculated. Sensitivities and specificities were also calculated using the value with the highest Youden Index as the cut-off value (Table 3 and S2 Table). The highest AUCs obtained for TBAg – Nil supernatants were shown by IL-10, IFN-γ, MCP-1 and IL-1RA (Fig 2). Several other cytokines, i.e., IL-5, -8, -12, -15, -17A, PDGF and RANTES, also showed statistical significance in differentiating active TB from LTBI (Table 3).

Nil supernatant

On the other hand, in the Nil supernatants, IL-1RA, MCP-1, IL-15, IL-12 and IL-10 showed higher AUCs than IFN-γ (S2 Table and S2 Fig). Many of the other cytokines also showed high AUCs, with statistical significance in discriminating active TB from LTBI (S2 Table and S2 Fig).

Accuracy of cytokine combinations in differentiating between active TB and LTBI

Next, combinations of multiple cytokine markers were examined to see if that would improve the accuracy in differentiating active TB from LTBI. For the combinations, we chose the four best cytokines based on their TBAg – Nil AUCs, namely, IL-10, IFN-γ, MCP-1 and IL-1RA (Table 3). As shown in Fig 3, the rate of identification of active TB increased with the total score. The total score of 4 for TBAg – Nil supernatants showed 100% identification of active TB (Fig 3).

GDA analysis of cytokine combinations in differentiating between active TB and LTBI

To test the accuracy of cytokine combinations in differentiating between active TB and LTBI, we performed GDA analysis using TBAg – Nil supernatants. We selected age, sex, IFN-γ, IL-1RA, -5, -8, -10, -17A, MCP-1 and PDGF as factors, and performed GDA analysis using Wilk's lambda. The final stepwise analysis selected IL-5 and MCP-1 with Wilk's lambda = 0.718 ($p < 0.001$), and the coefficients were -0.655 for IL-5 and 0.821 for MCP-1.

Accuracy of cytokine ratios and cytokine differences for differential diagnosis of active TB and LTBI

The levels of several cytokines, i.e., IL-2, -5, -10 and -15, were higher in TBAg – Nil supernatants of LTBI patients compared with active TB patients, which is the opposite

tendency from the other cytokines. For that reason, we calculated the ratios and differences of those cytokines relative to IFN-γ, IL-1RA and MCP-1. As a result, larger AUCs were shown by the difference between two cytokines than by their ratio. Our data show a larger AUC for the difference (0.8910) between IFN-γ and IL-2 compared with for their ratio (0.7164). The ratios of the other pairs of cytokines did not show AUCs above 0.8, but their differences by subtraction showed large AUCs, such as 0.8443 for IL-1RA – IL-2 (Fig 4).

Discussion

We found that several cytokines in Nil as well as TBAg-stimulated QFT supernatants were useful in differentiating active TB from LTBI. Although IFN-γ is considered to be unable to distinguish active TB from LTBI, our present study found that IL-1RA, IL-2, IL-5, MCP-1 and IL-10 —in addition to IFN-γ—are good candidates; especially when analyzed in combination, they increase the diagnostic potential of QFT for discriminating active TB from LTBI.

At present, the most specific immunoassays for diagnosing mycobacterial infections are probably IGRAs, including QFT. However, a problem in using IGRAs is that they are unable to discriminate active TB from LTBI. Indeed, for smear-negative patients, QFT has been estimated to show sensitivity of 75% and specificity of only 37%, suggesting that the diagnostic accuracy of QFT is especially low in those patients [5]. TST is also widely used in diagnostic testing for LTBI, but TST has low sensitivity of 80% [6] in subjects who had been vaccinated with BCG, which is common in Japan. Therefore, our aim here was to elucidate if we could improve diagnosis of active TB simply by assaying for a larger number of cytokines in the QFT supernatant used to detect IFN-γ. The major advantages in utilizing the QFT supernatant for differential diagnosis of active TB are its microbial specificity and methodological convenience for direct assay of cytokines induced by the TBAg-stimulation. The ability to discriminate active TB from LTBI by measuring multiple cytokines in a small amount of blood in an overnight assay would be a big advantage over the currently available examinations, including microbial culture.

Several cytokines showed a significant difference between active TB and LTBI in the TBAg – Nil supernatant. Interestingly, some of these cytokines showed the reverse pattern in TBAg – Nil supernatants between active TB and LTBI, i.e., higher in LTBI compared to active TB. In line with another study showing that TBAg-stimulated IL-10 is low in active TB [7], we found that IL-10 had the best AUC for discriminating active TB from LTBI, being higher in LTBI than in active TB. IL-10 is produced by various hematopoietic cells, and its main role is to suppress macrophage and dendritic cell functions [8]. IL-10 has also been reported to inhibit formation of mature fibrotic granuloma during M. tuberculosis infection [9]. We and others [7] showed that lymphocytes

from LTBI patients produce more IL-10 in response to in vitro TBAg exposure, suggesting that LTBI lymphocytes may contribute to attenuating inflammation during *M. tuberculosis* infection.

Other cytokines that showed good AUCs in distinguishing active TB from LTBI were MCP-1 and IL-1RA, i.e., higher in active TB compared to LTBI. MCP-1 induces chemotaxis of monocytes and granulocytes, a function that seems critical for protection against microbial infection [10]. The fact that a single nucleotide polymorphism (SNP) in the MCP-1 promoter correlated with increased susceptibility to active TB disease [11] suggests a close relationship between MCP-1 and the pathogenesis of active TB. On the other hand, IL-1RA is secreted by monocytes, neutrophils and such structural cells as epithelial cells, and its role is competitive inhibition of the proinflammatory effects of IL-1α and IL-1β [12, 13]. IL-1RA has been suggested as a plasma biomarker in many inflammatory and infectious diseases, including TB [10]. Studies have shown that IL-1RA is significantly increased in the serum [14], BAL fluid [15] and QFT supernatant [16] in active TB. According to our present data and reports from other groups showing the importance of IL-1RA in differentiating active TB from LTBI in children [17, 18], IL-1RA may be a critical player or a by-product in the pathogenesis of active TB. However, more detailed examinations are needed of the physiological functions and roles of IL-1RA and MCP-1 in both active TB and LTBI.

It is noteworthy that Nil supernatants (i.e., without TBAg stimulation) showed bigger differences in cytokine levels between active TB and LTBI than found for TBAg – Nil and showed the highest AUCs. The primary reason for this is probably that active TB cases had greater systemic inflammation compared to LTBI. However, another reason may be that non-blood cells that are not used for QFT measurement also produce the assayed cytokines, resulting in the differences in cytokine levels being larger in Nil supernatants than in TBAg-stimulated supernatants. Indeed, MCP-1 and IL-1RA are produced by fibroblasts as well as by such blood cells as monocytes, macrophages and neutrophils [19, 20]. Since only blood cells are used for QFT, there may not be significant cytokine induction in response to an antigen. Moreover, lymphocytes and monocytes from active TB patients may have already been maximally stimulated by antigen in vivo, such that their cytokine synthesis cannot be further increased in vitro, and resulting in differences in TBAg-Nil supernatants that are insufficient for discriminating between active TB and LTBI. It is also important that the levels of both MCP-1 and IL-1RA in Nil supernatants did not correlate positively with other clinical data related to inflammation (e.g., WBC, CRP, ESR) in our study (S3 Table). Thus, these cytokines may be independently and uniquely useful for differential diagnosis of active TB and LTBI, rather than being elevated due to a pro-inflammatory state.

When we analyzed combinations of

multiple cytokines for their ability to discriminate active TB from LTBI, TBAg – Nil supernatants showed good results. Not only the combinations of four cytokines showed accurate diagnosis of active TB: our GDA analysis showed combination of MCP-1 and IL-5 may also be a good candidate for discriminating active TB from LTBI. Another study of analysis of combinations of multiple cytokines in unstimulated plasma for distinguishing active TB from household contacts (QFT-positive and negative) found that the best model was a combination of fractalkine, IFN-γ, IL-4, IL-10 and TNF-α [21]. Others found that combination of EGF, sCD40L, VEGF, TGF-α and IL-1α was potent for discriminating active TB and LTBI [22]. Together, their and our data indicate that combinations of several cytokines may provide clearer identification of active TB from LTBI than a single cytokine assay. However, larger, prospective studies are still necessary to identify the best combination.

It has already been reported that IL-2 was higher in LTBI compared to active TB [23, 24] (although our present study found only a tendency, without statistical significance). For that reason, IL-2/IFN-γ has been reported to be a useful value for differentiating active TB from LTBI [23]. Our further analyses using IL-2 and IL-10—two cytokines that were more elevated in LTBI patients than in active TB—on the basis of their differences and ratios relative to other cytokines indicated that these cytokines can be additional useful markers for discriminating active TB from LTBI.

Limitations of the present study include the relatively small numbers of patients with LTBI and healthy control subjects who all worked in healthcare and had unknown histories with regard to old TB and BCG vaccinations. In addition, the samples had been collected and kept frozen for some time. However, our study found a robust IFN-γ response to TBAg that agreed with the results of QFT, suggesting that there was no deterioration of the samples or technical error. Although there were differences in age among the subject groups, an earlier study found minimal differences in cytokine levels among different age groups [25]. Another limitation of our present study is the lack of sick control patients or a disease control. The patients in our study had been diagnosed only with *M. tuberculosis*. Therefore, we cannot affirm that the elevated cytokine levels we observed in our study population were M. tuberculosis-specific. They may have been a non-specific phenomenon observed in general inflammatory conditions, including infection with other microorganism(s) [26]. In the future, larger, prospective studies are needed to identify the optimal combinations of cytokines, confirm the clinical utility of assay of them as diagnostic markers of mycobacterial infection, especially for differentiating active TB from latent infection, and also to confirm their cut-off values. Understanding the cytokines that differentiate active TB from LTBI may help us elucidate the differences in pathogenesis between active and latent

infections.

Acknowledgments

The authors thank Mr. Isao Asari and Ms. Sayaka Igarashi for their skilled technical assistance.

Grants

This project was supported by a grant from Banyu Life Science Foundation International and a grant from the Waksman Foundation of Japan, Inc. to Maho Suzukawa, and a Health Labour Sciences Research Grant from The Ministry of Health Labour and Welfare of Japan to Hideaki Nagai.

Disclosures

The authors declare there are no conflicts of interest related to this research.

References

1. Global Tuberculosis Report 2014. World Health Organization 2014. 2014.
2. Fiske CT, Yan FX, Hirsch-Moverman Y, Sterling TR, Reichler MR, Tuberculosis Epidemiologic Studies Consortium Task Order T. Risk factors for treatment default in close contacts with latent tuberculous infection. Int J Tuberc Lung Dis. 2014;18(4):421-7. doi: 10.5588/ijtld. 13.0688. PubMed PMID: 24670696; PubMed Central PMCID: PMCPMC40 60979.
3. Cohen T, Lipsitch M, Walensky RP, Murray M. Beneficial and perverse effects of isoniazid preventive therapy for latent tuberculosis infection in HIV-tuberculosis coinfected populations. Proc Natl Acad Sci U S A. 2006;103(18):7042-7. doi: 10.1073/pnas.0600349103. PubMed PMID: 16632605; PubMed Central PMCID: PMCPMC1459015.
4. Gibot S, Bene MC, Noel R, Massin F, Guy J, Cravoisy A, et al. Combination biomarkers to diagnose sepsis in the critically ill patient. American journal of respiratory and critical care medicine. 2012; 186 (1):65-71.doi: 10.1164/rccm.201201- 00 37 OC. PubMed PMID: 22538802.
5. Ling DI, Pai M, Davids V, Brunet L, Lenders L, Meldau R, et al. Are interferon-gamma release assays useful for diagnosing active tuberculosis in a high-burden setting? The European respiratory journal. 2011;38(3):649-56. doi: 10.1183/09031936.00181610. PubMed PMID: 21349910.
6. Pai M, Zwerling A, Menzies D. Systematic review: T-cell-based assays for the diagnosis of latent tuberculosis infection: an update. Annals of internal medicine. 2008;149(3):177-84. PubMed PMID:

18593687; PubMed Central PMCID: PMC2951987.

7. Hur YG, Gorak-Stolinska P, Ben-Smith A, Lalor MK, Chaguluka S, Dacombe R, et al. Combination of cytokine responses indicative of latent TB and active TB in Malawian adults. PloS one. 2013;8(11):e79742. Epub 2013/11/22. doi: 10.1371/journal.pone.0079742. PubMed PMID: 24260295; PubMed Central PMCID: PMCPmc3832606.
8. Redford PS, Murray PJ, O'Garra A. The role of IL-10 in immune regulation during M. tuberculosis infection. Mucosal Immunol. 2011;4(3):261-70. doi: 10.1038/mi.2011.7. PubMed PMID: 21451501.
9. Cyktor JC, Carruthers B, Kominsky RA, Beamer GL, Stromberg P, Turner J. IL-10 inhibits mature fibrotic granuloma formation during Mycobacterium tuberculosis infection. Journal of immunology (Baltimore, Md : 1950). 2013;190(6):2778-90. doi: 10.4049/jimmunol.1202722. PubMed PMID: 23396944; PubMed Central PMCID: PMCPMC3594073.
10. Chegou NN, Heyckendorf J, Walzl G, Lange C, Ruhwald M. Beyond the IFN-gamma horizon: biomarkers for immunodiagnosis of infection with Mycobacterium tuberculosis. The European respiratory journal. 2014;43(5):1472-86. doi: 10.1183/09031936.00151413. PubMed PMID: 24311770.
11. Flores-Villanueva PO, Ruiz-Morales JA, Song CH, Flores LM, Jo EK, Montano M, et al. A functional promoter polymorphism in monocyte chemoattractant protein-1 is associated with increased susceptibility to pulmonary tuberculosis. The Journal of experimental medicine. 2005;202(12):1649-58. doi: 10.1084/jem.20050126. PubMed PMID: 16352737; PubMed Central PMCID: PMCPMC2212957.
12. Arend WP. The balance between IL-1 and IL-1Ra in disease. Cytokine & growth factor reviews. 2002;13(4-5):323-40. PubMed PMID: 12220547.
13. Ruth JH, Bienkowski M, Warmington KS, Lincoln PM, Kunkel SL, Chensue SW. IL-1 receptor antagonist (IL-1ra) expression, function, and cytokine-mediated regulation during mycobacterial and schistosomal antigen-elicited granuloma formation. Journal of immunology (Baltimore, Md : 1950). 1996;156(7):2503-9. Epub 1996/04/01. PubMed PMID: 8786311.
14. Juffermans NP, Verbon A, van Deventer SJ, van Deutekom H, Speelman P, van der Poll T. Tumor necrosis factor and interleukin-1 inhibitors as markers of disease activity of tuberculosis. American journal of respiratory and critical care medicine. 1998;157(4 Pt 1):1328-31. doi: 10.1164/ajrccm.157.4.9709126. PubMed PMID: 9563758.
15. Tsao TC, Hong J, Li LF, Hsieh MJ, Liao SK, Chang KS. Imbalances between tumor necrosis factor-alpha and its soluble receptor forms, and interleukin-1beta and

interleukin-1 receptor antagonist in BAL fluid of cavitary pulmonary tuberculosis. Chest. 2000;117(1):103-9. PubMed PMID: 10631206.

16. Ruhwald M, Bjerregaard-Andersen M, Rabna P, Eugen-Olsen J, Ravn P. IP-10, MCP-1, MCP-2, MCP-3, and IL-1RA hold promise as biomarkers for infection with M. tuberculosis in a whole blood based T-cell assay. BMC research notes. 2009;2:19. Epub 2009/02/06. doi: 10.1186/1756-0500-2-19. PubMed PMID: 19193208; PubMed Central PMCID: PMCPmc2660909.
17. Tebruegge M, Dutta B, Donath S, Ritz N, Forbes B, Camacho-Badilla K, et al. Mycobacteria-Specific Cytokine Responses Detect Tuberculosis Infection and Distinguish Latent from Active Tuberculosis. American journal of respiratory and critical care medicine. 2015;192(4):485-99. doi: 10.1164/rccm.01501-0059OC. PubMed PMID: 26030187.
18. Chegou NN, Detjen AK, Thiart L, Walters E, Mandalakas AM, Hesseling AC, et al. Utility of host markers detected in Quantiferon supernatants for the diagnosis of tuberculosis in children in a high-burden setting. PloS one. 2013;8(5):e64226. Epub 2013/05/22. doi: 10.1371/journal.pone.0064226. PubMed PMID: 23691173; PubMed Central PMCID: PMCPmc3655018.
19. Rolfe MW, Kunkel SL, Standiford TJ, Orringer MB, Phan SH, Evanoff HL, et al. Expression and regulation of human pulmonary fibroblast-derived monocyte chemotactic peptide-1. Am J Physiol. 1992;263(5 Pt 1):L536-45. PubMed PMID: 1443157.
20. Chan LS, Hammerberg C, Kang K, Sabb P, Tavakkol A, Cooper KD. Human dermal fibroblast interleukin-1 receptor antagonist (IL-1ra) and interleukin-1 beta (IL-1 beta) mRNA and protein are co-stimulated by phorbol ester: implication for a homeostatic mechanism. J Invest Dermatol. 1992;99(3):315-22. PubMed PMID: 1387412.
21. Mihret A, Bekele Y, Bobosha K, Kidd M, Aseffa A, Howe R, et al. Plasma cytokines and chemokines differentiate between active disease and non-active tuberculosis infection. The Journal of infection. 2013;66(4):357-65. doi: 10.1016/j.jinf.2012.11.005. PubMed PMID: 23178506.
22. Chegou NN, Black GF, Kidd M, van Helden PD, Walzl G. Host markers in QuantiFERON supernatants differentiate active TB from latent TB infection: preliminary report. BMC pulmonary medicine. 2009;9:21. Epub 2009/05/19. doi: 10.1186/1471-2466-9-21. PubMed PMID: 19445695; PubMed Central PMCID: PMCPmc2696407.
23. Biselli R, Mariotti S, Sargentini V, Sauzullo I, Lastilla M, Mengoni F, et al. Detection of interleukin-2 in addition to interferon-gamma discriminates active tuberculosis patients, latently infected individuals, and controls. Clinical microbiology and infection : the official

publication of the European Society of Clinical Microbiology and Infectious Diseases. 2010;16(8):1282-4. doi: 10.1111/j.1469-0691.2009.03104.x. PubMed PMID: 19886902.

24. Borgstrom E, Andersen P, Atterfelt F, Julander I, Kallenius G, Maeurer M, et al. Immune responses to ESAT-6 and CFP-10 by FASCIA and multiplex technology for diagnosis of M. tuberculosis infection; IP-10 is a promising marker. PloS one. 2012;7(11):e43438. Epub 2012/11/13. doi: 10.1371/journal.pone.0043438. PubMed PMID: 23144772; PubMed Central PMCID: PMCPmc3493549.

25. Biancotto A, Wank A, Perl S, Cook W, Olnes MJ, Dagur PK, et al. Baseline levels and temporal stability of 27 multiplexed serum cytokine concentrations in healthy subjects. PloS one. 2013;8(12):e76091. Epub 2013/12/19. doi: 10.1371/journal.one.0076091. PubMed PMID: 24348989; PubMed Central PMCID: PMCPmc861126.

26. Clifford V, Tebruegge M, Zufferey C, Germano S, Denholm J, Street A, et al. Serum IP-10 in the diagnosis of latent and active tuberculosis. The Journal of infection. 2015;71(6):696-8. doi: 10.1016/.inf.2015.08.001. PubMed PMID: 26271898.

Relative resistance of HLA-B to down-regulation by naturally occurring HIV-1 Nef sequences

Macdonald Mahiti1,2,$, Mako Toyoda1,$, Xiaofei Jia3, Xiaomei T. Kuang4, Francis Mwimanzi1, Philip Mwimanzi1,4, Bruce D Walker5,6,7, Yong Xiong3, Zabrina L Brumme4,8, Mark A Brockman4,8, Takamasa Ueno1,2

1Center for AIDS Research, and 2International Research Center for Medical Sciences (IRCMS), Kumamoto University, Kumamoto, Japan; 3Department of Molecular Biophysics and Biochemistry, Yale University, New Haven, CT, USA; 4Simon Fraser University, Burnaby, BC, Canada; 5Ragon Institute of MGH, MIT and Harvard University, Boston, MA, USA, 6Division of Infectious Diseases, Massachusetts General Hospital, USA; 7Howard Hughes Medical Institute, USA, 8British Columbia Centre for Excellence in HIV/AIDS, Vancouver, BC, Canada

$MM and MT contributed equally to this work.

Running Title: HLA-B resists down-regulation by primary HIV-1 Nef

Abstract

HIV-1 Nef binds to the cytoplasmic region of HLA-A and HLA-B and down-regulates these molecules from the surface of virus-infected cells, thus evading immune detection by $CD8^+$ T cells. Polymorphic residues within the HLA cytoplasmic region may affect Nef's down-regulation activity. However the impact of HLA polymorphisms on recognition by primary Nef isolates remains elusive, as do the specific Nef regions responsible for down-regulation of HLA-A *versus* HLA-B. Here, we examined 46 Nef clones isolated from chronically HIV-1 subtype B-infected subjects for their ability to down-regulate various HLA-A, HLA-B, and HLA-C molecules on the surface of virus-infected cells. Overall, HLA-B exhibited greater resistance to Nef-mediated down-regulation compared to HLA-A, regardless of cell type examined. As expected, no Nef clone down-regulated HLA-C. Importantly, the differential ability of patient-derived Nef clones to down-regulate HLA-A and HLA-B inversely correlated with the sensitivity of HIV-infected target cells to recognition by effector cells expressing an HIV-1 Gag-specific T cell receptor. Nef codon-function analysis implicated amino acid variation at position 202 (Nef-202) in differentially affecting HLA-A and HLA-B down-regulation ability, an observation that was subsequently confirmed by site-directed mutagenesis. In silico and mutagenesis analyses further suggested that Nef-202 may interact with the C-terminal Cys-Lys-Val residues of HLA-A, which are absent in

HLA-B. Taken together, natural polymorphisms within Nef modulate its interaction with natural polymorphisms in the HLA cytoplasmic tails, thereby affecting the efficiency of HLA down-regulation and consequent recognition by HIV-specific T cells. Results thus extend our understanding of this complex pathway of retro
viral immune evasion.

Importance

Recognition of genetically diverse pathogens by the adaptive immune system represents a primary strategy for host defense, however pathogens such as HIV-1 can evade these responses to achieve persistent infection. The HIV-1 *nef* gene and the *hla class I* locus rank among the most diverse genes of virus and host, respectively. The HIV-1 Nef protein interacts with the cytoplasmic region of HLA-A and HLA-B and down-regulates these molecules to evade cellular immunity. By combining molecular, genetic, and in silico analyses, we demonstrate that patient-derived Nef clones down-regulate HLA-A more effectively than HLA-B molecules. This in turn modulates the ability of HIV-specific T cells to recognize HIV-infected cells. We also identify a naturally polymorphic site at Nef codon 202 and HLA cytoplasmic motifs ($GG_{314,315}$ and $CKV_{339\text{-}341}$) that contribute to differential HLA down-regulation by Nef. Our results highlight new interactions between HIV-1 and the human immune system that may contribute to pathogenesis.

Introduction

The HLA class I (HLA-I) gene region, comprising *HLA-A, HLA-B,* and *HLA-C* loci, ranks among the most polymorphic regions in the human genome, with 2,735 *HLA-A*, 3,455 *HLA-B* and 2,259 *HLA-C* alleles identified to date (IMGT HLA database; http://www.ebi.ac.uk/ipd/imgt/hla/) (see reviews, (1, 2)). HLA-I polymorphism is mainly concentrated within exons 2 and 3 (1) which primarily form the antigenic peptide-binding groove of the HLA-I complex (3) and play an important role in restricting $CD8^+$ T lymphocyte specificity. Other exons also exhibit polymorphism, albeit to a lesser extent. For example, HLA-A, HLA-B, and HLA-C alleles can be classified into 5, 2, and 7 polymorphic types, respectively, based on sequence variations within their cytoplasmic domains (encoded by exons 5 through 7 for HLA-B or 5 through 8 for HLA-A and HLA-C). Polymorphism in the cytoplasmic domain also influences receptor expression: for example, a unique amino acid conserved in all HLA-C allotypes (Ile-337, rather than Thr-337 in HLA-A and HLA-B) yields lower cell surface expression of HLA-C compared to HLA-A and HLA-B (4). However, the implications of HLA cytoplasmic polymorphisms on modulating antiviral immunity remain incompletely understood.

HLA-I restricted $CD8^+$ cytotoxic T lymphocyte (CTL) responses are important for controlling a wide range of viral infections (5, 6) including HIV-1 (7, 8), human T-cell leukemia virus type 1 (HTLV-1) (9), cytomegalovirus (10) and herpes simplex virus (11). In turn, viruses have evolved various mechanisms to evade HLA-I-restricted antiviral immunity, such as inhibiting intracellular antigen processing pathways and down-regulating HLA-I molecules from the infected cell surface (see reviews for (12-14)). In HIV-1, the 27-35 kDa accessory protein Nef down-regulates HLA-A and HLA-B molecules from the surface of HIV-1-infected cells (15, 16). Nef does not down-regulate HLA-C molecules due to the presence of unique residues at codons 320 and 327 in their cytoplasmic regions (17). As such, the antiviral activities of HLA-A and HLA-B-restricted CTLs are substantially reduced by Nef expression (18-20) whereas the antiviral activities of HLA-C-restricted CTLs are unaffected by Nef (21). Maintenance of HLA-C expression allows virus-infected cells to escape recognition by the innate immune system, as down-regulation of all HLA-I molecules would render HIV-infected cells susceptible to recognition by Natural Killer cells (22). Importantly, it was recently demonstrated that chimeric HLA-A02 molecules expressing various HLA-A and HLA-B cytoplasmic tails are differentially susceptible to Nef-mediated down-regulation and that this in turn has implications for infected cell recognition by HLA-A02-restricted CTLs (23). However, all prior studies focused on a limited number of prototypic laboratory-adapted HIV-1 strains (22, 23). It is thus unclear whether highly diverse naturally occurring (patient-derived) Nef sequences also display differential HLA-A *versus* HLA-B down-regulation ability, and if so, which Nef residue(s) modulate these interactions.

Nef ranks among the most diverse HIV-1 proteins (24, 25). Primary Nef clones isolated from patients at various infection stages and/or with different disease phenotypes exhibit substantial functional heterogeneity (26-31), including wide-ranging HLA-I down-regulation capacities (26, 28-30, 32-35). However, previous studies investigated a variety of HLA-I allotypes using different target cells and antibodies; as such, the possibility that these differences are influenced in part by experimental conditions cannot be conclusively ruled out. In this study, we assessed 46 subtype B Nef clones isolated from the same number of chronically HIV-1-infected patients for their ability to down-regulate various HLA-A, HLA-B, and HLA-C allotypes. Individual primary Nef clones exhibited differential ability to down-regulate HLA-I allotypes, with HLA-B molecules exhibiting decreased susceptibility to Nef-mediated down-regulation compared to HLA-A (whereas HLA-C was resistant to Nef's effects). Differential Nef-mediated downregulation of HLA-A versus HLA-B molecules in turn modulated the ability of HIV-specific effector T-cells to recognize HIV-infected target cells. By combining

statistical analysis, site-specific mutagenesis and structural interpretation, we identified natural polymorphisms within Nef and HLA cytoplasmic sequences that contribute to Nef's differential ability to down-regulate HLA-A and HLA-B molecules.

Results

Differential down-regulation of HLA-A, HLA-B, and HLA-C by HIV-1 laboratory strains.

To investigate differential down-regulation of various HLA-A, HLA-B, and HLA-C allotypes by HIV-1 Nef, we stably transfected HLA class I-deficient 721.221 cells with HLA-A*02:01 (A02), HLA-A*24:02 (A24), HLA-A*33:01 (A33), HLA-B*35:01 (B35), HLA-B*57:01 or HLA-C*04:01 (C04). Cytoplasmic tails of HLA-B molecules are three amino acids shorter than those of HLA-A and HLA-C molecules (Fig. 1A). Moreover HLA-A allotypes harbor aspartic acid and arginine at codons 314 and 315, respectively ($DR_{314,315}$); whereas HLA-B and HLA-C allotypes harbor dual glycines ($GG_{314,315}$). There are additional amino acid differences within the cytoplasmic regions between individual allotypes (Fig.1A). Cell surface expression of HLA-I molecules on 721.221 cells was stable and substantial (Fig. 1B, top row). Specifically, surface expression of the three HLA-A (A02, A24, and A33) and two HLA-B (B35 and B51) allotypes was comparable when stained with the pan-HLA specific mAb w6/32, whereas surface expression of an HLA-C allotype (C04) was lower, as expected. No changes in cell surface HLA-I expression were observed in cells infected with the HIV-1 reference strain NL43 engineered to lack Nef (NL43-ΔNef) (Fig. 1B middle row). In contrast, when cells were infected with vesicular stomatitis virus envelope glycoprotein (VSV-g)-pseudotyped $HIV\text{-}1_{NL43}$ expressing the Nef gene from the prototypic laboratory strain SF2 ($NL43\text{-}Nef_{SF2}$), all HLA-A and HLA-B allotypes were down-regulated from the cell surface whereas the HLA-C allotype was unaffected (Fig. 1B bottom row). As described in the methods, HLA-I down-regulation activity was quantified using a scale from 0% (denoting no HLA-I down-regulation activity in virus-infected cells) to 100% (denoting complete down-regulation activity). The greater the down-regulation activity value, the lower the residual cell surface expression of HLA-I. $Nef_{SF2's}$ ability to downregulate individual HLA-A and HLA-B molecules varied to some extent: down-regulation values, by allotype, were A02 (mean 71.4% ±standard deviation 3.1%), A24 (61.2%±3.7%), A33 (57.4%±2.4%), B35 (50.1%±2.4%) and B57 (52.4% ±3.1%) (Fig. 1C). Importantly, NefSF2's ability to down-regulate HLA-A alleles consistently exceeded that of HLA-B (Mann-Whitney, $p<0.001$). Two other laboratory HIV-1 Nef strains, NefNL43 and NefJRFL, were also evaluated for their ability to down-regulate A24 and B35 (Fig. S1). In both cases, their ability to down-regulate HLA-A exceeded that of HLA-B (Mann-Whitney, $p<0.001$), and neither

down-regulated C04.

Differential down-regulation of HLA-A, HLA-B, and HLA-C by natural Nef sequences.

We next assessed whether patient-derived Nef sequences differed in their ability to down-regulate HLA-A, HLA-B, and HLA-C allotypes. For these experiments we used 721.221 cells stably expressing A24, B35, and C04 as allotype representatives. A24 and B35 were chosen because they exhibited susceptibility to Nef-mediated down-regulation similar to the median values of the HLA-A and HLA-B allotypes tested (Fig. 1C); while C04 was chosen because the 721.221 cells expressing this allele exhibited the most stable cell surface HLA-C expression among our panel of 721.221 cells engineered to express various HLA-C allotypes. Representative HLA-I down-regulation data, derived from cells infected with HIV-1 NL43-derived strains encoding Nef clonal sequences from three chronic progressors (subjects CP66, 84, and 90) are shown in Fig. 2A. The three patient-derived Nef clones varied in their ability to down-regulate A24 and B35, but none down-regulated C04. For example, CP66-Nef's B35 down-regulation activity was 23%, which was approximately half of that of NefSF2 (49%, Fig. 1B). In contrast, CP84-Nef's A24 and B35 down-regulation activities of 66% and 56% respectively, were comparable to NefSF2. CP90-Nef down-regulated A24 and B35 by equivalent, but also relatively lower, levels (38% and 41%, respectively).

To quantify the ability of naturally occurring Nef sequences to down-regulate A24 and B35, we expanded this analysis to 46 patient-derived Nef clones. All 46 Nef clones displayed greater ability to down-regulate A24 (median activity of 60.8% [IQR 54.2-65.5]) compared to B35 (median activity 49.3% [IQR 41.0-55.5]) (Fig. 2B), a difference that was highly statistically significant (Mann-Whitney, $p<0.001$). No clone down-regulated C04. To quantify each virus' ability to differentially down-regulate A24 *versus* B35, we expressed the down-regulation values as pairwise ratios. Overall, the median ratio of A24/B35 down-regulation activity of patient-derived Nef clones was 1.25 [IQR 1.09-1.37], a value that differed significantly from the null expectation of a ratio of 1.0 (Wilcoxon one sample test, $p<0.001$) (Fig. 2C).

Cells normally express two different allomorphs of each of HLA-A, HLA-B, and HLA-C (homozygotes excepted). As such, a maximum of four different HLA-A and HLA-B allomorphs normally compete for Nef binding in infected cells (which differs from our 721.221 cell system where HLA alleles are expressed singly). We therefore tested Nef-mediated down-regulation of HLA-A and HLA-B in the T1 human $CD4^+$ cell line that endogenously expresses four different HLA-A and HLA-B alleles (see Methods). Among them, HLA-A*02:01 (A02) and HLA-B*51:01 (B51) are specifically detectable by mAbs for HLA-A2 (clone BB7.2) and alleles belonging to the HLA-Bw4 serotype group (clone TU109), respectively. The cytoplasmic tails of A02 and A24 differ by a single amino acid (Fig. 1A)

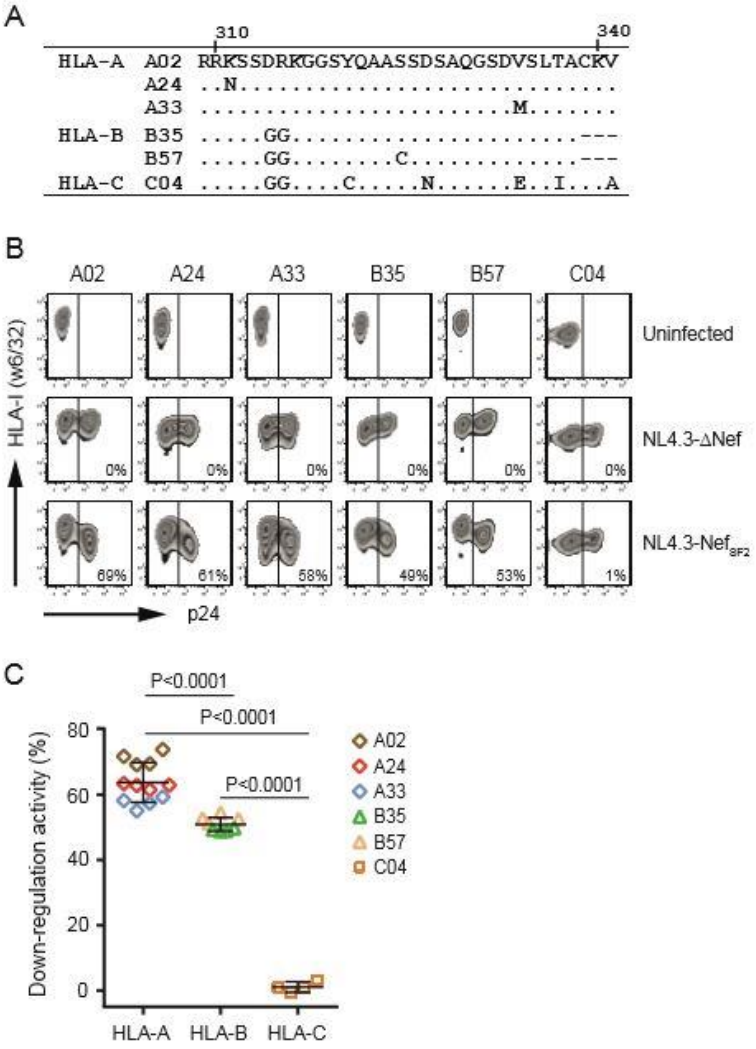

Fig. 1 Down-regulation of HLA-A, HLA-B, and HLA-C by laboratory SF2 Nef strain.

(A) Amino acid sequence of the cytoplasmic tails of HLA-A*02:01 (A02), A*24:02 (A24), A*33:01 (A33), B*35:01 (B35), B*57:01 (B57) and C*04:01 (C04) proteins. Dots denote amino acid residues identical to A02 and dashes denote the absence of amino acids at that position. (B) HLA-I-deficient 721.221 cells stably transfected with the indicated HLA-I molecule were infected with recombinant HIV-1 lacking Nef (ΔNef) or carrying Nef_{SF2}. Uninfected cultures were also used as controls. The cells were stained with an antibody to HLA class I (clone: w6/32), followed by intracellular staining with antibody to p24 Gag. Nef-mediated HLA down-regulation activities are shown on the flow cytometry plots. These values were calculated as the difference in HLA-I mean fluorescence intensity between the p24-negative and the $p24^+$ subsets divided by that of the p24-negative subset. (C) Quantitative assessment of Nef_{SF2}-mediated downregulation activity toward HLA-A, HLA-B and HLA-C alleles. Symbols denote measurements obtained from experiments performed in quadruplicate. Horizontal bars denote median and interquartile ranges. The Mann-Whitney U test was used to calculate statistical significance.

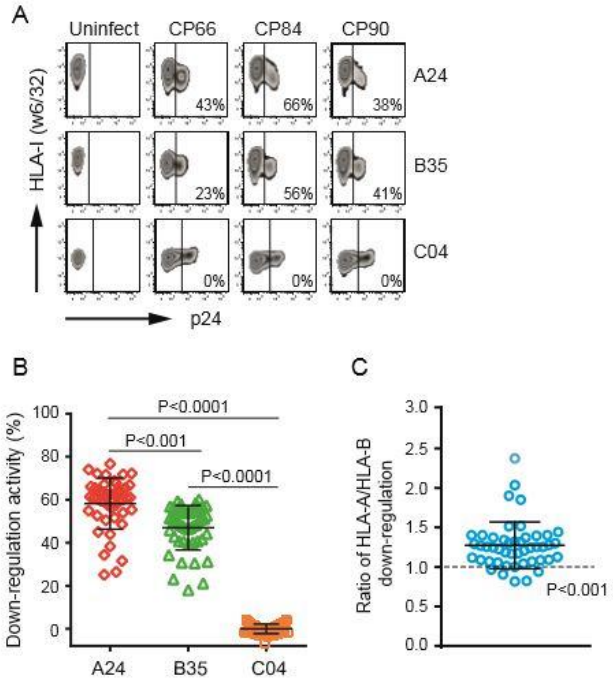

Fig. 2 Down-regulation of HLA-A, HLA-B, and HLA-C by primary Nef clones.

(A) 721.221 transfectants expressing A24, B35 or C04 were infected with recombinant viruses carrying Nef clones isolated from 46 HIV-infected patients. Three representative flow cytometry plots for the Nef clones from the patients, CP66, CP84, and CP90, are shown. Nef-mediated HLA-I down-regulation activities determined as above are indicated in the plots. (B) HLA-I down-regulation activity in 721.221 transfectants expressing A24, B35 or C04 by 46 patient-derived Nef clones are shown. Horizontal bars denote median and interquartile ranges. Each plot represents the mean of 3-4 independent assays. Statistical analysis was done by Mann-Whitney U test. (C) Ratio of down-regulation activity of A24 and B35 by 46 primary Nef isolates is shown. Horizontal bars denote median and interquartile ranges. Dotted line represents the null expectation of a ratio of 1.0. Statistical analysis was done by Wilcoxon one sample test.

Table 1. Nef amino acid residues associated with down-regulation ratios of HLA-A/HLA-B in 721.221 cells.

Nef codon[a]	AA[b]	Activity ratios[c]		No. of Subjects[d]		p value	q value
		AA+	AA-	AA+	AA-		
158	Glu	1.30	1.07	33	12	0.00064	0.13
202	Tyr	1.23	1.65	40	6	0.0017	0.17

[a]amino-acid codon numbers of Nef are as Nef_{HXB2}; [b]AA, amino acid residues; [c]median ratios of down-regulation activity of HLA-A*24/HLA-B*35; [d]the number of the subjects' sequences with or without the amino acid residue at the corresponding position, with the row total varies as the gap in the aligned sequence is considered as the missing data.

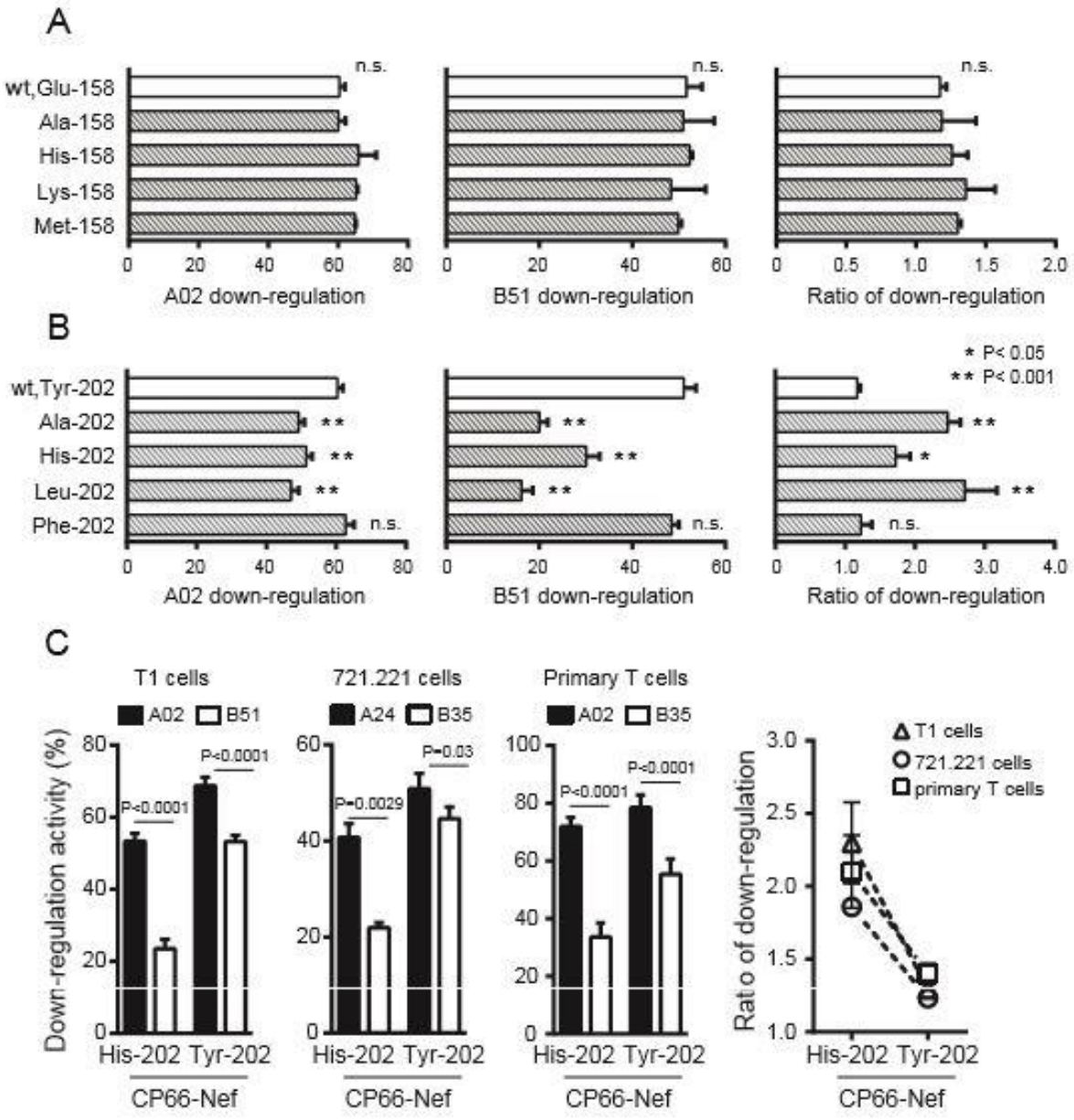

Fig. 3 Effect of defined Nef mutations on HLA-A and HLA-B down-regulation activity

(A, B) Nef_{SF2} and its variants at position 158 (*panel A*) and 202 (*panel B*) were tested for down-regulation activity toward A02 and B51 in T1 cells. The ratios of A02 versus B51 were also determined. Data shown are the mean ± SD of 3-4 independent experiments. Statistical analysis was performed by ANOVA with multiple comparisons *versus* wt. n.s., not significant. (C) CP66-Nef clones encoding His-202 and Tyr-202 were tested for down-regulation activity in T1 cells (for A02 and B51), 721.221 cells (A24 and B35), and human primary T lymphocytes isolated from an HIV-negative donor (expressing A02 and B35). The ratios of HLA-A and HLA-B down-regulation activity are also shown. Data shown are the mean ± SD of 3-4 independent experiments. Statistical analysis was performed by paired t test. Similar data were obtained using primary T lymphocytes isolated from another HIV-negative donor.

whereas that of B51 is identical to B35. Again, Nef_{SF2} down-regulated A02 more potently than B51 in T1 cells, with activity (mean ± SD) of 60.3 ± 1.6 and 51.6 ± 3.4, respectively (t test, $p<0.0001$). Moreover, all 46 patient-derived Nef clones down-regulated A02 (median 58.3 [IQR 54.5-63.2]) more potently than B51 (median 47.7 [IQR 44.2-50.7]) (Mann-Whitney, $p<0.0001$) (Fig. S2A). These values yielded a median ratio of A02/B51 down-regulation in T1 cells by patient-derived Nef of 1.24 [IQR 1.18 - 1.29] (Fig. S2B), which was again significantly different from the null expectation of a ratio of 1.0 (Wilcoxon one sample test, $p<0.001$).

HIV-1 Nef codons associated with differential HLA-A and HLA-B down-regulation

We next performed a pairwise Nef codon-function analysis to identify Nef amino acid residues associated with A24 and B35 down-regulation function. At the predefined threshold of $p<0.05$, $q<0.2$, no Nef residues were identified as being associated with A24 or B35 down-regulation ability (data not shown). However, when the analysis was performed using the A24/B35 down-regulation ratio as the functional variable, Nef clones carrying Glu-158 exhibited significantly higher A24/B35 down-regulation ratios than those carrying another amino acid at this site ($p=0.00064$, $q=0.13$). In contrast, Nef clones carrying Tyr-202 exhibited significantly lower ratios than those carrying another amino acid

at this site ($p=0.0017$, $q=0.17$) (Table 1). Using the T1 cell results as an independent validation dataset, we confirmed that Tyr-202 significantly associated with lower ratios (Mann-Whitney, $p=0.04$) while Glu-158 showed a trend towards higher ratios, though this was not statistically significant ($p=0.11$). These results suggested that amino acid residues at HIV-1 Nef codons 158 and 202 may play a role in this protein's differential recognition of HLA-A *versus* HLA-B allotypes.

Variation at Nef-202 modulates HLA-A and HLA-B down-regulation

To examine the effects of amino acid residues at 158 and 202 on selective down-regulation of HLA-A and HLA-B, we introduced various amino acid substitutions at these sites into Nef_{SF2} and analyzed the function of mutant viruses. We introduced Ala, His, Lys, and Met substitutions at codon 158 (wild type Glu), and Ala, His, Leu, and Phe substitutions at codon 202 (wild type Tyr). These substitutions included naturally occurring residues (Ala, Lys and Met at 158; His, Leu and Phe at 202) as well as residues not observed in natural Nef sequences (His at 158 and Ala at 202), as determined in our cohort and in N=1,470 publically available subtype B Nef sequences in the Los Alamos HIV sequence database. Steady-state levels of wild-type Nef protein and variants were comparable in virus-producing cells (data not shown). We then tested the Nef variants for A02 and B51 down-regulation activity in T1 cells. No mutation at 158 substantially influenced A02 or B51 down-regulation activity nor A02/B51 down-regulation ratios (Fig. 3A). In contrast, all mutations at codon 202 except Phe significantly decreased

Nef-mediated down-regulation of both A02 and B51 in T1 cells, compared to wild-type Tyr-202 (Fig. 3B). Moreover, these mutations impaired B51 down-regulation activity to a greater extent than A02, resulting in corresponding A02/B51 down-regulation ratios that were also significantly higher (Fig. 3B). Specifically, the A02/B51 down-regulation ratios for the Ala, His, and Leu-202 mutations were 2.47 ± 0.18, 1.72 ± 0.21, and 2.55 ± 0.42, respectively, values that were 2.1-, 1.5- and 2.2-fold higher, respectively, than wild type Nef_{SF2} (Tyr-202). Consistent results were also obtained in 721.221 cells expressing A24 and B35 (Fig. S3).

To further confirm the effect of Nef-202 on differential HLA-A and HLA-B down-regulation, we introduced a His-to-Tyr mutation into patient CP66's Nef clone at codon 202, thereby "reverting" this clone to the wild-type sequence at this position. This particular patient clone was chosen as it exhibited substantially impaired HLA-B down-regulation activity in T1 cells (A02/B51 down-regulation ratio 2.30 ± 0.28), 721.221 cells (A24/B35 down-regulation ratio 1.86 ± 0.04) and primary T cells (A02/B35 down-regulation ratio 2.16 ± 0.25) (Fig. 3C). Introduction of the His-to-Tyr reversion substantially increased both A02 and B51 down-regulation activity in T1 cells, A24 and B35 down-regulation activity in 721.221 cells, and A02 and B35 down-regulation activity in primary T cells (Fig. 3C). As the extent of functional rescue by this reversion was more pronounced for HLA-B compared to HLA-A allotypes, the ratio of HLA-A/HLA-B down-regulation activity of CP66-Nef decreased to 1.29 ± 0.06 in T1 cells, 1.23 ± 0.01 in 721.221 cells, and 1.43 ± 0.07 in primary T cells, values that are comparable to the median of patient-derived Nef clones (Fig. 2C). These data indicate that the amino acid polymorphism at Nef-202 alone can modulate Nef's ability to down-regulate HLA-B, and to a lesser extent HLA-A allotypes.

HLA-I cytoplasmic motifs that modulate sensitivity to Nef-mediated down-regulation

Nef-mediated down-regulation of cell surface HLA-I molecules occurs through interaction between the HLA cytoplasmic domain and Nef in conjunction with the clathrin adaptor protein complex 1 (AP1) (17, 36, 37). We sought to identify HLA-I cytoplasmic motifs that determine sensitivity to Nef-mediated down-regulation. As shown in Fig. 1A, HLA-A and HLA-B alleles differ in their amino acid residues at codons 314 and 315 as well as the presence (HLA-A) or absence (HLA-B) of the C-terminal Cys-Lys-Val ($CKV_{339\text{-}341}$) motif. We therefore created a chimeric A02 molecule possessing the cytoplasmic tail of B35 by introducing a $GG_{314,315}$ mutation into A02 and additionally deleting its C-terminal $CKV_{339\text{-}341}$ motif, and designated this sequence $A02_{GG,\,\Delta CKV}$. We then established Jurkat T cells stably expressing A02 and $A02_{GG,\,\Delta CKV,}$ which exhibited similar cell-surface expression of these molecules upon staining with anti-A2 antibody (MFI: 5664 ± 226 and 4989 ± 263, respectively) (Fig. 4A). Infection of these cells with an HIV-1 NL43

strain encoding NefSF2 resulted in down-regulation of A02 and $A02_{GG, \Delta CKV}$ to similar levels (Fig. 4A and Fig. 4B). As expected, introduction of the His-202 mutation into Nef_{SF2}, impaired its ability to down-regulate both A02 and $A02_{GG, \Delta CKV,}$ with the latter to a greater extent. Specifically, introduction of His-202 increased the A02/$A02_{GG, \Delta CKV}$ down-regulation ratio from 1.03 to 1.82, a 1.8-fold increase (Fig. 4C). Complementary results were obtained with the parental (His-202) and wild-type "revertant" (Tyr-202) CP66-Nef sequences. Specifically, the CP66 Tyr-202 "revertant" mutant exhibited A02 down-regulation activity comparable to NefSF2 and moderately lower $A02_{GG, \Delta CKV}$ down-regulation compared to Nef_{SF2} (Fig. 4A and 4B). In contrast, the parental CP66-Nef (His-202) exhibited substantially impaired $A02_{GG, \Delta CKV}$ down-regulation activity. Overall, the Tyr-to-His substitution increased the A02/$A02_{GG, \Delta CKV}$ down-regulation ratio of CP66-Nef from 1.15 to 2.86, a 2.5-fold increase (Fig. 4C).

We further investigated potential interactions between Nef codon 202 and the cytoplasmic tails of A02 and $A02_{GG, \Delta CKV}$ by examining the existing crystal structure of the A02 cytoplasmic tail and Nef in complex with the µ1 subunit of AP1 (37). This crystal structure exhibits that Tyr-202 of Nef involves in contacting a portion of the µ1 subunit of AP1 and forming a part of the groove for HLA-I binding (37) (Fig. 5A, 5B). Although the crystal structure did not include A02's cytoplasmic tail entirely (the last residue observed in the structure is Gly-331, which lies seven residues upstream of the C-terminal $CKV_{339-341}$ that is present in A02 but absent in HLA-B alleles, since the remaining region is disordered in three-dimensional space), the proximity of Gly-331 to the main chain atoms of Nef Tyr-202 suggested that $CKV_{339-341}$ could also be located nearby. Indeed, modeling of a seven-amino-acid spacer following Gly-331 indicated that $CKV_{339-341}$, could readily be positioned next to the side chain of Nef Tyr-202 for potential interaction (Fig. 5B). In contrast, the $DR_{314,315}$ residues of HLA-A, present in the crystal structure, do not directly contact any Nef residues (Fig. 5A). These data suggest that Nef codon 202 and the C-terminal $CKV_{339-341}$ motif present in HLA-A but not HLA-B alleles, in conjunction with the µ1 subunit of clathrin AP1, may form an interaction that enhances down-regulation of HLA-A over HLA-B.

Effects on T cell recognition

We postulated that Nef's differential ability to down-regulate HLA-A and HLA-B molecules would have consequences for T cell recognition of viral antigens presented on the surface of HIV-infected cells (18-20, 35). To test this hypothesis, we used a published reporter cell Co-culture assay that features

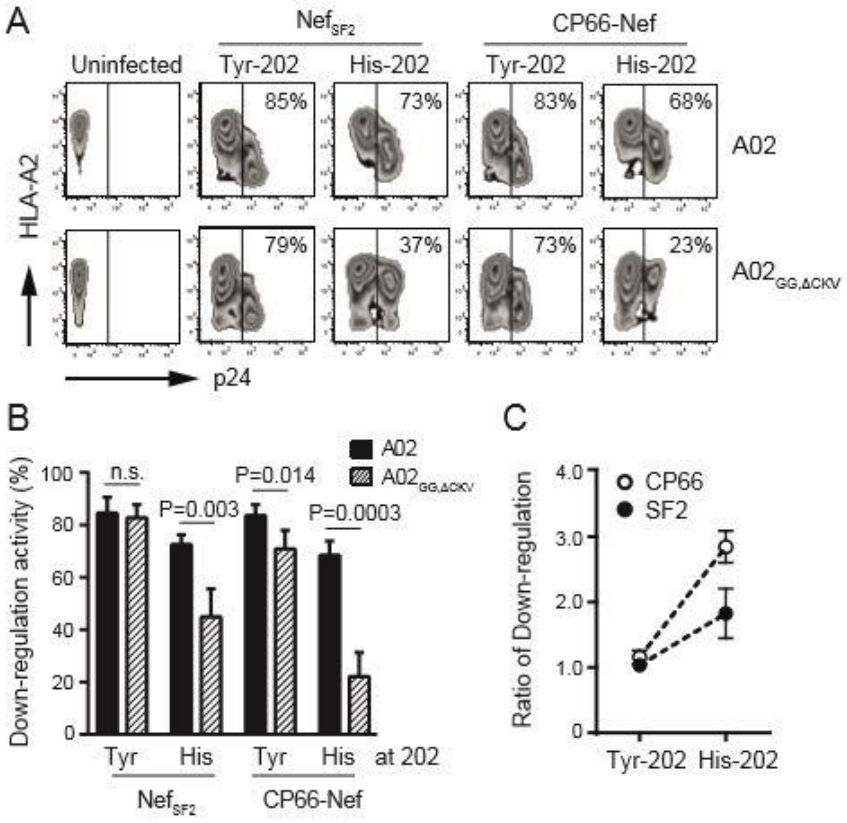

Fig. 4 Effects of HLA-I cytoplasmic tail polymorphisms on Nef-mediated HLA-A and HLA-B down-regulation activity.

(A) The amino acid sequence of the cytoplasmic region of A02 was mutated to encode $GG_{314,315}$ and a C-terminal deletion of the $CKV_{339\text{-}341}$ motif, resulting in a cytoplasmic sequence identical to B35 ($A02_{GG,\Delta CKV}$; see Fig. 1A). Jurkat transfectants stably expressing A02 and $A02_{GG,\Delta CKV}$ were infected by recombinant NL43 viruses encoding various Nef clones or remained uninfected. The Nef clones tested were Nef_{SF2}(Tyr-202), Nef_{SF2}(His-202), CP66-Nef (Tyr-202), and CP66-Nef (His-202). Representative flow cytometry plots are shown and the HLA down-regulation activities are indicated in the plots. (B, C) Quantitative assessment of the down-regulation activity (*panel B*) as well as the activity ratios (*panel C*) of A02 and $A02_{GG,\Delta CKV}$ are shown. The data shown are the mean ± SD of 3-5 independent assays. Statistical analysis was performed by paired t-test. n.s., not significant.

HLA-A*02:01-expressing target cells and HIV-1-specific "effector" cells that transiently express a T-cell receptor (TCR) specific for an HLA-A*02:01-restricted HIV-1 epitope in Gag (FK10; $Gag_{433\text{-}442}$: FLGKIWPSYK), human CD8-α chain, and an NFAT-driven luciferase construct (see methods). When target cells are infected with HIV, endogenously-derived viral peptide antigens are processed and presented in complex with A02 on their surface, though the HIV Nef protein counteracts this by down-regulating HLA-I. When HIV-infected target cells are co-cultured with A02-FK10-specific reporter cells, TCR-dependent signaling can be quantified based on luminescence. The ability of a given

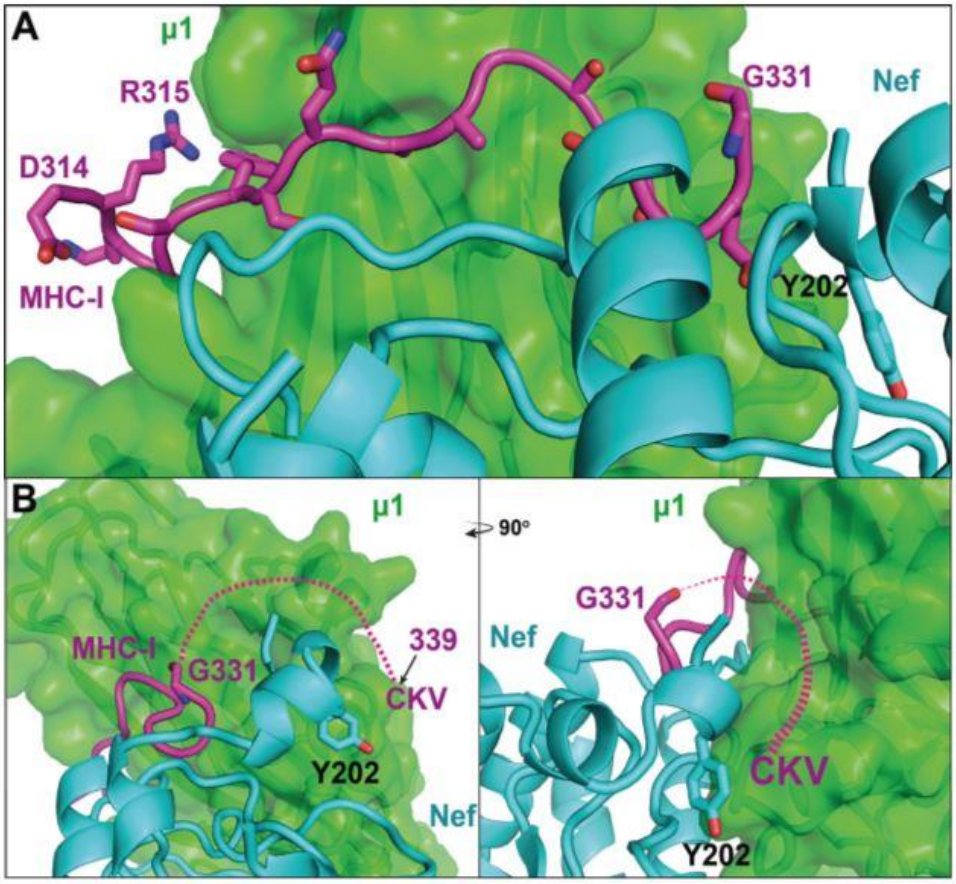

Fig. 5 Structural analysis of interaction between HLA-I cytoplasmic tail and Nef

(A) Interactions between A02 cytoplasmic domain, Nef and μ1 subunit of adaptor protein 1 (AP1) are illustrated based on coordinates from the tri-partite structure (PDB: 4EN2). The $DR_{314,315}$ motif in the HLA-A cytoplasmic domain, which corresponds to $GG_{314,315}$ in the HLA-B cytoplasmic domain, is indicated. The C-terminus of HLA-A was not observed in the structure, however the last observed C-terminal residue, G331, is located close to Nef Tyr-202. (B) Modeling suggests that the $CKV_{339-341}$ motif may be located in the vicinity of the side chain of Nef Tyr-202, allowing it to make a molecular contact. Dotted line depicts a potential path of the seven amino acids, SDVSLTA, leading from G331 to the terminal $CKV_{339-341}$ motif in HLA-A.

Nef sequence to down-regulate HLA-I on the target cell thus correlates inversely with TCR-mediated luminescence signal in effector cells.

We first undertook the following control experiments. Target cells expressing either A02 or $A02_{GG, \Delta CKV}$ were pulsed with increasing concentrations of FK10 peptide, co-cultured with A02-FK10-specific reporter cells, and the TCR-mediated signal was quantified by luminescence (Fig. 6A). As expected, luminescence intensity correlated positively with increasing FK10 peptide concentration in both A02 and $A02_{GG, \Delta CKV}$ target cells. Moreover, the magnitude of luminescence

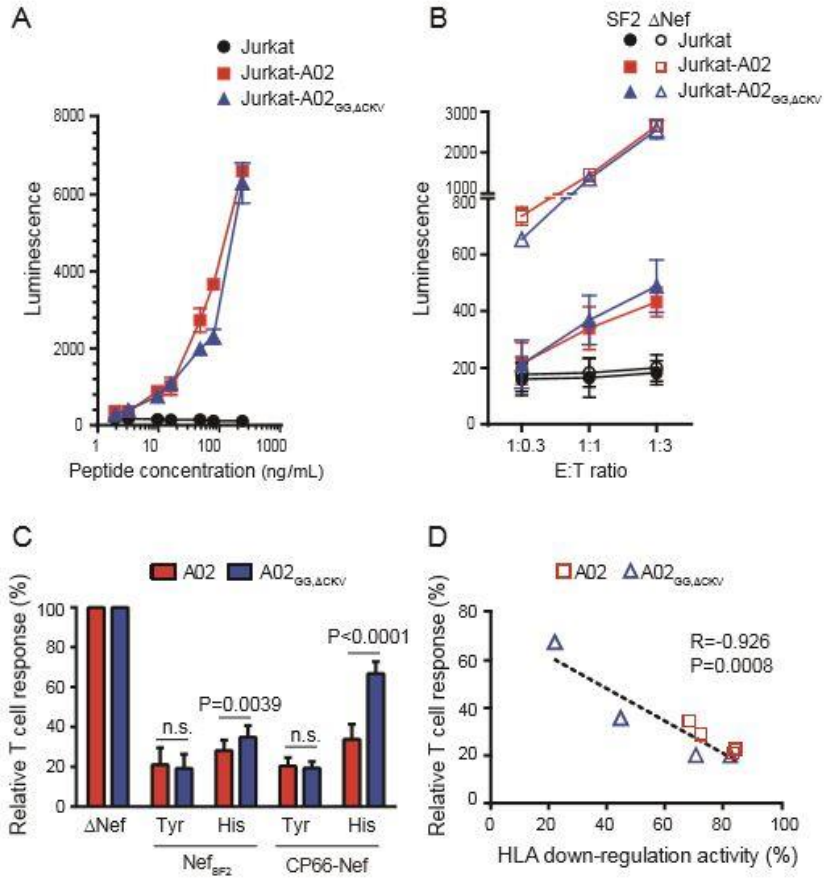

Fig. 6 Effect of differential Nef sensitivity to HLA-A and HLA-B on antigen-specific TCR recognition

(A) Luciferase-reporter effector T cells expressing an HLA-A*02-restricted HIV-1 Gag FK10-specific TCR were incubated with parental Jurkat target cells or Jurkat cells stably expressing A02 or $A02_{GG,\Delta CKV}$ in the absence or presence of the increasing concentrations of synthetic FK10 peptide at an E:T ratio of 1. T cell recognition is shown as luminescence signal detected at 6 hours. (B) The same effector cells were incubated with parental Jurkat target cells or those stably expressing A02 or $A02_{GG,\Delta CKV}$ that were infected with HIV-1 encoding NefSF2 or ΔNef at E:T ratios of 1:0.3, 1:1, or 1:3. T cell recognition is shown as luminescence signal detected at 6 hours. (C) The same effector cells were incubated with parental Jurkat target cells or those stably expressing A02 or $A02_{GG,\Delta CKV}$ infected with HIV-1 encoding Nef_{SF2}, CP66-Nef or their indicated residue 202 mutants. The relative T cell response was calculated as the luminescence signal at 6 hours, normalized to that of target cells infected with NL43ΔNef (set to 100%). Data shown for all panels represent the mean ± SD of 3-5 independent assays. Statistical analysis was performed by paired t-test. n.s., not significant. Over all experiments, background luminescence signal obtained by incubation of the effector cells alone was 141.5±20.2, and the frequency of HIV-infected cells within the target cell population as determined by intracellular expression of $p24^{Gag}$ protein was 45.7%±8.9%. (D) Correlation between relative T cell response and Nef's HLA down-regulation activity in both A02 and $A02_{GG,\Delta CKV}$-expressing cells infected with HIV-1 encoding Nef_{SF2}, CP66-Nef or their respective Nef-202 amino acid variants. Data for the relative T cell response and Nef's HLA down-regulation activity are derived from Fig. 6C and Fig. 4B, respectively. Statistical analysis was performed by Pearson's correlation analysis.

generated by effector cells was comparable regardless of whether A02 or $A02_{GG, \Delta CKV}$ target cells were used (Fig. 6A). This suggested that A02 and $A02_{GG, \Delta CKV}$ target cells were equally sensitive to recognition by A02-FK10-specific TCR. Importantly, no response was observed when parental target cells lacking HLA-A*02:01 were pulsed with FK10 peptide, confirming the HLA- and antigen-specific nature of the assay (Fig. 6A). Next, target cells were infected with HIV-1 NL43-Nef_{SF2} and ΔNef and incubated with effector cells at various effector:target (E:T) ratios (Fig. 6B). Effector cells cultured in the presence of A02 and $A02_{GG, \Delta CKV}$ target cells infected with HIV-1 NL43-ΔNef generated much greater luminescence signal compared to those cultured with control parental target cells lacking HLA-A*02:01. Furthermore, A02 and $A02_{GG, \Delta CKV}$ target cells stimulated comparable magnitudes of luminescence signal in effector cells across all E:T ratios examined (Fig. 6B). In contrast, effector cell responses were dramatically decreased when target cells were infected with NefSF2-expressing HIV-1 (Fig. 6B). Together,

these control experiments indicated that A02 and $A02_{GG, \Delta CKV}$ target cells were similarly functional as target cells and that wild-type Nef_{SF2} expression could substantially reduce T-cell recognition of HIV-infected cells.

We then tested effector T-cell responses following co-culture with target cells infected with HIV-1 expressing Nef_{SF2}, CP66-Nef or their respective Nef-202 mutants. Effector T cell responses toward these Nef^+ HIV-infected cells were quantified by luminescence and normalized to responses generated against HIV-1-ΔNef-infected target cells. Consistent with control experiments, effector T cell responses to A02 and $A02_{GG, \Delta CKV}$ target cells infected with HIV-1 Nef_{SF2} (encoding Tyr-202) were comparable in magnitude (Fig. 6C). In contrast, responses to $A02_{GG, \Delta CKV}$ target cells infected with HIV-1 Nef_{SF2} encoding the His-202 mutation were significantly higher compared to responses to A02 target cells infected with this virus (t test, $p=0.0039$) (Fig. 6C). Furthermore, while responses to A02 and $A02_{GG, \Delta CKV}$ target cells infected with the HIV-1-CP66-Nef (Tyr-202) revertant virus were comparable in magnitude and similar to those induced by Nef_{SF2}, we observed significantly greater T cell responsiveness towards $A02_{GG, \Delta CKV}$-expressing target cells infected with HIV-1 encoding the parental CP66-Nef (i.e., carrying the natural polymorphism His-202) compared to A02 target cells infected with the same virus (t test, $p<0.0001$) (Fig. 6C). Moreover, the magnitude of responses against the parental HIV-1-CP66-Nef virus was higher in both cells, compared to cells infected with HIV-1 strains encoding Nef_{SF2} or the CP66-Nef (Tyr-202) revertant. Finally, T cell responses as measured in this assay and Nef's HLA-I down-regulation activity as measured by flow cytometry showed a significant inverse relationship (Pearson, $R=-0.926$, $p=0.0008$) (Fig. 6D). Together, these results are consistent with our observation that the

naturally occurring His-202 mutation attenuates Nef's ability to down-regulate HLA-I, with a more pronounced impairment seen for HLA-B (here, modeled by the $A02_{GG, \Delta CKV}$ construct) compared to HLA-A. Our results further suggest that inefficient removal of HLA-B from the infected cell surface preferentially renders these cells more "visible" to HIV-specific, HLA-B-restricted effector T cells.

Discussion

In this study, we assessed the interplay between naturally occurring host (HLA-I) and virus (HIV-1 Nef) polymorphisms. We observed that HLA-B cytoplasmic tails display significantly decreased susceptibility to down-regulation by primary HIV-1 Nef clones compared to HLA-A cytoplasmic tails. On the host side, the relative resistance of HLA-B to down-regulation by patient-derived Nef clones appeared to be modulated by the $GG_{314,315}$ motif and/or the lack of C-terminal $CKV_{339\text{-}341}$ motif in the HLA-B cytoplasmic tail. On the viral side, HIV-1 Nef codon 202 was responsible, at least in part, for differential down-regulation of HLA-A and HLA-B allotypes by this protein. Importantly, results from our TCR recognition assays indicated that the differential susceptibility of HLA-I molecules to down-regulation by patient-derived Nef clones is likely to modulate T cell recognition of HIV-infected target cells presenting viral antigens in complex with HLA-I on their surface.

While it has long been known that HLA-B-restricted T cell responses exert a dominant influence on HIV-1 immune control (38, 39), it was not until recently that the relative resistance of HLA-B to Nef-mediated down-regulation was put forward as a possible underlying mechanism (23). The present study extends the previous work, which was performed using laboratory-adapted HIV-1 reference strains, by demonstrating that the majority of naturally occurring Nef sequences also down-regulate HLA-A to a greater degree than HLA-B. Our results thus identify differential susceptibility to HLA-A and HLA-B as a fundamental property of HIV-1 subtype B Nef sequences.

Introduction of various amino acid substitutions at Nef codon 202 (wild-type Tyr) substantially affected the protein's ability to down-regulate HLA-I, with greater impairment of HLA-B down-regulation compared to that of HLA-A. In particular, uncommon natural variants Leu and His, and unnatural variant Ala displayed this phenotype, while the common natural variant Phe conferred only modest effects compared to the wild-type Tyr. This provides a possible explanation for the relative frequency of these residues in natural subtype B HIV-1 Nef sequences. Of interest, the Nef Phe-202 polymorphism has been identified as being associated with host expression of HLA-A*30:01 and HLA-B*15:01 (40), suggesting that it may arise under immune selection pressure by these alleles *in vivo*, however we were unable to confirm this

experimentally due to limited availability of PBMC from this cohort. Also of interest, while Tyr and Phe are frequently observed at Nef codon 202 in all HIV-1 group M subtypes, the consensus at this residue in HIV-1 group O is Leu (Los Alamos HIV-1 sequence database). Given our observation that the Leu-202 substitution in Nef_{SF2} substantially increased the HLA-A/HLA-B downregulation ratio (Fig. 3B), it would be intriguing to investigate down-regulation of HLA-I molecules by naturally occurring HIV-1 group O Nef sequences.

Some limitations of this study merit mentioning. Although we investigated 46 patient-derived HIV-1 subtype B Nef clones, this panel of sequences did not capture the entirety of HIV-1 subtype B Nef genetic diversity. Nevertheless, relatively small subset of patient isolates exhibited a substantial dynamic range of HLA-A and HLA-B down-regulation function. Importantly, the majority of Nef clones was less able to down-regulate HLA-B compared to HLA-A molecules – an observation that remained true for all cell lines and primary T lymphocytes as well as all individual HLA alleles and cytoplasmic variants tested. As our goal was to investigate Nef-mediated HLA-A and HLA-B down-regulation on the surface of HIV-infected cells, we employed recombinant virus approaches (as opposed to transient transfection systems that are limited by Nef overexpression and potential cytotoxicity during plasmid delivery). Nevertheless, recombinant approaches are inherently limited by potential incompatibilities between insert and backbone (though all recombinant viruses were replication competent and demonstrated Nef polyfunctionality in various cell lines and primary T cells, as demonstrated in a previous published study of these clones (41)). The crystal structure of a ternary complex formed by Nef, the HLA-A02 cytoplasmic tail and the cargo-bonding µ1 subunit of AP1 was recently solved (37), yielding new insight into the molecular basis of Nef-mediated HLA-I down-regulation function. However, due to the disordered nature of the C-terminal end of the HLA-A02 cytoplasmic tail, this region was not included in the structure (37), rendering it impossible to directly investigate interactions between this region (notably the C-terminal $CKV_{339-341}$ motif) and Nef-202. Nevertheless, modeling of a seven-amino-acid spacer following Gly-331, the final residue of the HLA-A02 cytoplasmic tail observed in the structure, indicated that the $CKV_{339-341}$ motif could be positioned readily next to the side chain of Nef Tyr-202, supporting a possible interaction.

Despite these limitations, our study extends current understanding of Nef-mediated HLA-I down-regulation function by demonstrating that, on average, subtype B Nef sequences from untreated, chronically HIV-infected patients down-regulate HLA-A ~1.25-fold more efficiently than HLA-B. Moreover, these effects appear to be modulated, at least in part, by polymorphisms at Nef residue 202 as well as those located within the HLA-I cytoplasmic domain. Importantly, the

differential ability of Nef-mediated HLA-A and HLA-B down-regulation on HIV-infected cells modulates their subsequent recognition by HIV-specific T cells. Together, these results identify a new motif in HIV-1 Nef that differentially alters its ability to counteract HLA-A- and HLA-B-restricted CTL responses. Further studies will be necessary to determine whether Nef polymorphisms at residue 202 are associated with variation in immune-mediated control of infection or viral pathogenesis.

Materials and Methods

Patient-derived Nef clones and recombinant virus preparation

Recombinant viruses expressing patient-derived Nef clones in an HIV-1 NL43 proviral backbone were generated as part of previously published studies (28, 30, 41). Briefly, Nef sequences were isolated from plasma viral RNA of 46 HIV-1 subtype B chronically infected individuals recruited in the Boston area who were untreated at the time of sample collection, with median pVL 80500 [IQR 25121–221250] RNA copies/ml); median CD4 count 292.5 [IQR 72.5-440] cells/mm3, as described (30, 42, 43). This study was approved by the Institutional Review Boards at all relevant institutions and all participants provided written informed consent. Genbank accession numbers for clonal *nef* sequences used in this study are JX440926-JX440971 (41). To facilitate a consistent codon numbering scheme (based on the NefHXB2 reference strain), all clonal Nef sequences were pairwise-aligned to NefHXB2 and insertions stripped out. Patient-derived *nef* clones isolated as above were transferred into pNL43 plasmid and confirmed by sequencing as described (41). In addition, specific mutations (i.e., at Nef codons at 158 and 202) were introduced into the *nef* clone of SF2 strain using conventional overlapping PCR (33, 35) and the entire *nef* sequence was reconfirmed after subcloning into pNL43. The resultant DNA (5μg), along with a plasmid encoding vesicular stomatitis virus envelope glycoprotein (VSV-g) (1μg) was transfected into 10^6 293T cells and the virus-containing culture supernatants were harvested 48 hours later. Recombinant viruses harboring *nef* from HIV-1 subtype B reference strain SF2 (Nef_{SF2}), and lacking *nef* (ΔNef) were used as positive and negative controls, respectively, as previously described (30, 35).

Cells and antibodies for HLA analysis

Nef-mediated down-regulation of cell surface expression of HLA-I molecules was assessed by four different cell systems: (a) 721.221, an HLA-A, B, C-null human lymphoblastoid cell line, that was transfected to express a single HLA-I allele; (b) T1, a human $CD4^+$ monocytotic cell line that expresses 6 different autologous HLA-I alleles (each of 2 HLA-A, B, C alleles); (c) human primary T lymphocytes isolated from HIV-negative donors expressing autologous HLA-A*02 and HLA-Bw6 serotype alleles; (d) Jurkat, a human $CD4^+$ T cell line that was stably transfected with genes encoding

HLA-A*02:01 or its cytoplasmic tail mutant. For the first system, we used the HLA-A, B, C-null 721.221 cell line (44) that had been engineered to stably express single HLA class I allele: HLA-*A*02:01, A*24:02, A*33:03, B*35:01, B*57:01* or *C*04:01*. These transfectants were kindly provided by M. Takiguchi, Kumamoto University, Japan, or T. Yamamoto, Vaccine Research Center, NIH, USA. HLA-I expression for each of the 721.221 lines was validated by HLA genotyping methods as described (45), and HLA-I cell surface expression was confirmed by staining with a pan-HLA-I specific antibody (clone: w6/32, BioLegend Co.) followed by flow cytometry. For the second system, the human $CD4^+$ monocytotic cell line T1 was used. HLA-I genotyping results for T1 cells was HLA-*A*02:01, A*31:01, B*40:01, B*51:01, C01:02*, and *C03:04*. In the case of T1 cells, cell surface expression of specific HLA-I alleles, HLA-A*02:01 and HLA-B*51:01, was evaluated using HLA-A2 serotype-specific mAb (clone BB7.2, BioLegend) and HLA-Bw4 serotype-specific mAb (clone TU109, kindly provided by M. Takiguchi), respectively. For the third system, primary T lymphocytes were isolated from PBMC of HIV-negative donors followed by activation with phytohemagglutinin for five days. For the fourth system, the human $CD4^+$ Jurkat T cell line was used. Human cDNA encoding HLA-A*02:01 was cloned from PBMC of a healthy HLA-A*02:01+ volunteer into pcDNA3.1 plasmid. Mutations ($DR_{314,315}$ to $GG_{314,315}$ and deletion of $CKV_{339\text{-}341}$) were introduced into the cytoplasmic tail region of HLA-A*02:01, giving rise to HLA-$A02_{GG,\Delta CKV}$, in which cytoplasmic tail region is equivalent to that of HLA-B*35:01. In all cases, the cell surface expression of HLA-A02 and its cytoplasmic tail mutant was evaluated by an HLA-A2 serotype-specific mAb as above.

HLA-I down regulation assay

The 721.221, Jurkat, T1, and primary T cells were infected by the VSV-g-pseudotyped recombinant HIV-1 and harvested 48 hours later for staining with a pan HLA-I specific antibody (clone: w6/32, BioLegend Co.) or the serotype-specific mAbs, followed by 7-amino-actinomycin D (BioLegend Co) staining and intracellular $p24^{Gag}$ staining with anti-p24 Gag-FITC mAb (KC57, Beckman-Coulter) as previously described (30). Live cells (negative for 7-amino-actinomycin D) were gated and HLA-I expression in $p24^+$ and p24-negative subsets was analyzed by flow cytometry (FACS Canto II or FACS Verse; BD Biosciences). For calculation of the HLA-I down-regulation activity by Nef, the following formula was used (where MFI is mean fluorescence intensity):

(MFI of HLA-I in p24- subset - MFI of HLA-I in $p24^+$ subset)/ MFI of HLA-I in p24- subset

T cell recognition assay

The effects of Nef-mediated HLA-I down-regulation on T cell recognition were analyzed using a T cell receptor (TCR)-based reporter cell assay as previously described (46, 47). Briefly, the effector cells were prepared by

electroporation of Jurkat cells with expression plasmids encoding TCR-α andβ chains specific for the HLA-A*02:01-restricted HIV-1 Gag FK10 epitope [$Gag_{433-442}$: FLGKIWPSYK], human CD8-α chain (Invivogen), and NFAT-luciferase reporter (Affymetrix). The resultant cells were incubated for 24 hours, followed by separation of the CD8-expressing fraction by magnetic beads sorting (Milteyni). Target cells were prepared by infection of parental Jurkat cells (lacking A02) or Jurkat cells transfected with A02 or $A02_{GG, \Delta CKV}$ with recombinant HIV-1 encoding *nef* alleles of interest. For control experiments, uninfected target cells were pulsed with the synthetic FK10 peptide. Effector cells (5 x 10^4 cells) were co-cultured with target cells (5 x 10^4 cells, unless otherwise specifically indicated) for 6 hours and then harvested for the luciferase assay (Steady-glo luciferin kit, Promega). Luminescence was measured by a plate reader (CentroXS3, Berthhold Technologies) with the following conditions: 3000ms integration and 100 ms settle time.

Western blotting

HEK-293T cells were transfected with proviral DNAs encoding Nef_{SF2} or mutants for preparation of cell lysates as described previously (30, 31). Briefly, lysates were prepared in duplicate, subjected to SDS-PAGE, transferred to nitrocellulose membranes and stained with rabbit anti-Nef polycolonal antiserum (NIH AIDS Research and Reference Reagent Program) followed by secondary ECL Rabbit IgG, HRP-linked whole Ab (GE Healthcare Life Sciences) as reported (30). Band intensities were quantified using the Amersham Imager 600 (GE Healthcare Life Sciences).

Statistical analysis

Statistical analyses were performed using Graph Pad Prism 6.0. For codon-function analyses, the Mann-Whitney U test was used to identify amino acids associated with differential ability to down-regulate HLA-A and HLA-B (expressed as HLA-A/HLA-B down-regulation ratios). Multiple comparisons were addressed using q-values, the p-value analogue of the false discovery rate (FDR), which denotes the expected proportion of false positives among results deemed significant at a given p-value threshold (48). For example, at $q \leq 0.2$, we expect 20% of identified associations to represent false positives. In the present study, statistical significance was defined as $p<0.05$ (for univariate analyses) or $p<0.05$ and $q<0.2$ (for analyses correcting for multiple hypothesis testing).

References:

1. Hughes AL, Nei M. 1988. Pattern of nucleotide substitution at major histocompatibility complex class I loci reveals overdominant selection. Nature 335:167-170.
2. Lawlor DA, Zemmour J, Ennis PD, Parham P. 1990. Evolution of class-I MHC genes and proteins: from natural selection to thymic selection. Annu Rev Immunol

8:23-63.

3. Parham P. 1988. Function and polymorphism of human leukocyte antigen-A,B,C molecules. Am J Med 85:2-5.
4. Schaefer MR, Williams M, Kulpa DA, Blakely PK, Yaffee AQ, Collins KL. 2008. A novel trafficking signal within the HLA-C cytoplasmic tail allows regulated expression upon differentiation of macrophages. J Immunol 180:7804-7817.
5. Van Baalen CA, Schutten M, Huisman RC, Boers PH, Gruters RA, Osterhaus AD. 1998. Kinetics of antiviral activity by human immunodeficiency virus type 1-specific cytotoxic T lymphocytes (CTL) and rapid selection of CTL escape virus in vitro. J Virol 72:6851-6857.
6. Mackewicz CE, Ortega HW, Levy JA. 1991. Cd8+ Cell Anti-Hiv Activity Correlates with the Clinical State of the Infected Individual. Journal of Clinical Investigation 87:1462-1466.
7. Borrow P, Lewicki H, Hahn BH, Shaw GM, Oldstone MB. 1994. Virus-specific CD8+ cytotoxic T-lymphocyte activity associated with control of viremia in primary human immunodeficiency virus type 1 infection. J Virol 68:6103-6110.
8. Pereyra F, Jia X, McLaren PJ, Telenti A, de Bakker PI, Walker BD, Ripke S, Brumme CJ, Pulit SL, Carrington M, Kadie CM, Carlson JM, Heckerman D, Graham RR, Plenge RM, Deeks SG, Gianniny L, Crawford G, Sullivan J, Gonzalez E, Davies L, Camargo A, Moore JM, Beattie N, Gupta S, Crenshaw A, Burtt NP, Guiducci C, Gupta N, Gao X, Qi Y, Yuki Y, Piechocka-Trocha A, Cutrell E, Rosenberg R, Moss KL, Lemay P, O'Leary J, Schaefer T, Verma P, Toth I, Block B, Baker B, Rothchild A, Lian J, Proudfoot J, Alvino DM, Vine S, Addo MM, Allen TM, et al. 2010. The major genetic determinants of HIV-1 control affect HLA class I peptide presentation. Science 330:1551-1557.
9. Parker CE, Nightingale S, Taylor GP, Weber J, Bangham CR. 1994. Circulating anti-Tax cytotoxic T lymphocytes from human T-cell leukemia virus type I-infected people, with and without tropical spastic paraparesis, recognize multiple epitopes simultaneously. J Virol 68:2860-2868.
10. Reddehase MJ, Mutter W, Munch K, Buhring HJ, Koszinowski UH. 1987. CD8-positive T lymphocytes specific for murine cytomegalovirus immediate-early antigens mediate protective immunity. J Virol 61:3102-3108.
11. Cohen JI. 1998. Infection of cells with varicella-zoster virus down-regulates surface expression of class I major histocompatibility complex antigens. J Infect Dis 177:1390-1393.
12. Lybarger L, Wang X, Harris M, Hansen TH. 2005. Viral immune evasion molecules attack the ER peptide-loading complex and exploit ER-associated degradation pathways. Curr Opin Immunol 17:71-78.
13. Ambagala AP, Solheim JC, Srikumaran S. 2005. Viral interference with MHC class I antigen presentation pathway: the battle continues. Vet Immunol Immunopathol

107:1-15.

14. Petersen JL, Morris CR, Solheim JC. 2003. Virus evasion of MHC class I molecule presentation. J Immunol 171:4473-4478.

15. Le Gall S, Erdtmann L, Benichou S, Berlioz-Torrent C, Liu L, Benarous R, Heard JM, Schwartz O. 1998. Nef interacts with the mu subunit of clathrin adaptor complexes and reveals a cryptic sorting signal in MHC I molecules. Immunity 8:483-495.

16. Schwartz O, Marechal V, Le Gall S, Lemonnier F, Heard JM. 1996. Endocytosis of major histocompatibility complex class I molecules is induced by the HIV-1 Nef protein. Nat Med 2:338-342.

17. Williams M, Roeth JF, Kasper MR, Fleis RI, Przybycin CG, Collins KL. 2002. Direct binding of human immunodeficiency virus type 1 Nef to the major histocompatibility complex class I (MHC-I) cytoplasmic tail disrupts MHC-I trafficking. J Virol 76:12173-12184.

18. Collins KL, Chen BK, Kalams SA, Walker BD, Baltimore D. 1998. HIV-1 Nef protein protects infected primary cells against killing by cytotoxic T lymphocytes. Nature 391:397-401.

19. Tomiyama H, Akari H, Adachi A, Takiguchi M. 2002. Different effects of Nef-mediated HLA class I down-regulation on human immunodeficiency virus type 1-specific CD8(+) T-cell cytolytic activity and cytokine production. J Virol 76:7535-7543.

20. Yang OO, Nguyen PT, Kalams SA, Dorfman T, Göttlinger HG, Stewart S, Chen ISY, Threlkeld S, Walker BD. 2002. Nef-mediated resistance of human immunodeficiency virus type 1 to antiviral cytotoxic T lymphocytes. J Virol 76:1626-1631.

21. Adnan S, Balamurugan A, Trocha A, Bennett MS, Ng HL, Ali A, Brander C, Yang OO. 2006. Nef interference with HIV-1-specific CTL antiviral activity is epitope specific. Blood 108:3414-3419.

22. Cohen GB, Gandhi RT, Davis DM, Mandelboim O, Chen BK, Strominger JL, Baltimore D. 1999. The selective downregulation of class I major histocompatibility complex proteins by HIV-1 protects HIV-infected cells from NK cells. Immunity 10:661-671.

23. Rajapaksa US, Li D, Peng YC, McMichael AJ, Dong T, Xu XN. 2012. HLA-B may be more protective against HIV-1 than HLA-A because it resists negative regulatory factor (Nef) mediated down-regulation. Proc Natl Acad Sci U S A 109:13353-13358.

24. Foster JL, Molina RP, Luo T, Arora VK, Huang Y, Ho DD, Garcia JV. 2001. Genetic and functional diversity of human immunodeficiency virus type 1 subtype B Nef primary isolates. J Virol 75:1672-1680.

25. Huang Y, Zhang L, Ho DD. 1995. Characterization of nef sequences in long-term survivors of human immunodeficiency virus type 1 infection. J Virol 69:93-100.

26. Kirchhoff F, Easterbrook PJ, Douglas N,

Troop M, Greenough TC, Weber J, Carl S, Sullivan JL, Daniels RS. 1999. Sequence variations in human immunodeficiency virus type 1 Nef are associated with different stages of disease. J Virol 73:5497-5508.

27. Kuang XT, Li X, Anmole G, Mwimanzi P, Shahid A, Le AQ, Chong L, Qian H, Miura T, Markle T, Baraki B, Connick E, Daar ES, Jessen H, Kelleher AD, Little S, Markowitz M, Pereyra F, Rosenberg ES, Walker BD, Ueno T, Brumme ZL, Brockman MA. 2014. Impaired Nef Function Is Associated with Early Control of HIV-1 Viremia. J Virol 88:10200-10213.
28. Mahiti M, Brumme ZL, Jessen H, Brockman MA, Ueno T. 2015. Dynamic range of Nef-mediated evasion of HLA class II-restricted immune responses in early HIV-1 infection. Biochem Biophys Res Comm 463:248-254.
29. Mann JK, Byakwaga H, Kuang XT, Le AQ, Brumme CJ, Mwimanzi P, Omarjee S, Martin E, Lee GQ, Baraki B, Danroth R, McCloskey R, Muzoora C, Bangsberg DR, Hunt PW, Goulder PJ, Walker BD, Harrigan PR, Martin JN, Ndung'u T, Brockman MA, Brumme ZL. 2013. Ability of HIV-1 Nef to downregulate CD4 and HLA class I differs among viral subtypes. Retrovirology 10:100.
30. Mwimanzi P, Markle TJ, Martin E, Ogata Y, Kuang XT, Tokunaga M, Mahiti M, Pereyra F, Miura T, Walker BD, Brumme ZL, Brockman MA, Ueno T. 2013. Attenuation of multiple Nef functions in HIV-1 elite controllers. Retrovirology 10:1.
31. Toyoda M, Ogata Y, Mahiti M, Maeda Y, Kuang XT, Miura T, Jessen H, Walker BD, Brockman MA, Brumme ZL, Ueno T. 2015. Differential ability of primary HIV-1 Nef isolates to downregulate HIV-1 entry receptors. J Virol 89:9639-9652.
32. Lewis MJ, Balamurugan A, Ohno A, Kilpatrick S, Ng HL, Yang OO. 2008. Functional adaptation of Nef to the immune milieu of HIV-1 infection in vivo. J Immunol 180:4075-4081.
33. Mwimanzi P, Hasan Z, Hassan R, Suzu S, Takiguchi M, Ueno T. 2011. Effects of naturally-arising HIV Nef mutations on cytotoxic T lymphocyte recognition and Nef's functionality in primary macrophages. Retrovirology 8:50.
34. Noviello CM, Pond SL, Lewis MJ, Richman DD, Pillai SK, Yang OO, Little SJ, Smith DM, Guatelli JC. 2007. Maintenance of Nef-mediated modulation of major histocompatibility complex class I and CD4 after sexual transmission of human immunodeficiency virus type 1. J Virol 81:4776-4786.
35. Ueno T, Motozono C, Dohki S, Mwimanzi P, Rauch S, Fackler OT, Oka S, Takiguchi M. 2008. CTL-mediated selective pressure influences dynamic evolution and pathogenic functions of HIV-1 Nef. J Immunol 180:1107-1116.
36. Wonderlich ER, Williams M, Collins KL. 2008. The tyrosine binding pocket in the adaptor protein 1 (AP-1) mu1 subunit is necessary for Nef to recruit AP-1 to the

major histocompatibility complex class I cytoplasmic tail. J Biol Chem 283:3011-3022.

37. Jia X, Singh R, Homann S, Yang H, Guatelli J, Xiong Y. 2012. Structural basis of evasion of cellular adaptive immunity by HIV-1 Nef. Nat Struct Mol Biol 19:701-706.
38. Bihl F, Frahm N, Di Giammarino L, Sidney J, John M, Yusim K, Woodberry T, Sango K, Hewitt HS, Henry L, Linde CH, Chisholm JV, Zaman TM, Pae E, Mallal S, Walker BD, Sette A, Korber BT, Heckerman D, Brander C. 2006. Impact of HLA-B alleles, epitope binding affinity, functional avidity, and viral coinfection on the immunodominance of virus-specific CTL responses. J Immunol 176:4094-4101.
39. Kiepiela P, Ngumbela K, Thobakgale C, Ramduth D, Honeyborne I, Moodley E, Reddy S, de Pierres C, Mncube Z, Mkhwanazi N, Bishop K, van der Stok M, Nair K, Khan N, Crawford H, Payne R, Leslie A, Prado J, Prendergast A, Frater J, McCarthy N, Brander C, Learn GH, Nickle D, Rousseau C, Coovadia H, Mullins JI, Heckerman D, Walker BD, Goulder P. 2007. CD8+ T-cell responses to different HIV proteins have discordant associations with viral load. Nat Med 13:46-53.
40. Carlson J, Listgarten J, Pfeifer N, Tan V, Kadie C, Walker B, Ndung'u T, Shapiro R, Frater J, Brumme Z. 2012. Widespread impact of HLA restriction on immune control and escape pathways of HIV-1. J Virol 86:5230 - 5243.
41. Mwimanzi P, Markle TJ, Ogata Y, Martin E, Tokunaga M, Mahiti M, Kuang XT, Walker BD, Brockman MA, Brumme ZL, Ueno T. 2013. Dynamic range of Nef functions in chronic HIV-1 infection. Virology 439:74-80.
42. Miura T, Brockman MA, Brumme ZL, Brumme CJ, Pereyra F, Trocha A, Block BL, Schneidewind A, Allen TM, Heckerman D, Walker BD. 2009. HLA-associated alterations in replication capacity of chimeric NL4-3 viruses carrying gag-protease from elite controllers of human immunodeficiency virus type 1. J Virol 83:140-149.
43. Pereyra F, Addo MM, Kaufmann DE, Liu Y, Miura T, Rathod A, Baker B, Trocha A, Rosenberg R, Mackey E, Ueda P, Lu Z, Cohen D, Wrin T, Petropoulos CJ, Rosenberg ES, Walker BD. 2008. Genetic and immunologic heterogeneity among persons who control HIV infection in the absence of therapy. J Infect Dis 197:563-571.
44. Shimizu Y, Geraghty DE, Koller BH, Orr HT, DeMars R. 1988. Transfer and expression of three cloned human non-HLA-A,B,C class I major histocompatibility complex genes in mutant lymphoblastoid cells. Proc Natl Acad Sci USA 85:227-231.
45. Itoh Y, Mizuki N, Shimada T, Azuma F, Itakura M, Kashiwase K, Kikkawa E, Kulski JK, Satake M, Inoko H. 2005. High-throughput DNA typing of HLA-A, -B, -C, and -DRB1 loci by a PCR-SSOP-Luminex method in the

Japanese population. Immunogenetics 57:717-729.
46. Anmole G, Kuang XT, Toyoda M, Martin E, Shahid A, Le AQ, Markle T, Baraki B, Jones RB, Ostrowski MA, Ueno T, Brumme ZL, Brockman MA. 2015. A robust and scalable TCR-based reporter cell assay to measure HIV-1 Nef-mediated T cell immune evasion. J Immunol Method in press.
47. Shahid A, Olvera A, Anmole G, Kuang XT, Cotton LA, Plana M, Brander C, Brockman MA, Brumme ZL. 2015. Consequences of HLA B*13-associated escape mutations on HIV-1 replication and Nef function. J Virol in press.
48. Storey JD, Tibshirani R. 2003. Statistical significance for genomewide studies. Proc Natl Acad Sci U S A 100:9440-9445.

Acknowledgments

We thank Yoko Ogata, Michiyo Tokunaga, Doreen Kamori, and Tristan Markle for their technical contributions to this study; Brad Jones (George Washington University) and Mario Ostrowski (University of Toronto) for providing the CTL clone from which the FK10-specific TCR was isolated; and Tao Dong and Ushani Rajapaksa at University of Oxford for productive discussion. This study was supported by a grant from Japan Agency for Medical Research and Development, AMED (Research Program on HIV/AIDS), an AIDS International Collaborative Research Grant from the Ministry of Education, Science, Sports, and Culture (MEXT) of Japan, the Imai Memorial Trust for AIDS Research, the Waksman Foundation of Japan (to TU), and US National Institutes of Health (NIH) grant AI102778 (to YX). FM is supported by the scholarship for The International Priority Graduate Programs; Advanced Graduate Courses for International Students (Doctoral Course), MEXT, Japan. PM is supported by Postdoctoral Fellowships from the Michael Smith Foundation for Health Research (MSFHR) and the Canadian Institutes of Health Research (CIHR). MAB holds a Canada Research Chair (Tier 2) in Viral Pathogenesis and Immunity from the Canada Research Chairs Program. ZLB is the recipient of a CIHR New Investigator Award and a Scholar Award from MSFHR.

Supplementary

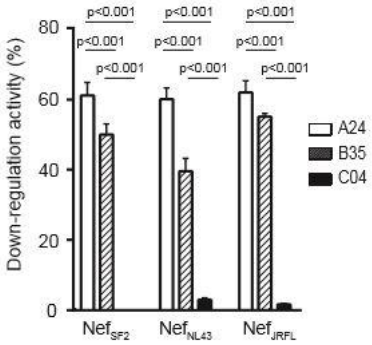

Fig. S1 Down-regulation of HLA-A, HLA-B, and HLA-C by laboratory Nef clones.

721.221 transfectants expressing A24, B35 or C04 were infected with recombinant viruses carrying Nef clones of the laboratory strains of SF2, NL43 and JRFL. HLA-I down-regulation activity by these Nef clones are shown. The data shown are the mean±SD of a minimum of three independent assays. Statistical analysis was done using the Mann-Whitney U test.

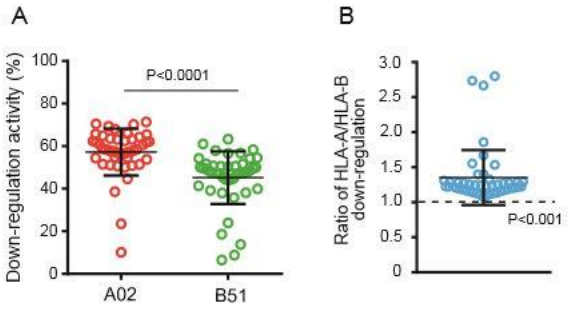

Fig. S2 Down-regulation of HLA-A and HLA-B by primary Nef clones in T1 cells.

(A) HLA-I down-regulation activity in T1 cells by 46 patient-derived Nef clones are shown. Horizontal bars denote median and interquartile ranges. Each plot represents the mean of a minimum of three independent assays. Statistical analysis was done using the Mann-Whitney U test. (B) Ratio of down-regulation activity of A02 and B51 by 46 primary Nef isolates is shown. Horizontal bars denote median and interquartile ranges. Dotted line represents the null expectation of a ratio of 1.0. Statistical analysis was done using the Wilcoxon one sample test.

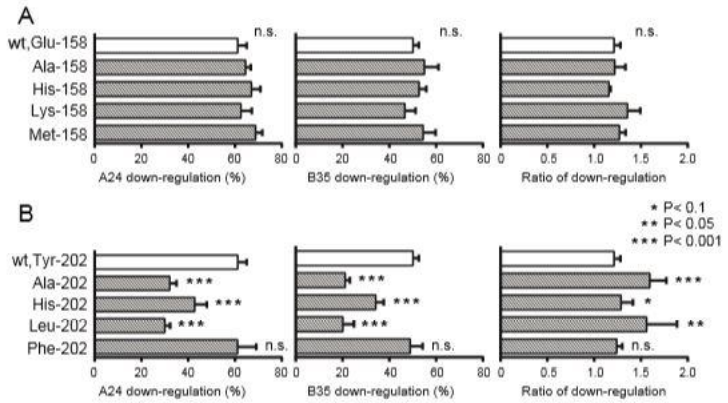

Fig. S3 Effect of defined Nef mutations on HLA-A and HLA-B down-regulation activity in 721.221 cells.

(A, B) Nef_{SF2} and its variants at position 158 (*panel A*) and 202 (*panel B*) were tested for down-regulation activity toward A24 and B35 in 721.221 cells. The ratios of A24 *versus* B35 were also determined. Data shown are the mean ± SD of a minimum of three independent experiments. Statistical analysis was performed using ANOVA with subsequent pairwise comparisons performed versus wild-type. n.s., not significant.